

Conceptual Analysis on Guyed Monopiles for Offshore Wind Turbine Generators in Deep Water

T. J. B. van Doormaal

Delft University of Technology



Conceptual Analysis on Guyed Monopiles for Offshore Wind Turbine Generators in Deep Water

by

T. J. B. van Doormaal

To obtain the degree of Master of Science
at the Delft University of Technology,
to be defended publicly on Thursday March 2, 2023 at 2:00 PM.

Student number:	4473361	
Project duration:	May 2022 - March 2023	
Institution:	Delft University of Technology	
Company:	KCI the Engineers B.V.	
Chair Committee:	Prof. dr. ir. M. Veljkovic,	TU Delft
Committee member:	Dr. ir. F. Kavoura,	TU Delft
Committee member:	Dr. ir. P. van der Male	TU Delft
Company supervisor:	ir. J.H. van den Ouden	KCI the Engineers B.V.
Company supervisor:	ir. M. Del Buono	KCI the Engineers B.V.

Preface

This thesis marks the conclusion of my studies in Structural Engineering and signifies the end of my journey as a student at the Delft University of Technology. My thesis aims to analyze the boundaries of a guyed monopile and overcome issues which occur for monopiles when applied in deep waters. Through extensive modelling and analysis, I have gained valuable insights and knowledge in the field of offshore wind turbine generators. The process of completing this thesis has not only enhanced my understanding of the subject matter but has also taught me valuable skills in critical thinking and problem-solving.

I am very grateful to the TU Delft, KCI the Engineers and SIF Group for giving me the opportunity to complete this important phase of my academic career with a project encompassing nearly all aspects of my studies. It was a perfect learning experience that blended academia and industry. I hope that this thesis will make a meaningful contribution to the field of offshore wind turbine generators. I sincerely hope that these research findings will inspire further studies and provide a foundation for future work in this area.

My gratitude goes to everyone who contributed to my thesis, particularly my supervisors from KCI the Engineers. Marcello Del Buono, you were available whenever I struggled with my topic. Thanks for teaching me a part of your programming skills. Also, your support and passion have provided me with useful information throughout my research. Eric-Jan van den Ouden, thanks for inspiring me through the whole project and giving me your insights into engineering. Also, for helping me out with your knowledge of Ansys workbench. I sometimes had the feeling that both of you liked my project even more than I did.

Thanks to all supervisors from TU Delft, who have provided invaluable guidance and support throughout my research. Without you, my road to graduation would have been totally different and more practical probably. Milan Veljkovic, thanks for your guidance and justified criticism whenever it was needed. You helped me take the extra steps necessary. Pim van der Male, thanks for all your knowledge on offshore engineering. You warned me that a thesis like this might be complicated and that my prior knowledge may have been inadequate. I must admit, you were not wrong. However, your guidance helped me overcome some of the obstacles I encountered. Florentia Kavoura, thanks for helping me out with finding a topic. You advised me on the structure of my thesis and helped me out with the basic questions I had during my thesis.

I would also like to express my gratitude to my friends and family for their support and encouragement. You helped me with sometimes much-needed distractions during my graduation. You also had to cope with my mood, which may not always have been optimal. Finally, I want to thank Angela. You had to cope with me during this turbulent period. Thanks for listening and always supporting me. You improved my thesis a lot without maybe even knowing it!

Thijn van Doormaal
Delft, February 2023.

Abstract

The demand for offshore wind energy has never been higher, yet the number of ideal areas for wind farm installations is decreasing. As a result, larger wind turbines are being placed in deeper waters, which poses opportunities for floating foundations. However, due to the industry's inability to scale up the production of relatively expensive floaters, companies are exploring alternative foundation methods for offshore wind turbine generators in deep water, including the extension of the use of monopiles, which are now being considered for use in water depths up to 60 meters. However, higher loads in deep water require increased stiffness in the monopile structure, which is typically achieved by using larger thicknesses and diameters, resulting in XXL-monopiles. The steel used for these XXL-monopiles increases exponentially for greater water depths, and the designs cross the production limits.

This study investigates the use of a guyed monopile as a more favorable alternative to a conventional monopile for deepwater applications with large wind turbine generators in the range of 60-120 meters of water depth and a rated power of 15 MW. The guyed monopile concept involves adding moorings to a conventional monopile to provide additional stiffness at a certain elevation, reducing the required material within the monopile.

A numerical model is elaborated where the structure is represented by a one-direction FEM model having two degrees of freedom. The model is supported by springs that represent the soil and mooring system. The soil is modelled by a series of p-y reaction curves. For the mooring stiffness, a nonlinear stiffness approach is used where the axial stiffness and geometry of the mooring are considered. The method is used to determine the maximum stiffness that a mooring system can bring. After that, the mooring system is included in the FEM model. Static and dynamic analyses are performed to determine the response of the structure. The described methodology also implements requirements based on potential resonance (1P and 3P frequencies), ultimate limit state (yield strength, column buckling, and local buckling), and fatigue limit state (fatigue damage due to wind and waves). The static and dynamic responses are validated using Ansys. It is concluded that the moorings can provide enough stiffness to reduce the impact of the acting loads on the structure.

A case study is conducted to compare the use of a conventional monopile and a guyed monopile for a foundation based on realistic wind and wave loads. Data of a reference wind turbine and a reference location is taken to find the advantages of a guyed monopile for a realistic case. The study iterates the process for different water depths and varying numbers of moorings. Greater water depths lead to more issues due to resonance and fatigue, which can only be overcome by increasing the diameter and thickness of conventional monopiles. This can also be overcome for guyed monopiles by increasing the mooring stiffness. The results show that the guyed monopile is favored over the conventional monopile in all cases, with up to a 45% reduction in steel required.

The case study's findings are used to identify key parameters in the design of a guyed monopile. The sensitivity of the mooring system stiffness is compared to other key design parameters, including monopile diameter, thickness, and embedded length. The study finds that the moorings have a favourable effect on the system's natural frequency. Also, bending and shear stress may be reduced when moorings are applied.

Contents

Preface	i
Abstract	ii
Nomenclature	vi
List of Figures	viii
List of Tables	x
1 Introduction	1
1.1 Offshore wind	1
1.2 Problem description.	1
1.2.1 Monopiles	2
1.2.2 Guyed monopiles	3
1.3 Objective and research questions.	4
1.4 Methodology	4
2 Literature Review	6
2.1 Terminology.	6
2.2 Deep water	6
2.3 Preliminary design of monopiles	7
2.4 Geometric design criteria.	7
2.5 Mooring system.	8
2.5.1 Mooring type	9
2.5.2 Tensioning systems	9
2.5.3 Anchoring	9
2.6 Resonance criteria	10
2.7 Static Analysis.	10
2.7.1 Dynamic amplification factor.	10
2.7.2 Morison equation	11
2.8 Fatigue analysis	11
2.8.1 Stress Concentration Factor.	11
2.8.2 Damping ratio.	12
2.8.3 S-N curves.	12
3 Structural Model	14
3.1 Mass matrix	15
3.1.1 Steel structure	15
3.1.2 Rotor Nacelle Assembly.	15
3.1.3 Seawater	16
3.2 Stiffness matrix	16
3.2.1 Structural beam stiffness	16
3.2.2 Geotechnical stiffness.	17
3.2.3 Mooring stiffness	18
4 Mooring stiffness analysis	19
4.1 Mooring Stiffness	19
4.1.1 Suspended mooring stiffness	20
4.1.2 Mooring sensitivity	23
4.2 Anchor stiffness	24
4.3 Monopile stiffness.	25
4.3.1 Three mooring layout.	25

4.4	Horizontal spring model	26
4.5	Conclusions	27
5	Static Analysis	29
5.1	Loads	29
5.1.1	Permanent Loads	29
5.1.2	Wind load	29
5.1.3	Hydrodynamic loads	30
5.2	Static Response	31
5.2.1	Internal forces.	31
5.2.2	Internal stresses.	32
5.3	Requirements	32
5.3.1	Von Mises	33
5.3.2	Local buckling analysis	33
5.3.3	Column buckling analysis.	37
5.3.4	Geotechnical capacity check	40
6	Dynamic Analysis	41
6.1	Modal Analysis	41
6.2	Harmonic load response	42
6.3	Damage equivalent bending moment	43
6.3.1	Damage equivalent bending moment for wind	43
6.3.2	Damage equivalent bending moment for waves	44
6.3.3	Total damage equivalent bending moment	46
7	Parametric case study: North Sea	48
7.1	Assumptions.	48
7.1.1	Wind turbine generator.	48
7.1.2	Environmental data.	49
7.1.3	Soil characteristics	50
7.2	Structural design	50
7.3	Modal Analysis	51
7.4	Static Analysis.	51
7.4.1	Wind loads	51
7.4.2	Hydrodynamic loads	51
7.4.3	Internal forces.	53
7.4.4	Internal stresses.	53
7.5	Dynamic analysis	54
7.5.1	Damage-equivalent loads	55
7.5.2	Damage-equivalent moment	55
7.5.3	Fatigue criteria	55
7.6	Parametric study	56
8	Ansys validation	58
8.1	Geometry	58
8.2	Supports.	58
8.3	Modal analysis	58
8.4	Static analysis.	60
8.4.1	Dynamic response.	62
9	Sensitivity Analysis	63
9.1	Natural frequencies	63
9.1.1	First natural frequency	64
9.1.2	Second natural frequency	65
9.2	Internal Stresses	65
9.2.1	Axial stress	66
9.2.2	Bending stress.	66
9.2.3	Shear stress	67

10 Conclusions & Recommendations	69
10.1 Conclusions	69
10.2 Recommendations	70
References	75
A Results Conventional Monopile	76
B Results Guyed Monopile	84
C Geometries parametric study	92
D Modal results parametric study	97
E ULS and FLS results parametric study	100
F Stream function wave	105

Nomenclature

Latin Symbols

A	cross-sectional area
A_{eff}	effective cross-sectional area
\underline{B}	Bouyancy vector
c	wave celerity
C_a	the added water mass coefficient
D	monopile outer diameter
d	water depth
E	modulus of elasticity (Young's modulus)
EA	axial stiffness
f	frequency
F	force
F_D	Morison's drag force
F_M	Morison's inertia force
G	shear modulus
\underline{G}	weight vector
H_s	significant wave height
h	vertical component of the mooring in z-direction
I	moment of inertia
i	number of the mode of vibration
j	imaginary unit
k	spring constant
K_{soil}	soil spring stiffness
K_{sys}	mooring system stiffness
L	Unstretched length of a mooring
L_w	width of weld at the surface
M	bending moment
\underline{M}	bending moment vector
$\underline{\underline{M}}$	mass matrix
$\underline{\underline{M}}_{ss}$	steel structure mass matrix
$\underline{\underline{M}}_{RNA}$	rotor nacelle assembly mass matrix
$\underline{\underline{M}}_{SWI}$	seawater inside the monopile mass matrix
$\underline{\underline{M}}_{SWO}$	seawater outside the monopile mass matrix
m_i	mass of a beam element.
m_{RNA}	mass of the RNA.
N	axial force
n	number of nodes
\underline{Q}_{IN}	the inertial force vector
t	wall thickness
t_{mg}	marine growth thickness
T_p	peak period
\underline{V}	shear force vector
v	velocity

\dot{v}	acceleration
W	section modulus
w	weight per unit length
\underline{Y}	Displacement vector
$\underline{\underline{Y}}$	the 2n acceleration vector.
z	elevation
z_{hub}	the elevation of the hub
z_{IFC}	the elevation of the tower-monopile interface
z_{RNA}	the elevation of the rotor-nacelle assembly

Greek Symbols

α_W	angle of the wind direction.
α_H	angle of the wave direction.
β	shape parameter
γ	scale parameter
γ_G	partial load vector due to permanent loads
γ_w	partial load vector due to wind loads
δ_0	the misalignment inherent in the SN data and analysis procedure.
δ_t	the eccentricity due to a change in thickness.
δ_m	the maximum misalignment.
λ	wavelength
μ	soil linearization factor
ω_i	the eigenvalue of the i-th mode of vibration.
ω	angular speed.
Φ_i	the eigenvector of the i-th mode of vibration.
ϕ	wind-wave misalignment angle.
ρ_w	the density of sea water.
σ_a	axial stress
σ_M	axial stress
σ_{max}	the maximum stress.
σ_{ref}	the nominal reference stress
τ	shear stress
ξ	damping ratio
ξ_s	steel material damping.
ξ_G	soil damping.
ξ_H	hydrodynamic damping
ξ_D	damping due to damping devices
ξ_W	aerodynamic damping.

Abbreviations

1P	one-blade passing frequency
3P	three-blade passing frequency
CM	Conventional Monopile
CoG	Center of Gravity
DAF	Dynamic Amplification Factor
DEL	Damage Equivalent Load
DEM	Damage Equivalent bending Moment
DFF	Design Fatigue Factor
FEM	Finite-Element Method
FLS	Fatigue Limit State
GM	Guyed Monopile
IEA	International Energy Agency
IF	Internal Force
LCoE	Levelized Costs of Energy
MSL	Mean Sea Level
RNA	Rotor Nacelle Assembly
SCF	Stress Concentration Factor
SDoF	Single Degree of Freedom
SF	Safety Factor
ULS	Ultimate Limit State
WTG	Wind Turbine Generator

List of Figures

1.1	Fixed foundation concepts for offshore wind turbines generators [30]	2
1.2	Floating foundation concepts for offshore wind turbines generators [16]	2
1.3	Schematic view guyed monopile	3
1.4	Flowchart to answer the main question	4
2.1	Overview of chosen terminology	6
2.2	Monopile design steps, Source: Malekjafarian et al. [35] and [3]	8
2.3	Geometry and fabrication tolerances for butt welds in tubular sections, source:DNVGL-RP-C203 [14]	11
2.4	S-N curves in seawater with cathodic protection. Source: DNVGL-RP-C203 [14]	13
3.1	Finite-element model for wind turbine generator	14
3.2	Linearization of P-Y model for pile-soil interaction	17
4.1	Finite-element model for wind turbine generator with added stiffeners	19
4.2	Mooring type characteristics for Dyneema rope. [9]	20
4.3	Suspended mooring parameters. Source: Al-Solihat and Nahon[43]	20
4.4	Marine growth influence on the mooring stiffness	22
4.5	Mooring stiffness for varying diameter	23
4.6	Mooring stiffness sensitivity parameters	23
4.7	Influence of the mooring stiffness	23
4.8	Finite-element model of a pinpile	24
4.9	Displacement(left) and rotation(right) of a pinpile	24
4.10	Example of monopile ring stiffness analysis for a guyed monopile with 3 moorings	25
4.11	Monopile ovalization stiffness for 3 moorings applied	26
4.12	Horizontal spring model for a monopile supported by 3 moorings	26
4.13	Conclusions on mooring stiffness analysis	27
5.1	Current velocity profile	30
5.2	Cross section class for circular hollow sections. Source: Eurocode 3 EC-1993-1-1[18]	32
5.3	Buckling deformations of a cantilever, simply supported cantilever and guyed cantilever	37
6.1	Cross section points where the damage is calculated	43
6.2	Example of a JONSWAP spectrum. Source:Ma et al.[33]	44
6.3	Example of an Airy wave	44
7.1	Monopile geometry	50
7.2	1P and 3P Frequencies check for reference WTG for CM and GM	51
7.3	Current velocity for 80m water depth	52
7.4	Applied stream function wave	52
7.5	Applied static force envelopes	53
7.6	Internal forces	53
7.7	Internal Stresses	54
7.8	Unity Checks	54
7.9	Maximum of the criteria of every node	54
7.10	Damage equivalent bending moments	55
7.11	Fatigue damage utilization for the conventional and guyed monopile	56
7.12	Total foundation mass resulting from the parametric study	57
8.1	Geometry of the beam model in Ansys	58

8.2	Springs representing the moorings	59
8.3	Modal analysis results from Ansys	60
8.4	Comparison internal forces: bending moment (left) and shear force (right)	61
8.5	Ansys deformed internal force results	61
8.6	Deformations of Ansys-Numerical model validation	62
8.7	Harmonic responses Ansys and Numerical model	62
9.1	Influence of the mooring stiffness in comparison to other main design parameters on the first natural frequency	64
9.2	Influence of the mooring stiffness in comparison to other main design parameters on the second natural frequency	65
9.3	Influence of the mooring stiffness in comparison to other main design parameters on the axial stress	66
9.4	Influence of the mooring stiffness in comparison to other main design parameters on the bending stress	67
9.5	Influence of the mooring stiffness in comparison to other main design parameters on the shear stress	68
C.1	All geometries for 60-meter water depth	93
C.2	All geometries for 80-meter water depth	94
C.3	All geometries for 100-meter water depth	95
C.4	All geometries for 120-meter water depth	96
D.1	All resonance checks for 60-meter water depth	97
D.2	All resonance checks for 80-meter water depth	98
D.3	All resonance checks for 100-meter water depth	98
D.4	All resonance checks for 120-meter water depth	99

List of Tables

3.1	Structural beam mass matrix	15
3.2	RNA mass matrix	15
3.3	Sea water inside monopile mass matrix	16
3.4	Sea water outside monopile mass matrix	16
3.5	Structural beam stiffness matrix	17
3.6	Geotechnical stiffness matrix	18
3.7	Mooring system stiffness matrix	18
4.1	Equations for mooring type characteristics, source: Ma et al. [33]	20
4.2	marine growth thickness t_{mg} over the sea water depth	21
5.1	Imperfection factor α for buckling curve, source: EC1993-1-1 [18]	39
6.1	DEL data provided by WTM	43
7.1	Rotor nacelle assembly data, according to the IEA 15MW wind turbine generator[24] . .	49
7.2	Tower geometry	49
7.3	Extreme oceanographic data including return period, source: Lohmann, Hunt, and Redanz [32]	49
7.4	Soil characteristics, source: Fugro	50
7.5	Wind loads	51
7.6	Assumed DEL data	55
8.1	Natural frequencies Ansys vs. numerical model	59
9.1	Design parameter ranges	63

1

Introduction

1.1. Offshore wind

Since the finishing of the first offshore wind farm in Denmark in 1991, the demand for Wind Turbine Generators (WTGs) kept increasing exponentially, and the expectation is that this growth will continue in the future as well. In May 2022, the European Commission launched a plan to rapidly reduce the dependency on Russian fossil fuels, named REPowerEU [20]. In this plan, it is stated that there is an urgency to transform Europe's energy system to end the necessity of Russian fossil fuels and to tackle the climate crisis. Therefore, an accelerated roll-out of renewable energy is more urgent than ever. This acceleration should result in a proposed 45% increase in the renewable energy industry by 2030, according to the report of the European Commission [20]. A large proportion of this increase will be because of wind energy generation. In 2020, more than one-third of the total energy generated by renewable sources in Europe was due to wind power, both onshore as well as offshore [21]. Because of the higher wind speeds and high general acceptance, mainly offshore wind is expected to be increasing in the near future. Offshore wind is one of the renewable energy resources which is known to be secure, steady, and solid. The global offshore wind market is set to expand significantly over the next two decades, growing by 13% per year, according to data from the International Energy Agency [28]. It is also concluded that offshore wind energy has the potential to generate 18 times the total global electricity demand of 2019.

To reduce the costs of offshore wind farms, within the offshore wind industry, there is a development going on to generate more power per WTG. A typical nowadays offshore WTG can generate 12 MW. However, a prototype of Vestas' W236 Wind turbine of 15 MW is already being tested, and it is planned to have it in operation at the wind farm project Hollandse Kust West front of the coast of the Netherlands. On top of that, turbines with a capacity of more than 20MW are currently being designed [4][44]. The increasing power generation results in larger blade diameters and even higher wind turbine towers. This includes a new challenge to design the turbines with higher forces that need to be transferred within the tower wall towards the support structure of the WTG.

Next to the larger structures, sustainability becomes more and more of an issue. The production of a ton of steel makes up for 1.85 tons of carbon dioxide pollution into the atmosphere, and of the total emitted carbon dioxide is 8% due to steel production [26]. Therefore, the minimization of material use and optimization of all conceivable structures is very important. This also implies the offshore wind industry and, thus, the foundations of WTGs. There is an eternal demand from the WTG industry to minimize the Levelized Cost of Energy (LCoE). The LCoE is a method to measure the total cost of generated energy from a particular power source. The lower the LCoE, the more profitable a WTG gets. Having a more affordable foundation also decreases the LCoE. Hence, a lighter foundation structure for an offshore WTG is more desirable.

1.2. Problem description

Figure 1.1, six typical fixed support structure concepts for wind turbine generators. These are (a) gravity-based foundation, (b) monopile foundation, (c) suction can foundation, (d) multi-pin pile tripod founda-

tion, (e) multi-suction can tripod foundation and (f) jacket foundation. On top of these concepts, floating support structure concepts are of more importance these days. Four of these are shown in figure 1.2: (g) semi-submersible, (h) spar, (i) tension leg platform, and (j) barge.

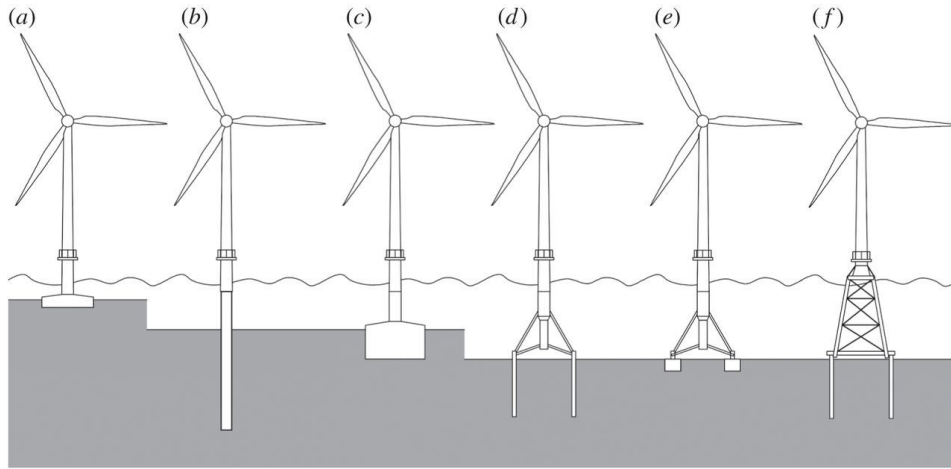


Figure 1.1: Fixed foundation concepts for offshore wind turbines generators [30]

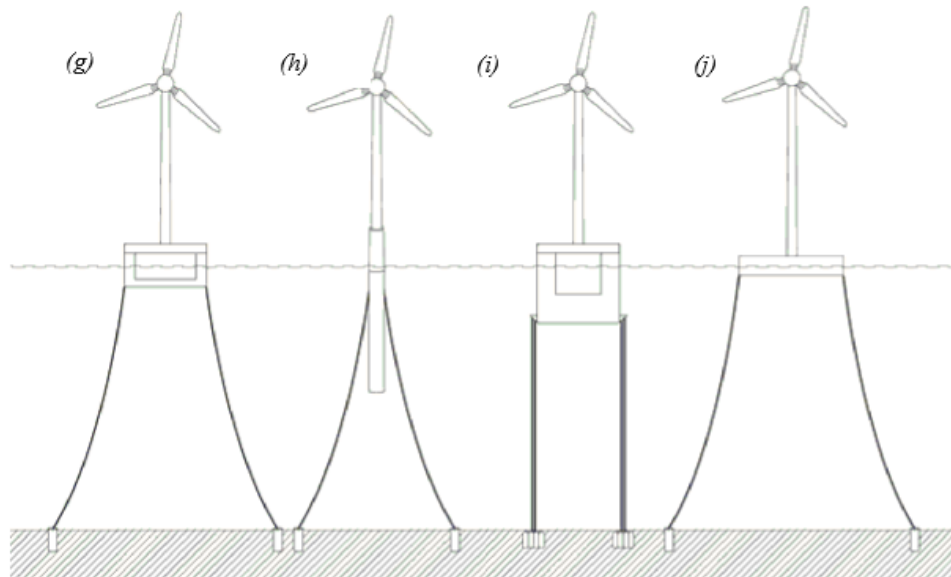


Figure 1.2: Floating foundation concepts for offshore wind turbines generators [16]

1.2.1. Monopiles

From all of the concepts, monopiles are still the most used support structure with a share of 81.2% of all installed offshore WTGs in Europe by the end of 2020 [47]. The construction costs of fixed foundation concepts are quite low, and the installation is easy. But as described in the previous section, as WTGs will be built more often in deep waters, the monopiles might not be suitable anymore due to higher costs. In a report of the Norwegian registrar and classification society DNV GL, it is predicted that floating offshore wind will generate 264 GW of energy by 2050[11]. This is equal to 15% of all generated offshore wind energy. The technology of floating structures is promising, and a big advantage is that the structures can also be placed in deep waters. DNVGL expects that eventually, floating wind might perform even better than bottom fixed offshore wind [11]. There is only one big issue with floating wind energy; the LCoE of the technology is way higher. "Today, floating foundation costs are five times higher than bottom fixed", - according to the DNV GL report. Therefore, shortly, fixed bottom structures will still be the best way of supporting WTGs.

Monopiles are steel tubes that are driven and hammered into the sea bed. Due to easy installation and manufacturing, monopiles are considered the cheapest option for supporting a WTG. A monopile support structure consists of the monopile itself and a Transition Piece (TP) on top. This TP carries secondary elements such as boat landings, ladders, and platforms. These are used for the accessibility of the WTG. However, a trend is developing in which the transition piece is left out, the so-called TP-less monopile, as it requires less steel. Due to the increasing size of WTGs and the increasing water depths in which the generator is placed, the monopiles are also required to grow in diameter. That is why the development of XXL monopiles has been going on for the last couple of years. Also, XXL monopiles are used more often. These are monopiles that have diameters over 8 meters.

Monopile structures are now often assumed to be suitable for only shallow (<25m) and mid-deep waters (<50m) [30]. However, a recent MSc thesis conducted by TU Delft has suggested that, from a technical point of view, monopiles can be used in even deeper waters, i.e. until 120 meters [49]. The greater the water depth where a WTG foundation is placed, the more steel for monopile support is needed. This is due to the higher forces that act on the wind turbine. Because of the extra depth, the hydrodynamic forces are higher. This also applies to the wind loads due to the higher wind speeds described in the previous section. Furthermore, the deeper the water, the longer the monopile needs to be, and the more the pile stiffness decreases. To avoid resonance resulting from the periodic loads of the turbine, this stiffness needs to be increased by widening the diameter of the monopile or increasing the embedding length. Therefore, a monopile's thickness or diameter will increase as the depth increases.

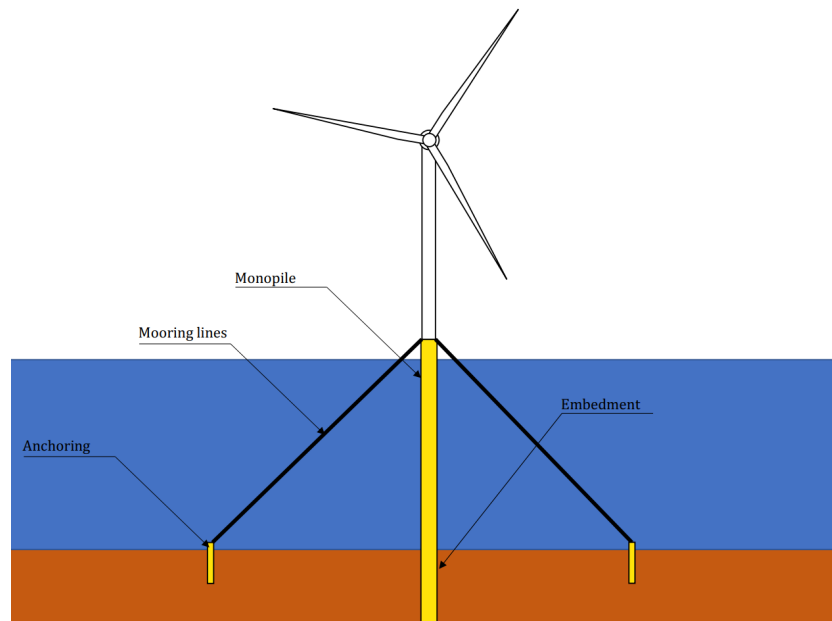


Figure 1.3: Schematic view guyed monopile

1.2.2. Guyed monopiles

In 1984, a thesis was conducted by Taconis for the Delft University of Technology[45]. In this paper, a guyed tower offshore wind turbine has been developed for intermediate water depths (75m). A slender truss tower has been designed to show the feasibility of the application of a guyed system for a truss tower where 16 moorings and anchors are used for stiffening the structure. A guyed tower wind turbine generator appears feasible for water depths of 75-100 m. Also, research conducted by Bunce and Carey concluded that a guyed WTG could have a significant benefit compared to a tripod solution for wind turbines. Its weight is reduced by a third, which leads to multiple cost-beneficial advantages. However, the installation costs are often believed as too expensive. As even bigger WTGs are placed in deeper waters, a guyed WTG design may become relevant again.

1.3. Objective and research questions

This MSc thesis aims to structurally analyze the effect of adding pretensioned moorings onto a monopile foundation for offshore wind turbine generators in deep water. The objective is to elaborate that a guyed monopile is favourable over conventional monopiles in deep waters for large wind turbine generators having a rated power of 15 MW. The goal of this research will be achieved by answering the following research questions:

1. What order of magnitude of stiffness can the mooring system for a guyed monopile provide?
2. Given a case of environmental conditions, what would be the weight reduction of a monopile foundation that can be achieved by the application of moorings for different water depths?
3. What is the influence of the mooring system stiffness compared to other design variables, and how does it affect the response of the structure?

1.4. Methodology

To overcome the problems stated in the previous sections and find a solution for the research questions (RQs), this thesis is divided into five sections:

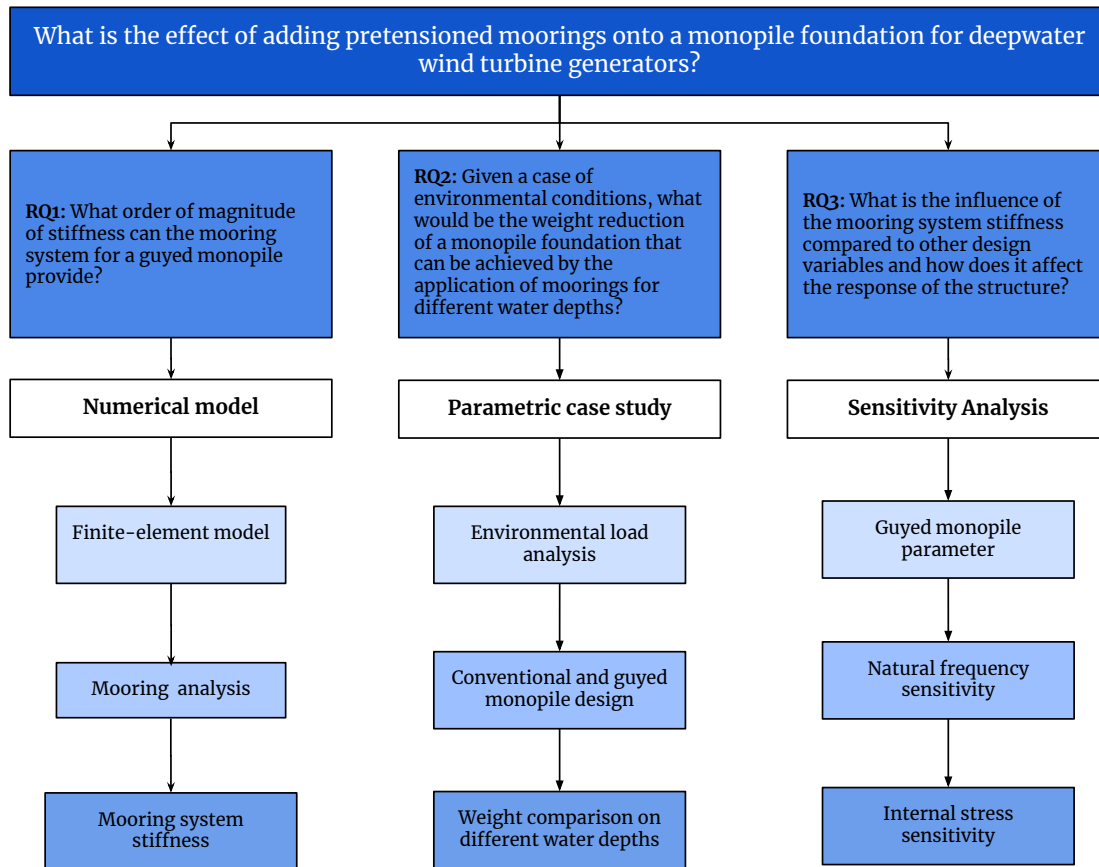


Figure 1.4: Flowchart to answer the main question

1. Numerical model (RQ1)

In this thesis, first, a numerical model is built. This is done by designing the mooring system stiffness. Therefore, a 1D beam finite element model for a monopile is established using Python. The model is supported by springs representing the soil and the mooring system. An exact nonlinear approach is used to model the mooring system's springs, where the moorings for floating offshore structures are usually modelled. The stiffness of the soil is modelled using the p-y method; this is an approach to analyze the response of laterally loaded piles. The model also comprehends static

(ULS) and dynamic (FLS) analyses to determine the structure's response. For the static analysis, column buckling of the monopile and yield stress of the material is evaluated. The dynamic analysis comprehends a fatigue study in which the cumulative damage from dynamic loading on a WTG is calculated. This is done for every circumferential weld within the monopile.

2. Parametric case study (RQ2)

The analytical model of the previous parts presents a preliminary design of a WTG foundation for a reference 15MW wind turbine and a reference site with a water depth of 80 meters. As fewer data are known for deep water locations, the data of a shallow water project is chosen. The selected location's metocean-, soil and environmental data are gathered and used to determine the loads on the WTG. This section ends with a study in which the boundaries of a guyed monopile are investigated. The foundation for the same WTG and location as in the case study is considered, but with varying water depths: 60, 100, and 120 meters and a variable number of moorings.

3. Sensitivity analysis (RQ3)

In the sensitivity analysis, the influence of the different variables in the numerical model of the previous section is investigated. This section is divided into two parts. In the first part, the natural frequencies are analyzed, and the impact of every mooring stiffness parameter will be shown. Next to that, the internal stresses of guyed monopile design variables are examined. These parameters are monopile diameter, thickness, embedded length, and mooring stiffness, which are compared to each other to show what variable influences the design of a guyed monopile.

2

Literature Review

2.1. Terminology

In figure 2.1, an overview is given of the chosen terminology for this thesis.

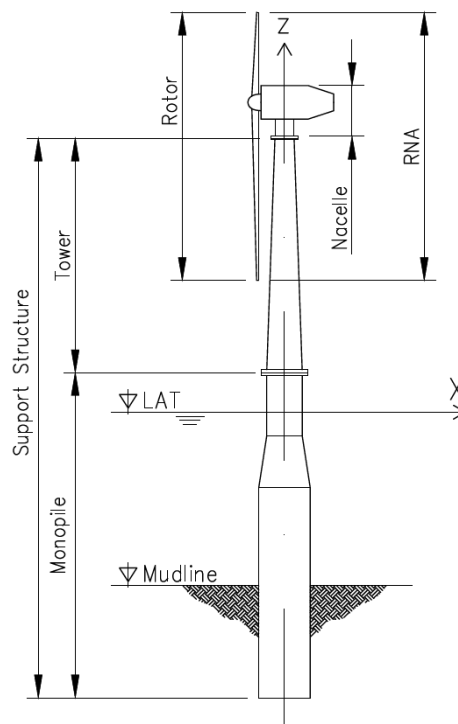


Figure 2.1: Overview of chosen terminology

2.2. Deep water

Monopiles are hammered into the seabed. By doing this, the soil provides the needed stiffness to withstand the forces acting on the monopile. Therefore, a monopile-supported WTG is assumed to be fixed, and the WTG is considered a cantilever. For a cantilevered column with a perpendicular point load at the end of the column, the bending moment increases linearly over the whole beam. Applying moorings somewhere over the column decreases the maximum bending moment in the cantilever. Burton et al. states that: "The design of wind turbine foundations is largely driven by the tower base overturning moment under extreme wind conditions"[7]. With deeper water, this overturning moment will increase even more. The deformation of a cantilever grows exponentially over the length of the column as no rotation is allowed at the clamped support. In the case of a guyed monopile, the moorings act as spring

support in a perpendicular direction to the column[33]. The higher the mooring attachment, the more displacement due to the load can be achieved. That is why it is believed that water depths below 60 meters are assumed to be impractical for guyed monopiles. So, the deeper the water, the more benefits a guyed monopile might give over a conventional monopile.

In this range, only jackets are believed to be applicable in water depths of 50 - 80 meters as a bottom-fixed structure. Otherwise, floating becomes economically more attractive. However, for floating wind reducing the LCoE is mainly necessary for overall wind energy generation. Upscaling is a critical factor for the reduction [38]. No floating foundation manufacturer is now able to produce multiple foundations in a relatively short time. This is necessary to have enough WTGs in production to satisfy the ambition of governments to become energy neutral shortly. Paya and Du state: "To fabricate one hundred monopiles and jackets is a challenge, but it has been done. The fabricators in the Northern Europe / North Sea area can do it and have learned from existing projects. However, it has never been done for floaters, which may be the real bottleneck for some development projects" [40]. As monopiles and moorings are relatively easy to fabricate, the guyed monopile could replace foundations of WTGs in the range of 60 - 120 meters water depth.

2.3. Preliminary design of monopiles

In the preliminary design phase for monopiles, the basis of design is drafted. The basis of design contains the process, assumptions and data necessary to meet the client's requirements. Information on design, guidelines, to-be-used materials and the forces the foundation must withstand can be found in the document. On top of that, it describes the local soil-, wind- and wave conditions. In this phase also, the geometry of the tower is handled. The size of the WTG tower is considered and the weight of the tower as well as the weight of the RNA. Also, the requirements for resonance, buckling and fatigue are described. Finally, the location is described in detail. The assembly of the seabed is (briefly) investigated in the preliminary design phase, as it has to be built up out of good soil to give stable and firm support for the foundation of the WTG. For every WTG, site-specific metocean data needs to be determined. The mean sea level and maximum sea level for ULS calculations. Also, sea level rise due to climate change must be considered. Afterwards, a probability analysis of the incoming wind, waves and their chances of appearing in the same direction is performed. These are called scatter tables or wind and wave roses. Conservatively, in this research, the maximum load is taken as the 1-year return period for the maximum wind (gust) speed is taken and 50 year return period for the maximum speed in ULS calculations. Arany et al. developed a model to design a monopile in 10 steps [3]. Malekjafarian et al. visualised the model by a flowchart which can be seen in figure 2.2. This model is used as a basis for this research. The process for designing a WTG foundation starts by guessing initial pile diameters. As this thesis focuses on deep waters, the expectancy is that resonance issues will play a big role in developing monopiles in deep water. Therefore, this check will be done first.

2.4. Geometric design criteria

To shift the use of monopiles towards greater water depths, there is a need to push the limits of the monopiles' cross-section characteristics and material properties. The design of monopiles is now often governed by its production-, storage-, transportation- and installation limits. This will also be the case for guyed monopiles. Helpful literature is analysed to determine limits on which the monopile can be designed.

D/t ratio

The Diameter-to-thickness (D/t) ratio, or slenderness, refers to the relative size of the diameter of a structural element compared to its thickness. This ratio is often used to evaluate the stability and strength of the component. In the case of monopiles, the D/t ratio is an essential factor in their design. The more slender a monopile becomes, the more issues occur due to local bending. Also, the increasing size of the monopiles results in more transportation and storage issues. Because monopiles are hammered into the seabed, the maximum value for the D/t ratio is 160. [46]

Can length

A monopile consists of cans that are connected using butt welds. These cans consist of thick steel plates whose size is limited due to transportation and production reasons [10]. The plates are manufactured

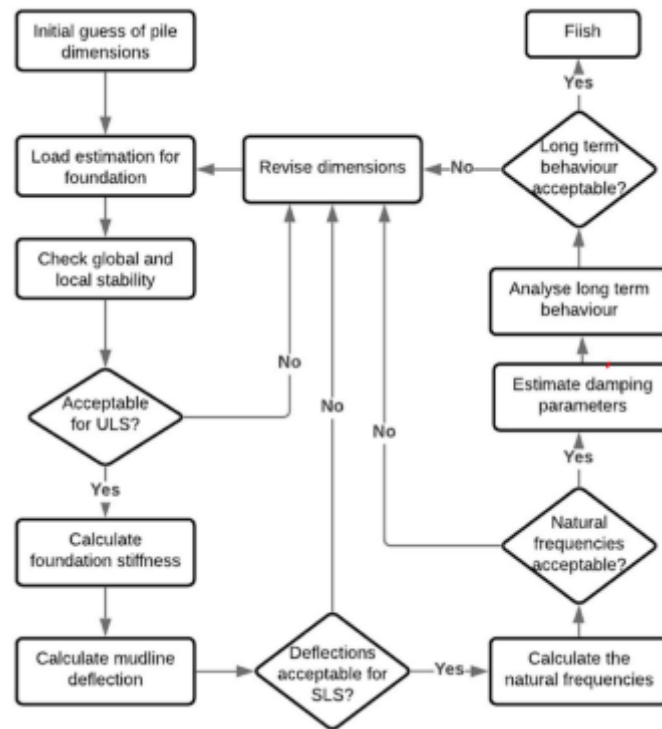


Figure 2.2: Monopile design steps, Source: Malekjafarian et al. [35] and [3]

using a technique called the thermo-mechanical control process. The plates are rolled into the desired diameter and afterwards welded together, forming the cans. There is a maximum value for the weight per plate due to transportation and deliverability issues. Therefore, the wider they are, the less length per plate can be used, more plates per can are necessary and more welds are needed to form a can. This study assumes a maximum can length value of 4.5 meters.

Steel thickness

Heavy plate manufacturer Dillinger mainly produces steel plates for the offshore and pipeline industry. These plates are better resistant to the aggressive environment where the plates are used due to the influence of seawater. The company produces the plates by using steel which is thermomechanically rolled fine-grained. There is a limit to what thickness this method can be used, which is approximately 150mm [10]. Therefore, the maximum steel thickness used in this study is also set at 150 mm.

Conical section

Monopiles often have a conical or tapered section over the monopile's height, especially for water depths greater than 20 meters. This conical section is used in the design to reduce loads resulting from waves onto the cross-section and account for the increase in bending moment towards the seabed[29]. The slope of a tapered section between the monopile may not exceed 4° due to production limits.

Weight

The weight of monopiles is often limited and governed due to transportation and manufacturability issues. The total weight for a pile will take over 2400 tonnes shortly when XXL monopiles are used[46]. Also, bigger boats might be necessary as their lifting capacity might not be large enough. However, as earlier discussed, the boundaries of a monopile have to be extended for the use of a guyed monopile; therefore, no limit for the (can) weight is assumed in this research.

2.5. Mooring system

The moorings of a guyed monopile will be one of the critical parameters in the design. They are permanently installed and need to provide excellent stiffness to the monopile to have an effect. In this section, the mooring type and anchoring are described.

2.5.1. Mooring type

A guyed system contains three main components: the mooring type, the mooring itself and the anchor to connect the mooring with the seabed; these are described in the following sections. Two mooring systems can be recognized: a taut mooring system and a catenary mooring system. In a taut system, all moorings are considered straight, and the system stiffness is achieved from the elasticity and, thus, the axial stiffness of the moorings. The main advantage is that less mooring is necessary than for a catenary system. However, this is mainly of importance for waters deeper than 100 meters. When a taut system is assumed, the weight of the mooring is neglected, and the sag of the mooring is not considered. However, in reality, all moorings have weight, a perfect straight mooring is not achievable. The catenary system also implies the weight and the lift of the moorings. As the weight is considered a distributed load onto the mooring, the catenary system has a curved shape, and the mooring is not straight. This also brings a non-linearity to the system. A Catenary system often comprehends the application of chains. A mooring is a line that connects an offshore component to an anchor in the seabed. In floating platforms, moorings are applied and pre-tensioned for reducing their motions. Mooring systems can have a temporary as well as a permanent lifetime. As WTGs are built for a lifetime of about 25 years. The mooring system is also considered permanent [37]. That is why components like the moorings, pre-tensioning system and anchoring of the mooring system for a guyed monopile must also be designed with permanent elements. Steel chain is one of the most common ways of offshore mooring structures. It is considered very heavy, which is why it cannot be used for a taut mooring system. In an all-chain setup, chains are mainly utilised in catenary systems. Which means that one mooring entirely consists of a chain. It can also be used in a combined setup, where the end parts are built out of the chain. But, the middle portion (often the longest) consists of a rope of another material Ma et al. Multiple chain grades with different strength grades. moorings often consist of steel wires, which have high elasticity and, therefore, a higher axial stiffness than steel chains. They are also lighter than chains as less steel is used for the same stiffness. For permanent moorings, corrosion also is important. Therefore, sheathed spiral strands, which often consist of polyethylene, can be utilised. Also, galvanized steel can be used to have resistance against rust or other types of corrosion [33]. Steel wires suffer from excessive bending, therefore often used as a 'chain-wire-chain' system. This means that the moorings' ends are manufactured as chains, and the middle part consists of wire rope.

2.5.2. Tensioning systems

Pre-tensioning has to be applied to provide enough stiffness to the guyed monopile. In a recent study conducted by Ma et al.[34], state-of-the-art practices in the oil and gas industry are reviewed and documented to elaborate on the benefits and downsides of the upcoming floating offshore wind turbine projects. Ma et al. states that a hydraulic chain jack or a winch for steel chains is the most common way of pre-tensioning. These might also be the most cost-effective for application in the floating wind industry. On top of that, an in-line tensioner might also be beneficial. An in-line tensioner is a device which is permanent in the mooring line. A few advantages are that the tensioner can also be used underwater and placed at multiple locations along the mooring line.

2.5.3. Anchoring

At the end of the mooring, there needs to be sufficient anchoring for the mooring to resist the acting loads on the mooring. Ma et al. describes the two most-used methods for permanent anchoring moorings into the seabed: (1) suction pile anchor and (2) driven (pin) pile anchor [33]. For anchors, structural design and geotechnical design need to be evaluated. As the anchors are expensive due to installation, reducing the number of anchors is beneficial. A way to overcome this problem is to apply more moorings per anchor. A downside is that the resulting horizontal force onto the anchor is more significant, and a more excellent pile resistance is needed.

Suction piling

Suction piling means anchoring with cylindrical hollow tubes placed onto the seabed. Due to the self-weight of the anchor, the piles are installed and sunken until a certain depth beneath the mudline. After that, the remaining air is sucked out of the can so that the piles are located at the desired penetration depth, making no heavy and expensive hammering equipment is needed for installation[33].

Pin piling

Pin piles are driven into the seabed until the desired penetration depth. Their structural behaviour is quite the same as for monopiles. The main advantage is that pin piles can be used in challenging soil conditions and are believed to be the most cost-beneficial way of anchoring. They have good vertical and lateral load resistance, which is essential for applying pretensioned moorings.

2.6. Resonance criteria

It needs to be made sure that the structure's natural frequencies do not interfere with the angular speed of the rotor. A WTG manufacturer provides the minimum and maximum values for the rotor angular speed, Ω_{min} and Ω_{max} . For the IEA wind, this is, for example, 5.0 rpm and 7.56 rpm, respectively [24]. This angular speed is also called the rotors' rotational frequency during power production (1P). Consequently, next to the 1P frequency, the 3P frequency can be calculated. This is the blade-passing frequency (3P) of the rotor. Suppose one of the natural frequencies interferes between these. In that case, there is the possibility that resonance occurs, which needs to be avoided as the collapse of the structure might be a consequence of this behaviour.

First, the 1P and 3P spectra are calculated for the corresponding WTG. The minimum and maximum of the design 1P frequencies are as follows:

$$f_{1P,min} = \Omega_{min}/SF \quad (2.1)$$

$$f_{1P,max} = \Omega_{max} \cdot SF \quad (2.2)$$

Where:

- Ω_{min} = the minimum value for the rotor angular speed.
- Ω_{max} = the maximum value for the rotor angular speed.
- SF = Safety factor for confirming safety.

The same is applied for the minimum and maximum of the design 3P frequencies:

$$f_{3P,min} = 3 \cdot \Omega_{min}/SF \quad (2.3)$$

$$f_{3P,max} = 3 \cdot \Omega_{max} \cdot SF \quad (2.4)$$

Where:

- Ω_{min} = the minimum value for the rotor angular speed.
- Ω_{max} = the maximum value for the rotor angular speed.
- SF = Safety factor for confirming safety.

The foundation structure of the WTG must be designed such that the natural frequencies following from equation 6.6 do not interfere with these spectra. Note that a safety factor is already considered for the calculation, generally accepted as 5% according to DNVGL-ST-0126. The stability requirement can then be described as follows:

$$\forall \omega_i : \omega_i < f_{1p,min} \vee f_{1p,max} < \omega_i < f_{3p,min} \vee \omega_i > f_{3p,max} \quad (2.5)$$

Where:

- ω_i = the i-th natural frequency of the structure.
- $f_{1P,min}$ = the minimum value for the design 1P frequency.
- $f_{1P,max}$ = the maximum value for the design 1P frequency.
- $f_{3P,min}$ = the minimum value for the design 3P frequency.
- $f_{3P,max}$ = the maximum value for the design 3P frequency.

2.7. Static Analysis

2.7.1. Dynamic amplification factor

The dynamic amplification factor (DAF) is the ratio of the dynamic response amplitude to the static response. The DAF for an SDOF-system is as follows, according to Xi et al.:

$$DAF = \frac{X_{dyn}}{X_{stat}} = \frac{1}{\sqrt{(1 - (\frac{f_e}{f_0})^2)^2 + (2\xi \frac{f_e}{f_0})^2}} \quad (2.6)$$

As offshore WTGs are systems with multiple DoFs, the calculation is more complicated. Xi et al. performed a parametric study in which numerous wave scenarios were analyzed to see the different DAFs. It is concluded that the DAF often ranges between 1.10 and 1.26 [48]. In this study, the DAF is conservatively taken as 1.26.

2.7.2. Morison equation

Hydromechanics in offshore engineering are often described by the Morison equation. The method gives a relationship between the drag and inertia force. This equation is a superimposed way to calculate the total force on a structure loaded by a wave based on the linear inertia force and the quadratic drag force. The drag force, thrust force, and total force due to the current can be described as follows, respectively:

$$F_D = \frac{1}{2} C_D \rho_w D v |v| \quad (2.7) \quad F_T = \frac{1}{2} C_T(D) \rho_w \pi D^2 \dot{v} \quad (2.8) \quad F_{tot}(t) = F_D(t) + F_T(t) \quad (2.9)$$

Where:

- C_D = Morison's drag coefficient, taken in this study as 1.1.
- C_M = Morison's inertia coefficient, taken in this study as 2.1.
- ρ_w = the density of the seawater.
- D = diameter of the monopile.
- $v(z)$ = the velocity of a water particle.
- $\dot{v}(z)$ = the acceleration of a water particle.

2.8. Fatigue analysis

2.8.1. Stress Concentration Factor

A stress concentration is a location in a structural component where the stress deviates from the nominal (Euler-Bernoulli) stress. This effect is seen due to geometric discontinuities of the element, such as sharp corners, holes, and welded connections having different thicknesses. This stress concentration is primarily described in terms of the Stress Concentration Factor (SCF), i.e. the ratio of the highest stress in a component to a nominal reference stress:

$$SCF = \frac{\sigma_{max}}{\sigma_{ref}} \quad (2.10)$$

The SCF is used in fatigue design to predict the component's life subjected to cyclic loading, which is the case for WTGs. Stress concentrations in monopile design are mainly seen at the cable power holes and circumferential butt welds, as only the latter is assumed to be in the scope. This thesis will focus on the welded sections between the cans of a guyed monopile. In general, the SCF needs to be minimized such that the fatigue life increases. Therefore, the difference in thickness of two neighbouring cans should be chosen to be small enough that the SCF is as small as possible. Proper post-weld treatment is recommended when the fatigue life is not sufficient for the design life. A method to calculate the SCF for the butt welds is given in DNV-GL-RP-C203 [14]. A schematic view of such a butt weld is shown in figure 2.3. Here, the SCF is calculated as follows:

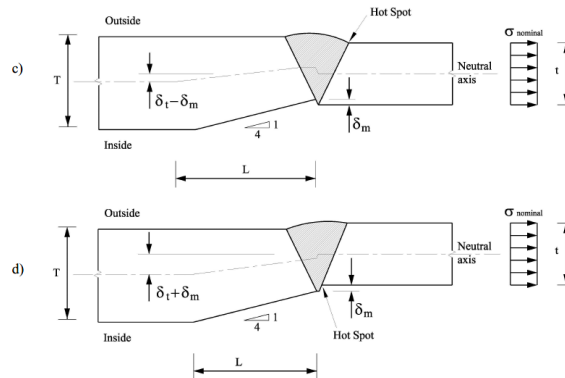


Figure 2.3: Geometry and fabrication tolerances for but welds in tubular sections, source:DNVGL-RP-C203 [14]

$$SCF = 1 + \frac{6(\delta_t + \delta_m - \delta_0)}{t} \frac{1}{1 + (\frac{T}{t})^\beta} e^{-a} \quad (2.11)$$

Where:

$$\begin{aligned} \alpha &= \frac{1.82L_w}{\sqrt{Dt}} \cdot \frac{1}{1 + (\frac{T}{t})^\beta} \\ \beta &= 1.5 - \frac{1.0}{\log(\frac{D}{t})} + \frac{3.0}{(\log(\frac{D}{t}))^2} \\ \delta_t &= 0.5 \cdot (T - t) \\ &\quad \text{the eccentricity due to a change in thickness} \\ \delta_m &= \text{the maximum misalignment} \\ \delta_0 &= 0.05 \cdot t \text{ is the misalignment inherent in the } S_N \text{ data and analysis procedure.} \\ L_w &= \text{width of weld at the surface.} \end{aligned}$$

2.8.2. Damping ratio

OWTs are damped structures with a wide range of total damping. The damping ratio (ξ) is expressed as a percentage of critical damping, $c_{crit} = 2 \cdot \sqrt{km}$ with m and k being the modal mass and stiffness, respectively. For WTGs, the damping ratio can range from 1 to 3 per cent for parked turbines and 7 to 10 per cent for those in operation [35]. Five different components are recognized as a sum of the damping ratio:

- Steel material damping (ξ_s)
- Soil damping (ξ_G)
- Hydrodynamic damping (ξ_H)
- Damping due to damping devices (ξ_D)
- Aerodynamic damping (ξ_W)

Due to the larger water depth, the damping of the seawater may have a stronger influence than the study of Malekjafarian et al. indicates. However, this type of analysis is assumed to be out of the scope of this study. Misalignment of wind and wave gives different damping ratios. Passon states, "The effective aerodynamic damping for the hydrodynamic response is reduced in case of misaligned wind and waves. Concerning the rotor orientation and wind direction, this reduction corresponds approximately to the absolute cosine-cubed value of the wind-wave misalignment angle ϕ , i.e. $|\cos^3(\phi)|$ " [39]. Therefore the damping ξ can be calculated as follows:

$$\xi(\alpha_W, \alpha_H) = \begin{cases} \xi_{W,p} & \text{parked condition} \\ \xi_{W,90} + (\xi_{W,0} - \xi_{W,90}) \cdot |\cos(\alpha_W - \alpha_H)|^3 & \text{operational condition} \end{cases} \quad (2.12)$$

Where:

$$\begin{aligned} \alpha_w &= \text{the wind direction.} \\ \alpha_H &= \text{the wave direction.} \\ \xi_{W,90} &= \text{Minimum total damping ratio, } 90^\circ \text{ wind-wave misalignment, taken as 1\%. [35]} \\ \xi_{W,0} &= \text{Maximum total damping ratio, } 0^\circ \text{ wind-wave misalignment, taken as 10\%. [35]} \\ \xi_{W,P} &= \text{total damping ratio in parked condition.} \end{aligned}$$

2.8.3. S-N curves

When a particular material is repeatedly loaded by cyclic stress, it will fail after a certain number of cycles. In fatigue tests, these materials are tested until failure, and the results are visualized in S-N curves. These are graphs where the stress range against the critical number of cycles that produces fatigue failure is plotted for a specific detail. In figure 2.4, an example of fatigue curves is shown for steel material in seawater where cathodic protection is applied, which is the case for the part of the monopile above MSL. DNVGL-RP-C203 describes that curve C2 may be used for grinded cans and curve D may be applied for non-grinded cans where circular welds are applied. Here it can be seen that grinding positively affects the fatigue life of the material around the weld because the stress range may be higher for the same number of cycles. For this thesis, it is assumed that grinding is applied at all welds, i.e. S-N curve C2

is used throughout this research. Also, cathodic protection against seawater is assumed to be sufficient over the lifetime of the structure.

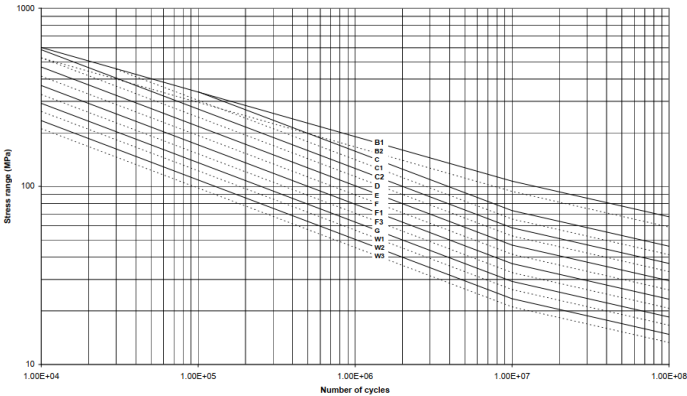


Figure 2.4: S-N curves in seawater with cathodic protection. Source: DNVGL-RP-C203 [14]

3

Structural Model

For the structural model of a WTG combined with a guyed monopile, the Finite Element Method (FEM) is used to determine the static response and modal response. This is built up by using Euler-Bernoulli beam elements over the whole support structure, from the monopile tip to the top where the rotor nacelle assembly is placed. The 2D model is divided into a number of nodes by choosing a certain element size, dz , as shown in figure 3.1. The total amount of nodes becomes then:

$$n = \frac{z_{total}}{dz} + 1 \quad (3.1)$$

The number of beam elements is as follows:

$$n_{elements} = n - 1 \quad (3.2)$$

Where the reference coordinate system has its origin in the center of the monopile at LAT elevation and the z-axis is directed vertically. In this model, only lateral deflections and node rotations are predicted.

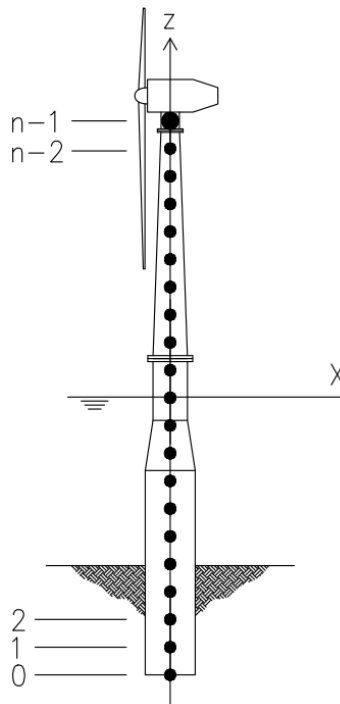


Figure 3.1: Finite-element model for wind turbine generator

3.1. Mass matrix

The mass matrix following from the FEM model is built up consisting of multiple partial matrices: steel structure (\underline{M}_{ss}), RNA (\underline{M}_{RNA}), seawater inside the submerged part of the monopile (\underline{M}_{SWI}) and the added seawater mass outside (\underline{M}_{SWO}) of the 2n degrees of freedom, 2n-DOF system with n nodes. The corresponding force vector is:

$$\underline{Q}_{IN} = \underline{M} \cdot \ddot{\underline{Y}} \quad (3.3)$$

Where:

$$\begin{aligned} \underline{Q}_{IN} &= \text{the 2n inertial force vector} \\ \underline{M} &= \text{the 2nx2n mass matrix } (= \underline{M}_{ss} + \underline{M}_{RNA} + \underline{M}_{SWI} + \underline{M}_{SWO}) \\ \ddot{\underline{Y}} &= \text{the 2n acceleration vector and the second derivative: } \ddot{\underline{Y}} = \frac{d^2 \underline{Y}}{dt^2} \end{aligned}$$

3.1.1. Steel structure

consistent mass matrix of discretized beam monopile and tower

Table 3.1: Structural beam mass matrix

	Column i <i>Unit linear acceleration of node i</i>	Column n+i <i>unit angular acceleration of node i</i>
Row i-1 <i>Inertial force applied to node i-1</i>	$+54/420 \cdot m_{i-1}$	$-13/420 \cdot L_{i-1} \cdot m_{i-1}$
Row i <i>Inertial force applied to node i</i>	$+156/420 \cdot (m_1 + m_{i-1})$	$+22/420 \cdot (L_1 \cdot m_1 - L_{i-1} \cdot m_{i-1})$
Row i+1 <i>Inertial force applied to node i+1</i>	$+54/420 \cdot m_1$	$+13/420 \cdot L_1 \cdot m_1$
Row n+i-1 <i>Inertial moment applied to node i-1</i>	$+13/420 \cdot L_{i-1} \cdot m_{i-1}$	$-3/420 \cdot L_{i-1}^2 \cdot m_{i-1}$
Row n+i <i>Inertial moment applied to node i</i>	$+22/420 \cdot (L_1 \cdot m_1 - L_{i-1} \cdot m_{i-1})$	$+4/420 \cdot (L_1^2 \cdot m_1 + L_{i-1}^2 \cdot m_{i-1})$
Row n+i+1 <i>Inertial moment applied to node i+1</i>	$-13/420 \cdot L_1 \cdot m_1$	$-3/420 \cdot L_1^2 \cdot m_1$

Where:

$$\begin{aligned} m_i &= \text{the mass of the beam element between node i and node i+1.} \\ L_i &= \text{the length of the beam element between node i and node i+1.} \end{aligned}$$

3.1.2. Rotor Nacelle Assembly

The RNA is placed on top of the top node, and the resulting components onto the mass matrix are as follows:

Table 3.2: RNA mass matrix

	Column n-1 <i>Unit linear acceleration of the top node</i>	Column 2n-i <i>unit angular acceleration of the top node</i>
Row n-1 <i>Inertial force applied to the top node</i>	m_{RNA}	$m_{RNA} \cdot (z_{RNA} - z_{n-1})^2$
Row 2n-1 <i>Inertial moment applied to the top node</i>	$m_{RNA} \cdot (z_{RNA} - z_{n-1})^2$	$J_{y, RNA} + m_{RNA} \cdot (z_{RNA} - z_{n-1})^2$

Where:

$$\begin{aligned} m_{RNA} &= \text{the mass of RNA.} \\ z_{RNA} &= \text{the elevation of the RNA centre of gravity.} \\ z_{n-1} &= \text{is the elevation of the tower top flange (node N-1).} \\ J_{y, RNA} &= \text{is the moment of inertia around y-axis of the RNA.} \end{aligned}$$

3.1.3. Seawater

The inertia of the seawater is divided into two components: the seawater inside of the monopile and the seawater outside of the monopile. Both following matrices are lumped and described in table 3.3 and table 3.4:

Table 3.3: Sea water inside monopile mass matrix

	Column i Unit linear acceleration of submerged node i	Column n+i unit angular acceleration of submerged node i
Row n-1 Inertial force applied to submerged node i	$\frac{\rho_w \cdot \pi \cdot d_i^2}{4} \cdot \frac{(z_{i+1} - z_{i-1})}{2}$	0
Row 2n-1 Inertial moment applied to the submerged node i	0	0

Table 3.4: Sea water outside monopile mass matrix

	Column i Unit linear acceleration of submerged node i	Column n+i unit angular acceleration of submerged node i
Row n-1 Inertial force applied to submerged node i	$\frac{C_A \cdot \rho_w \cdot \pi \cdot (D_i^2 + 2t_{MG,i})}{4} \cdot \frac{(z_{i+1} - z_{i-1})}{2}$	0
Row 2n-1 Inertial moment applied to the submerged node i	0	0

Where:

- ρ_w = the density of the (sea) water.
- C_A = the added water mass coefficient (1.0).
- z_i = is the elevation of node i.
- d_i = is the internal diameter of the monopile.
- D_i = is the external diameter of the monopile.

3.2. Stiffness matrix

The total stiffness matrix is the sum of three components: structural stiffness matrix, geotechnical stiffness matrix, and mooring system stiffness matrix, of which the last two are shown in figure 4.1.

$$\underline{Q} = \underline{\underline{K}} \cdot \underline{Y} \quad (3.4)$$

Where:

- \underline{Q} = the 2n corresponding force vector.
- $\underline{\underline{K}}$ = the 2nx2n stiffness matrix.
- \underline{Y} = the 2n displacement vector.

3.2.1. Structural beam stiffness

The structural stiffness of the beam is described as the stiffness following Euler-Bernoulli beam elements. The resulting components of the stiffness matrix are as follows:

Table 3.5: Structural beam stiffness matrix

	Column i <i>Unit linear displacement of node i</i>	Column n+i <i>unit angular displacement of node i</i>
Row i-1 <i>Force applied to node i-1</i>	$-12 \cdot EI_{i-1}/L_{i-1}^3$	$+6 \cdot EI_{i-1}/L_{i-1}^2$
Row i <i>Force applied to node i</i>	$+12 \cdot (EI_i/L_i^3 + EI_{i-1}/L_{i-1}^3)$	$+6 \cdot (EI_i/L_i^2 - EI_{i-1}/L_{i-1}^2)$
Row i+1 <i>Force applied to node i+1</i>	$-12 \cdot EI_i/L_i^3$	$-6 \cdot EI_i/L_i^2$
Row n+i-1 <i>Moment applied to node i-1</i>	$-6 \cdot EI_{i-1}/L_{i-1}^2$	$+2 \cdot EI_{i-1}/L_{i-1}$
Row n+i <i>Moment applied to node i</i>	$+6 \cdot (EI_i/L_i^2 - EI_{i-1}/L_{i-1}^2)$	$+4 \cdot (EI_i/L_i - EI_{i-1}/L_{i-1})$
Row n+i+1 <i>Moment applied to node i+1</i>	$+6 \cdot EI_i/L_i^2$	$+2 \cdot EI_i/L_i$

Where:

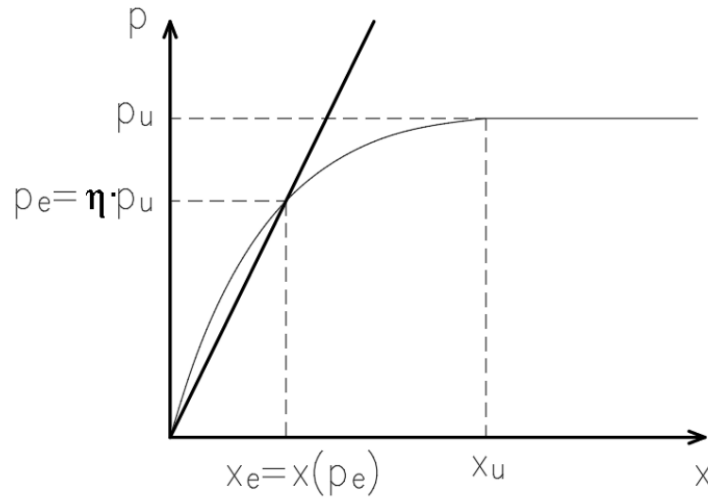
E = Young's modulus.

I_i = the second moment of area of the beam element between node i and node i+1.

L_i = the length of the beam element between node i and node i+1.

3.2.2. Geotechnical stiffness

Beneath the mudline, the nodes of the FEM model are supported by the soil, which is represented as horizontal springs, as can be seen in figure 3.1. The stiffness of each spring is determined according to p-y curves for the soil-pile interaction. These springs are non-linear, and for simplification and faster calculations, this has been linearized according to the p-y method, as shown in figure 3.2.

**Figure 3.2:** Linearization of P-Y model for pile-soil interaction

The soil reaction at a certain depth can be described as following:

$$\frac{\mu \cdot p_u}{x(\mu \cdot p_u)} \cdot dz \quad (3.5)$$

Where:

- p_u = the ultimate lateral pressure of the soil strip at a depth z .
 $x(p)$ = the inverse of the $p(x)$ soil reaction curve function.
 μ = soil linearization factor is defined as the fraction of ultimate pressure at which the linear reaction curve matches the non-linear $p(x)$ curve, which is the point (x_e, p_e) in figure 3.2.

The resulting components of the stiffness matrix are as follows:

Table 3.6: Geotechnical stiffness matrix

	Column n-1 <i>unit linear displacement of buried node i</i>	Column 2n-i <i>unit angular displacement of buried node i</i>
Row n-1 <i>Force applied to buried node i</i>	$\frac{\mu \cdot p_u}{x(\mu \cdot p_u)} \cdot \frac{z_{i+1} - z_{i-1}}{2}$	0
Row 2n-1 <i>Force applied to buried node</i>	0	0

3.2.3. Mooring stiffness

The stiffness of the moorings is calculated as in chapter 4. Then, it is added to the FEM model by supplementing it to the stiffness matrix of equation 3.4, where the translational stiffness of the nodes without moorings is equal to 0:

Table 3.7: Mooring system stiffness matrix

	Column n <i>Unit linear acceleration of mooring node i</i>	Column n+i <i>unit angular acceleration of mooring node i</i>
Row n-1 <i>Inertial force applied to mooring node i</i>	$K_{sys} = \sum k_1, k_2 \dots k_i$	0
Row 2n-1 <i>Inertial moment applied to the mooring node i</i>	0	0

4

Mooring stiffness analysis

In this chapter, the stiffness of a mooring system is determined by analytical modelling. The mooring stiffness is modelled in the structural FEM model as a horizontal linear spring, indicated as K_{sys} in figure 4.1. The spring is applied to the node at the tower and the monopile interface.

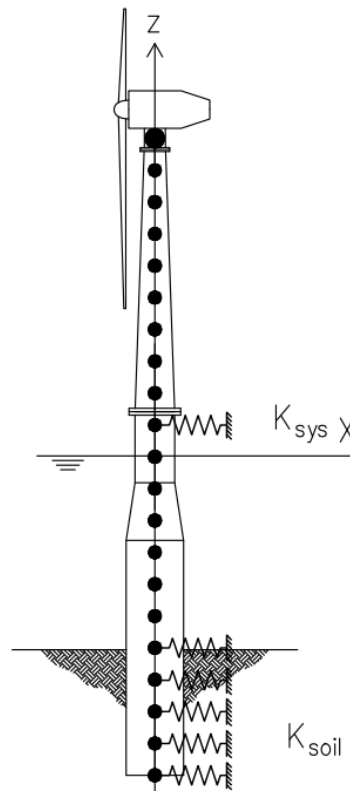


Figure 4.1: Finite-element model for wind turbine generator with added stiffeners

4.1. Mooring Stiffness

It is believed that a high mooring stiffness is necessary for a guyed monopile. Next to that, the weight of the moorings might contribute to a stiffness reduction in the mooring. Therefore, only sagged moorings are assumed in this research, where no part of the mooring is lying on the seabed. Three mooring types are selected for the stiffness analysis, i.e. chain, wire rope, and Dyneema. Ma et al. describes three characteristics that mainly influence the stiffness of a mooring [33]. These are the Minimum Breaking Strength (MBS), the weight of the mooring and the axial stiffness. Values for these characteristics for chains and wire ropes are given as equations for the diameter by Ma et al. These are shown in table 4.1.

Mooring type	MBS (kN)	Submerged weight (N/m)	Axial stiffness (kN)
Chain (stud, R5)	$0.0320 \cdot d^2 \cdot (44 - 0.08 \cdot d)$	$0.187 \cdot d^2$	$101 \cdot d^2$
Wire rope	$0.9 \cdot d^2$	$0.043 \cdot d^2$	$88.7 \cdot d^2$
Dyneema rope	$0.8299 \cdot d^2 - 24.497 \cdot d + 241.58$	$0.0048 \cdot d^2$	$46.844 \cdot d^2 - 1545.7 \cdot d + 24424$

Table 4.1: Equations for mooring type characteristics, source: Ma et al. [33]

For Dyneema rope, similar equations are determined by summarizing the strength tables of the Deeprupe manual [9] and fitting a polynomial curve within the data. This can be seen in figure 4.2. The results of the fitted curves can also be seen in table 4.1.

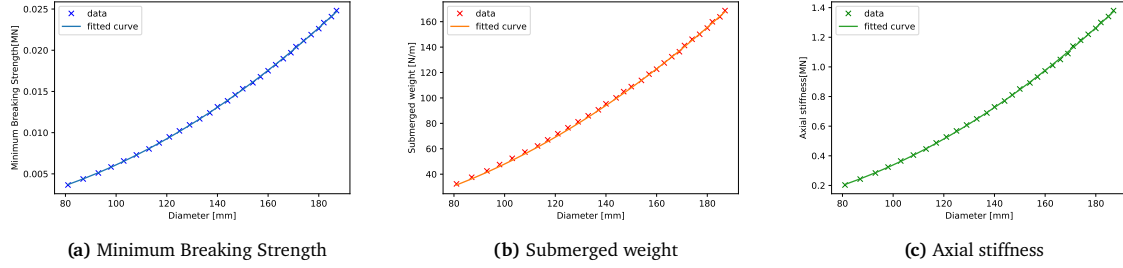


Figure 4.2: Mooring type characteristics for Dyneema rope. [9]

In this research, the stiffness is determined for all three mooring types. 20% pre-tensioning of the MBS is recommended by Ma et al. [33] and Taconis[45], therefore this is taken as a standardized value within the model.

4.1.1. Suspended mooring stiffness

In this research, suspended moorings are assumed, which are lifted off the seabed and no part is lying on the seabed. To calculate the stiffness of such a mooring, the method is used according to Al-Solihat and Nahon [43]. It is assumed that no part of the mooring lies on the seabed for a suspended cable. The parameters for this analysis can be seen in figure 4.3.

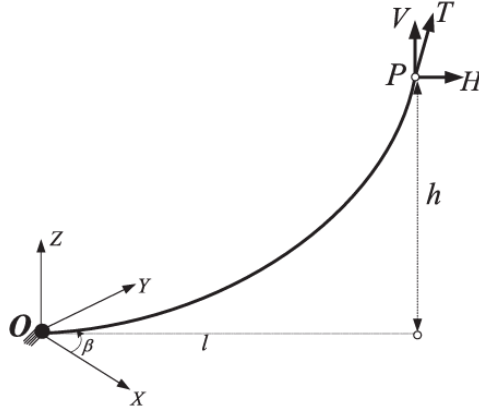


Figure 4.3: Suspended mooring parameters. Source: Al-Solihat and Nahon[43]

The stiffness of such a mooring can be solved numerically as follows:

$$l = (HL/EA) + (H/w)[\sinh^{-1}(V/H) - \sinh^{-1}((V - wL)/H)] \quad (4.1)$$

$$h = (wL^2/EA)[(V/(wL) - 0.5) + (H/w) \times [\sqrt{1 + (V/H)^2} - \sqrt{1 + ((V - wL)/H)^2}]] \quad (4.2)$$

Where,

EA = is the axial stiffness of the mooring
 h = height of the mooring.
 H = horizontal tension component.
 l = horizontal length of the mooring.
 L = unstretched length of the mooring.
 V = vertical tension component.
 w = weight per unit length.

In these equations, the horizontal and vertical components of the tension are unknown. These are solved numerically using Python. The differential equations of equations 4.1 and 4.2 are then expressed in matrix form [43] [50]:

$$\begin{Bmatrix} dl \\ dh \end{Bmatrix} = \begin{bmatrix} \frac{\partial l}{\partial H} & \frac{\partial l}{\partial V} \\ \frac{\partial h}{\partial H} & \frac{\partial h}{\partial V} \end{bmatrix} \begin{Bmatrix} dH \\ dV \end{Bmatrix} \quad (4.3)$$

The derivatives of the mooring profile l and h due to the tension components H and L are then expressed as follows, according to [43]:

$$\frac{\partial l}{\partial H} = \frac{L}{EA} + \frac{1}{w} \left[\sinh^{-1} \left(\frac{V}{H} \right) - \sinh^{-1} \left(\frac{V - wL}{H} \right) \right] + \frac{1}{w} \left[-\frac{V}{\sqrt{H^2 + V^2}} + \frac{V - wL}{\sqrt{H^2 + (V - wL)^2}} \right] \quad (4.4)$$

$$\frac{\partial l}{\partial V} = \frac{\partial h}{\partial H} = \frac{1}{w} \left[\frac{H}{\sqrt{H^2 + V^2}} - \frac{H}{\sqrt{H^2 + (V - wL)^2}} \right] \quad (4.5)$$

$$\frac{\partial h}{\partial V} = \frac{L}{EA} + \frac{1}{w} \left[\frac{V}{\sqrt{H^2 + V^2}} - \frac{V - wL}{\sqrt{H^2 + (V - wL)^2}} \right] \quad (4.6)$$

To obtain the stiffness in the horizontal direction, or in other words, the differential change of H due to a certain change of l . i.e. $\frac{\partial H}{\partial l}$, the stiffness matrix needs to be determined by taking the inverse of the matrix of equation 4.3:

$$\begin{bmatrix} \frac{\partial l}{\partial H} & \frac{\partial l}{\partial V} \\ \frac{\partial h}{\partial H} & \frac{\partial h}{\partial V} \end{bmatrix}^{-1} = \begin{bmatrix} \frac{\partial H}{\partial l} & \frac{\partial H}{\partial h} \\ \frac{\partial V}{\partial l} & \frac{\partial V}{\partial h} \end{bmatrix} \quad (4.7)$$

Solving this matrix gives the differential change in horizontal tension and thus the mooring stiffness.

Marine growth

Marine life will grow onto the moorings after some time. The weight of the mooring will increase due to this phenomenon. As a result, the sag of the mooring will increase, and the stiffness will decrease. The question arises of how big the influence of marine growth on the mooring stiffness is. Therefore the weight of the marine growth is determined. According to DNVGL-RP-C205, the density of marine growth is equal to $\rho_{MG} = 1325 \text{ kg/m}^3$ [15]. The thickness of the marine growth differs over the water depth, as can be seen in table 4.2

Table 4.2: marine growth thickness t_{mg} over the sea water depth

elevation [m]	thickness [mm]	Density[kg/m ³]
0-10	150	1325
>10	100	1325

For simplicity, the thickness over the depth of marine growth is conservatively set at 150 millimeters. The area per unit length of the marine growth will be as follows:

$$A_{MG} = \pi \cdot (t_{mg}^2 + t_{mg} \cdot d) \quad (4.8)$$

Where d_{mo} is the diameter of the mooring. Here, it is assumed that the marine life will grow onto a mooring as a perfect circle. The total unit weight of the mooring due to marine growth is as follows:

$$w_{chain} = w_{chain,0} + \delta w = 0.187 \cdot d^2 + \rho_{mg} \cdot A_{mg} w_{wire} = w_{wire,0} + \delta w = 0.043 \cdot d^2 + \rho_{mg} \cdot A_{mg} \quad (4.9)$$

Where:

- w_{chain} = unit weight of a chain including marine growth.
- w_{wire} = unit weight of a wire including marine growth.
- $w_{chain,0}$ = initial weight per unit length of a chain.
- $w_{wire,0}$ = initial weight per unit length of a wire.
- δw = the extra weight due to marine growth.

Substituting the unit weight of equation 4.9 into the equations of section 4.1.1 gives the mooring stiffness after the presence of marine growth. The influence of the marine growth thickness over time is determined for five chains having different diameters, which can be seen in figure 4.4a. In this figure, the influence on the total stiffness for a growing marine thickness is shown. As can be seen, for chains having diameters of 80 - 200 mm, the mooring stiffness is not affected when the marine growth is growing. However, for chains with a smaller diameter, i.e. 40 mm, the mooring stiffness is affected. The difference in mooring stiffness for chains, steel and Dyneema for varying diameters is shown in figure 4.4b. Here it can be seen that the mooring stiffness does indeed not change for larger diameters. For 40mm moorings, the reduction equals 48%, 69% and 98% for chains, wires, and Dyneema, respectively. This thesis uses only moorings with larger diameters over 100 mm. Therefore, the influence of marine growth on the moorings is neglected.

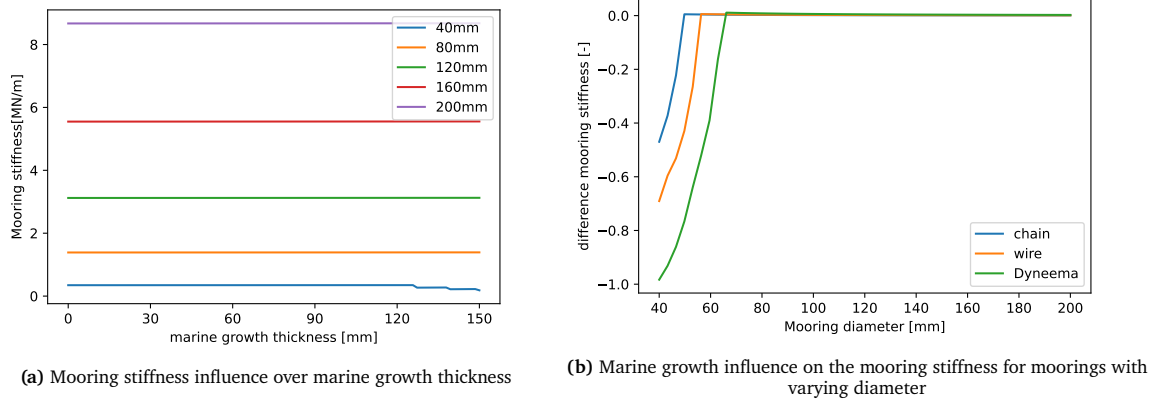


Figure 4.4: Marine growth influence on the mooring stiffness

Comparison mooring type

Chain, steel wire, and Dyneema rope and compared to each other by their stiffnesses. To do this, the stiffness is calculated for a varying diameter according to section 4.1.1. The diameters are chosen between 80mm and 200mm. The mooring characteristics are determined according to table 4.1. The result of the mooring stiffness is shown in figure 4.5

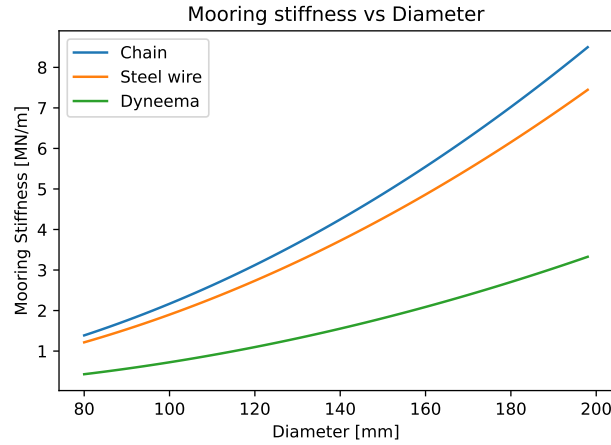


Figure 4.5: Mooring stiffness for varying diameter

As can be seen in the figure, steel chains can provide the largest stiffness for a mooring system, followed by steel wire, and Dyneema provides the least stiffness per diameter of the mooring. However, all three mooring types can provide similar stiffnesses to a guyed monopile and are considered sufficient for application in a guyed monopile. However, for this research, the mooring type is chosen with the largest contributing stiffness and therefore chains are selected.

4.1.2. Mooring sensitivity

The individual stiffness of each mooring is analyzed. To do this, table 4.1 contains the minimum breaking strength, the submerged weight, and the axial stiffness. These parameters highly influence the stiffness of the moorings. In the table, it can be seen that all of these characteristics are dependent on the diameter of the mooring. The stiffness is calculated in section 4.1.1. Here the MBS, submerged weight, and axial stiffness are all implemented in the calculation of the mooring stiffness. Two other parameters influencing the stiffness are the horizontal and the vertical distance between the origin and the endpoint of the mooring, i.e. h and l , respectively. These two depend on the chosen angle between the seabed and the z-axis, as shown in figure 4.6.

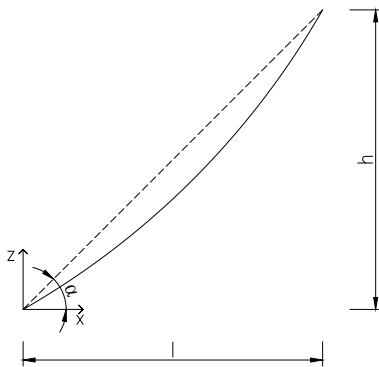


Figure 4.6: Mooring stiffness sensitivity parameters

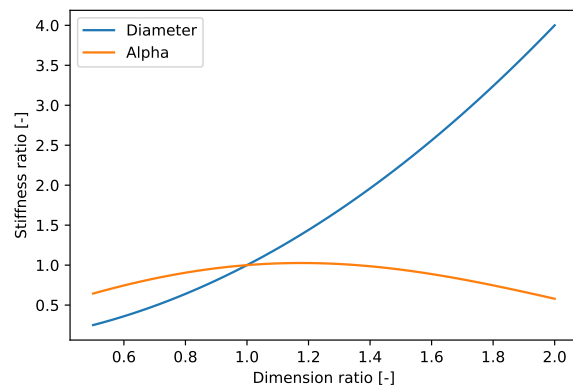


Figure 4.7: Influence of the mooring stiffness

Therefore, the α and the diameter of the mooring are chosen as influence parameters of the stiffness. These mooring characteristics are then compared by taking α of 30° and a chain with a diameter of 100mm as a starting point. Then the angle and the diameter are changed separately to show the influence on the stiffness. The results are plotted on dimensionless axes, given as ratios from the initial design, shown in figure 4.7.

When the seabed angle is decreased, the stiffness also decreases. This makes sense as a lower angle

means that the horizontal length increases, which leads to more material use and also to a higher length and a higher weight of the cable, resulting in a lesser stiffness, according to equations 4.1 and 4.2. When the angle becomes more extensive, it results in higher stiffness, and eventually, it decreases. The ideal α was found at 35° . The mooring stiffness increases exponentially when the diameter increases. Hence, a twice as bigger diameter gives a stiffness four times larger. When a higher stiffness is needed for a GM, it makes more sense to increase the diameter than to increase the horizontal distance of the mooring. The same results were found for a steel wire rope according to table 4.1.

4.2. Anchor stiffness

According to the standards of the American Petroleum Institutes(API), the pinpile is modelled with the use of API RP2Geo. To describe the pile reaction given a horizontal displacement due to the attached mooring, a FEM model is made of the pinpile. The pinpile is divided into Euler-Bernoulli beam elements. The nodes of this model are supported by the soil, which is represented as horizontal springs, as shown in figure 4.8. The FEM model is made the same way as the model is made for the WTG in Chapter 3.

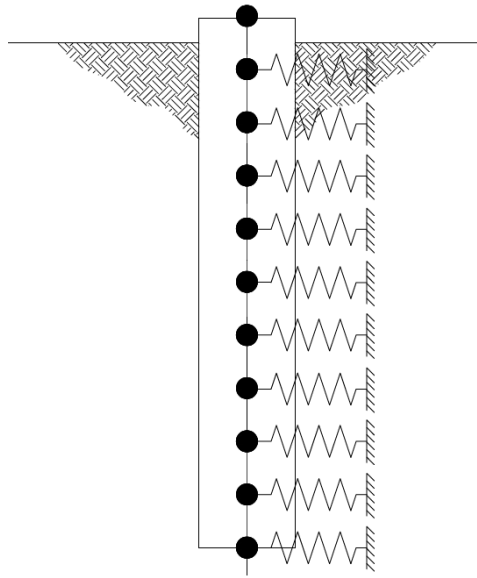


Figure 4.8: Finite-element model of a pinpile

The stiffness of each spring is determined using the p-y method, which means that p-y curves are used for modelling the soil-pile interaction, see section 3.2.2. For simplification, again a uniform soil consisting of sand has been chosen. By applying a certain force at the last node, the resulting reaction forces within the pinpile can be calculated. Thereafter, the displacement is determined and rewritten into the stiffness of one anchor. The results for a 20m long, 1.5m diameter wide pinpile with a thickness of 50mm are shown in figure 4.9.

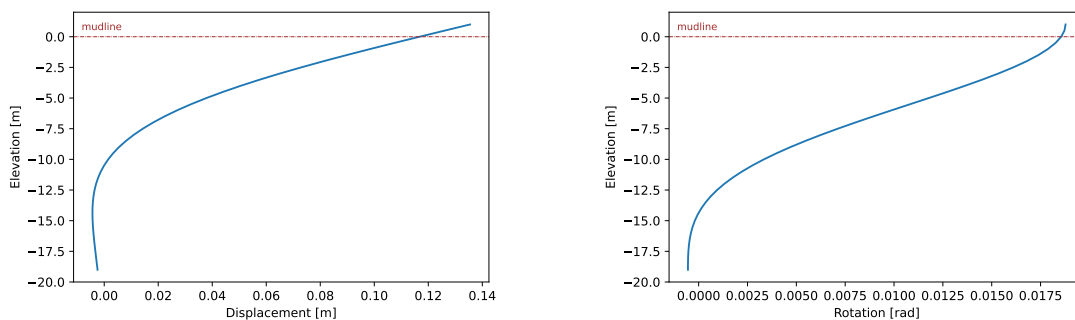


Figure 4.9: Displacement(left) and rotation(right) of a pinpile

The anchor stiffness can then be calculated according to Hooke's law:

$$k_{a,i} = \frac{F_{H,topnode}}{x_{topnode}} \quad (4.10)$$

Where,

$F_{H, top node}$ = Horizontal force in the mooring, in the connection.
 $x_{top node}$ = Horizontal displacement at the connection.

4.3. Monopile stiffness

Due to forces acting perpendicular to the cross-section of the monopile, the cross-section will deform which gives a decrease in the effect of the mooring pretensioning. Therefore, an empirical study has investigated the monopile stiffness following this principle. Ansys has been used to create the part of the monopile where the moorings are attached. An example of the used geometry is shown in figure 4.10. Then, the structure is meshed using 2D shell elements. The top and bottom of the ring are constrained in the y direction and can only move horizontally. On both, the top and bottom of the ring are then a horizontal load is applied. The displacements resulting from these loads are determined and using Hooke's law, the stiffness can be calculated. For the calculation of the monopile stiffness, no stiffening or connection plates are taken into account.

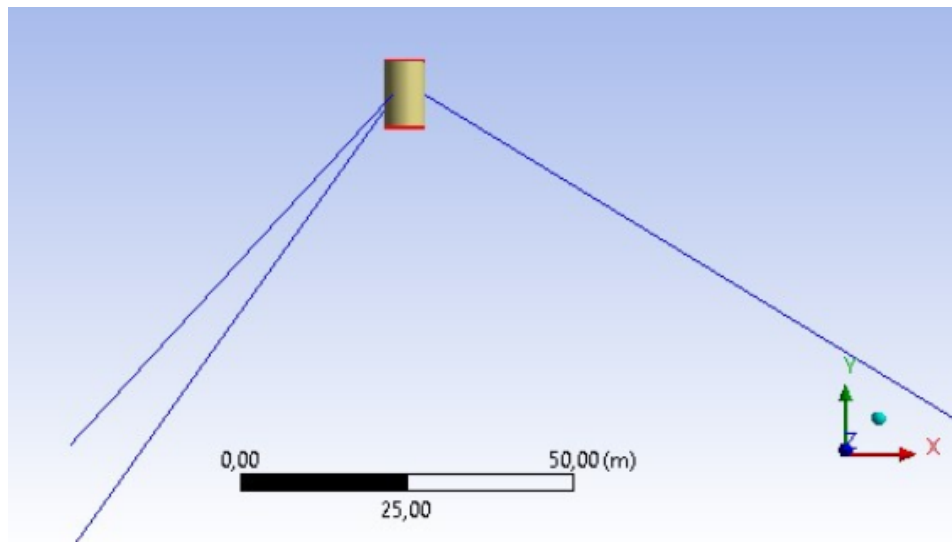


Figure 4.10: Example of monopile ring stiffness analysis for a guyed monopile with 3 moorings

4.3.1. Three mooring layout

This has been repeated using a parametric approach in which the diameter and the thickness of the monopile are changed. The results of this empirical analysis are shown in figure 4.12. In this figure, every blue dot is the result of one iteration.

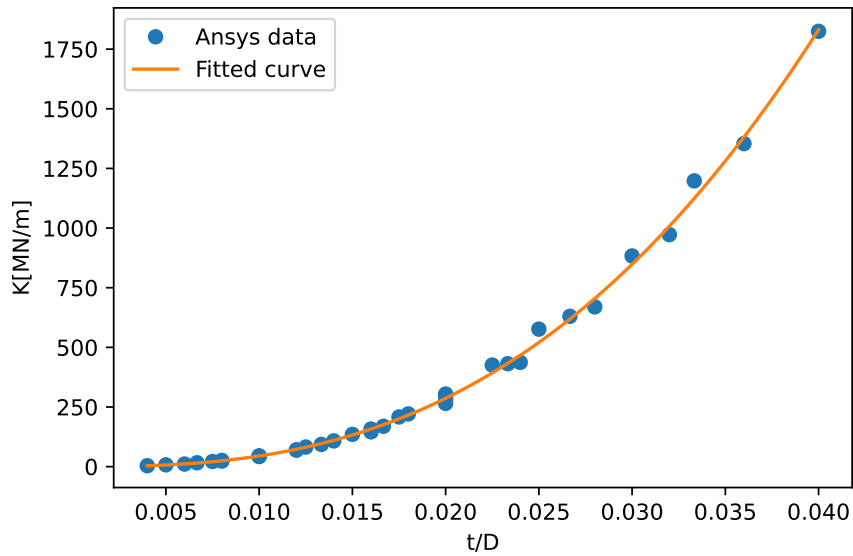


Figure 4.11: Monopile ovalization stiffness for 3 moorings applied

The stiffness of the monopile is then approximated with a fitted curve using Excel. The monopile stiffness is dependent on the ratio between the thickness and diameter of the monopile, as shown in figure 4.12. It can be determined using a power equation:

$$k_m = a \cdot \left(\frac{t}{D}\right)^\alpha \quad (4.11)$$

where:

- k_m = Monopile stiffness
- a = 10085232.47 MN/m
- t/D = ratio between the thickness and the diameter of the monopile
- α = 2.676

4.4. Horizontal spring model

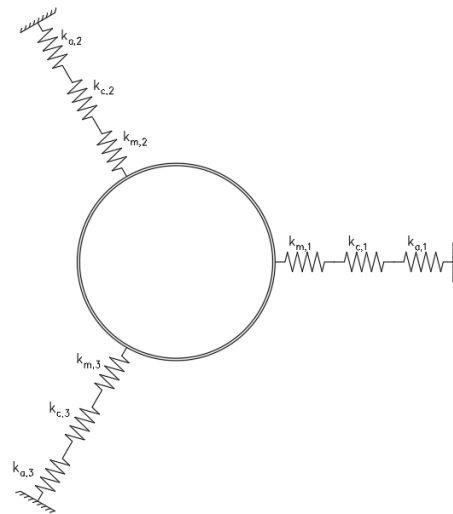


Figure 4.12: Horizontal spring model for a monopile supported by 3 moorings

The resulting stiffness of one mooring is then the resulting stiffness of the three parameters combined: monopile stiffness, mooring stiffness, and anchoring stiffness, as is shown in figure 4.12. As the three parameters work together in a serial spring system, the mooring stiffness can be described as:

$$\frac{1}{k_i} = \frac{1}{k_{m,i}} + \frac{1}{k_{c,i}} + \frac{1}{k_{a,i}} \quad (4.12)$$

Where:

- k_i = stiffness of the three components combined of mooring i
- $k_{m,i}$ = stiffness of the monopile cross-section of mooring i
- $k_{c,i}$ = stiffness of the mooring of mooring i
- $k_{a,i}$ = stiffness of the anchor of mooring i
- i = number of mooring

The total system stiffness of all moorings can be described using the equivalent spring constant for a parallel spring system which acts in the same direction as the displacement due to the resulting loads which are applied:

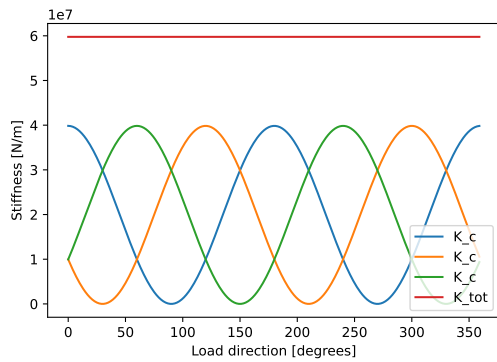
$$K_{sys} = \sum_{i=1} k_i \quad (4.13)$$

Where:

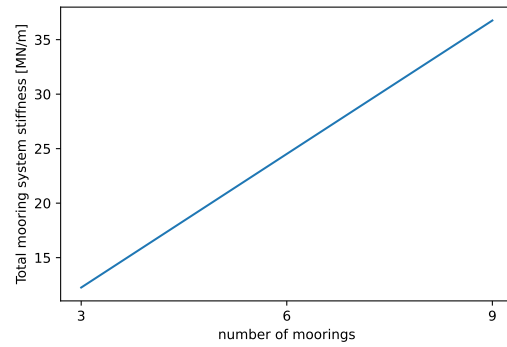
- k_i = stiffness of the three components combined of mooring i.
- i = the number of mooring.

4.5. Conclusions

In figure 4.13a, the stiffness diagram is shown for a varying load direction for a three-moorings system. Here, it can be seen that the stiffness of one mooring depends on the direction of the displacement of the monopile. This is reasonable as a mooring is stretched less when loaded perpendicularly to the geometry of the mooring, and it is stretched more when loaded in a parallel manner. However, the total stiffness of multiple moorings is found to be linear and not changing for different load directions. Therefore, the total system stiffness is independent of the direction of the displacement of the wind turbine. There are two requirements for this behaviour: (1) a minimum of 3 anchors is used, and (2) the moorings are evenly distributed over the cross-section of the monopile. In other words, when three moorings are applied, they are placed at 120-degree angles. If this is not the case and one or multiple moorings have an offset, the total stiffness also has a sinusoidal form.



(a) Total stiffness against the direction of the load for a three-moorings system



(b) The total system stiffness against the number of moorings

Figure 4.13: Conclusions on mooring stiffness analysis

A parametric study on the number of moorings is conducted to show the effect on the total mooring system stiffness. Here, a water depth of 60 meter is assumed and the anchoring stiffness and ovalization

stiffness is set at infinite to find the maximum total stiffness due to the moorings. As the anchoring will be the most expensive, more moorings per anchor will be most beneficial. Hence, three anchors are used throughout this thesis and the number of mooring is a multiple of three. The results are shown in figure 4.13b. Here, it can be seen that the total stiffness has a linear distribution over the number of moorings. Also, the theoretical maximum stiffness is infinite. This is in reality not possible as there is a trade-off between the maximum number of moorings to be feasible to be applied for the attachment between the moorings and the monopile. Therefore, a maximum of nine moorings applied at three anchors is assumed for this thesis. For a 60-meter water depth where chains having a diameter of 200 millimeters are used, this provides a maximum theoretical system stiffness of 35.5 MN/m.

5

Static Analysis

The monopile is designed according to a static and dynamic analysis. In this chapter, the static analysis is determined. First, the static loads that act on the structure are determined in section 5.1. With these loads, the structure's response is calculated in section 5.2, whereof the internal stresses can be established. The stresses are then compared to the resistance of the material in section 5.3. Therefore, Von Mises, column and local buckling checks and a geotechnical check are performed to ensure that failure due to static forces is not occurring.

5.1. Loads

5.1.1. Permanent Loads

The permanent loads can be described by the weight of the RNA, tower, monopile, and marine growth. These are all axial loads onto the structural model. The permanent load vector can be described as follows:

$$\underline{G} = \gamma_{G,1} \cdot (\underline{G}_{RNA} + \underline{G}_{STR}) + \gamma_{G,2} \cdot \underline{B} \quad (5.1)$$

Where:

$\gamma_{G,1}$	=	Partial load factor due to unfavourable permanent loads.
$\gamma_{G,2}$	=	Partial load factor due to favourable permanent loads.
\underline{G}_{RNA}	=	the vector having all components equal to zero except for the last node which is equal to the weight of the RNA.
\underline{G}_{STR}	=	Vector due to the weight of the structural beam elements.
\underline{B}	=	vector due to the buoyancy of the beam elements

5.1.2. Wind load

The ULS wind load of a WTG is provided by WTG manufacturers as if it is a force and a bending moment at the interface between the tower and foundation. This is the static equivalent wind load. These forces are then calculated as if applied at the hub, which is in reality the case. The wind load vector Q_w is a vector filled with zeros except for the components relatable to the hub height:

$$Q_{w,F,hub} = \gamma_w \cdot F_w \quad (5.2)$$

$$Q_{w,M,hub} = \gamma_w \cdot M_w - F_w \cdot (z_{hub} - z_{IFC}) \quad (5.3)$$

Where:

γ_w	=	Partial load factor for wind loads.
F_w	=	Force due to wind load provided by WTG manufacturer.
M_w	=	Bending moment due to wind load provided by WTG manufacturer.
z_{hub}	=	Elevation of the hub.
z_{ifc}	=	elevation of the tower-monopile interface

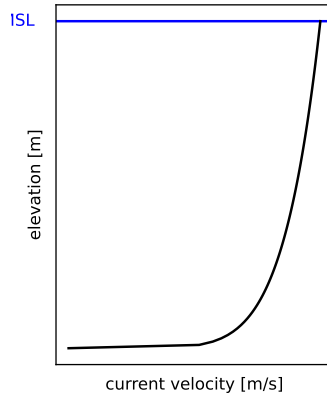


Figure 5.1: Current velocity profile

5.1.3. Hydrodynamic loads

Wave loads

Stream function wave theory is used, according to section 3.2.6 of DNV-GL-RP-C205[15]. Where the wave profile is assessed numerically with a given maximum wave height, its corresponding wave period, and the water depth. The general form of the solution of a stream function wave is as follows:

$$\Psi(x, z) = cz + \sum_{n=1}^N X(n) \sinh nk(z + d) \cos nkx \quad (5.4)$$

Where:

- c = wave celerity ($=\lambda/T$).
- z = the surface elevation, taken as the distance between the still water level and the wave surface.
- x = the horizontal coordinate of the point where the wave is propagating.
- d = the constant water depth.
- N = the order of the wave theory, depending on the steepness and water depth.
- k = the wave number ($=2\pi/\lambda$).
- T = the wave period.
- λ = the wave length.

An example of all stream function wave orders is shown in appendix F.

Currents

The current velocity is modeled with a power law according to §A.9.3 of NEN-EN-ISO 19901-1[1]. In the standard, it is described that the current profile may be described as follows:

$$v_c(z) = v_{c0} \cdot \left(\frac{z + h}{h} \right)^\alpha \quad (5.5)$$

Where:

- $v_c(z)$ = the velocity of a water particle at elevation z .
- v_{c0} = the surface current speed.
- d = the water depth.
- α = the power exponent, taken as $\frac{1}{7}$.

The resulting profile is shown in figure 5.1. The used method is usually taken for shallow waters, however, deeper waters normally require a more thorough analysis of the current profile, which can be done according to long-term measured data sets. For simplification, the shallow water method is used.

The hydrodynamic loads are calculated using the Morison equation as described in section 2.7.2. Here, the water particle acceleration is calculated by the acceleration of the wave. The water particle velocity is calculated by taking the wave and current velocity. The resulting force vector of the wave function is then calculated as follows, having all non-submerged nodes a 0 component:

$$Q_{k,i} = \gamma_H \cdot DAF \cdot F_{tot} \cdot dz \quad (5.6)$$

Where:

- γ_H = Partial load factor for hydrodynamic loads.
- DAF = Dynamic Amplification Factor, as described in section 2.7.1.
- dz = Finite-element step size.

5.2. Static Response

The deflection resulting from a static load \underline{Q} can be determined as follows:

$$\underline{Y} = \underline{K}^{-1} \cdot \underline{Q} \quad (5.7)$$

The internal forces following from the deflection \underline{Y} are as following:

$$\underline{Q}_s = \underline{K}_s \cdot \underline{Y} \quad (5.8)$$

The shear forces and bending moments in the monopile are then calculated as follows:

$$V_i = \sum_{k=i}^{n-1} \underline{Q}_{s,k} \quad (5.9)$$

$$M_i = \sum_{k=i}^{n-1} \underline{Q}_{s,n+k} + \sum_{k=i}^{n+k} \underline{Q}_{s,k} \cdot (z_k - z_i) \quad (5.10)$$

Equations 5.7 - 5.10 are then summarized within the following matrix equation:

$$\underline{IF} = \underline{R} \cdot \underline{Y} \quad (5.11)$$

Where:

- \underline{IF} = the internal force vector.
- \underline{Y} = the displacement vector.
- \underline{R} = Matrix having for i-th column the internal forces vector generated by a unit force applied to the i-th DOF. Each column can be calculated as shown in previous equations.

5.2.1. Internal forces

The axial force can be determined as the sum of all permanent loads as described in equation 5.1.

$$N_i = \sum_{k=i}^{n-1} G_{k,i} \quad (5.12)$$

The shear forces and bending moments resulting from the wind loads are calculated with the static analysis as described in section 5.2. The total shear force and total bending moment vectors are determined by adding the vectors of wind and hydrodynamic loads, resulting from this analysis:

$$\underline{V} = \underline{V}_w + \underline{V}_h \quad (5.13)$$

$$\underline{M} = \underline{M}_w + \underline{M}_h \quad (5.14)$$

5.2.2. Internal stresses

The axial stress can be described as equation 2.2.2 as in DNVGL-RP-C202:

$$\sigma_a(z) = \frac{N(z)}{\pi \cdot D(z) \cdot t(z)} \quad (5.15)$$

Where:

- $N(z)$ = The axial force at elevation z .
- $D(z)$ = The mean diameter of the monopile at elevation z .
- $t(z)$ = The is the monopile thickness at elevation z .

The bending moment stress can be described as equation 2.2.3 as in DNVGL-RP-C202:

$$\sigma_M(z) = \frac{4 \cdot M(z)}{\pi \cdot D(z)^2 \cdot t(z)} \quad (5.16)$$

Where:

- $M(z)$ = The bending moment at elevation z .
- $D(z)$ = The mean diameter of the monopile at elevation z .
- $t(z)$ = The thickness of the monopile at elevation z .

The shear stress can be described as equation 2.2.7 as in DNVGL-RP-C202:

$$\tau(z) = \frac{2 \cdot V(z)}{\pi \cdot D(z) \cdot t(z)} \quad (5.17)$$

Where:

- $V(z)$ = The shear force at elevation z .
- $D(z)$ = The mean diameter of the monopile at elevation z .
- $t(z)$ = The thickness of the monopile at elevation z .

5.3. Requirements

The cross-section of a circular hollow section of a monopile is not stiffened. This means that it needs to be made sure that the elastic buckling strength of the unstiffened circular cylinders is sufficient. These are shell buckling and column buckling. In figure 5.2 the classification of steel cross-sections is shown, according to EC-1993-1-1.


Cross-section part	Type I	Type II	Type III
	$d / t_p \leq 50 \epsilon^2$	$d / t_p \leq 70 \epsilon^2$	$d / t_p \leq 90 \epsilon^2$

Figure 5.2: Cross section class for circular hollow sections. Source: Eurocode 3 EC-1993-1-1[18]

By following the approach of the Eurocode, it is found that the cross sections of monopiles mostly consist of cans having cross sections with type III and type IV, The monopile is therefore checked for its yield strength and buckling, i.e. shell buckling and column buckling [36].

5.3.1. Von Mises

The total occurring stress in a structure must be lower than the yield strength of the steel material to prevent the yielding of the material, This is called the Von Mises stress check. The maximum distortion according to the von Mises criterion is as follows [12]:

$$\sigma_y = \sqrt{(\sigma_a + \sigma_M)^2 + 3 \cdot \tau^2} \quad (5.18)$$

Where:

- σ_a = the axial stress as described in equation 5.15.
- σ_M = the bending moment stress as described in equation 5.16.
- τ = the shear stress as described in equation 5.17

This distortion must be smaller than the steel yield capacity:

$$\sigma_y \leq \frac{f_y}{\gamma_M} \quad (5.19)$$

Where:

- f_y = the characteristic yield stress of the steel.
- γ_M = the material factor, set to 1.1 according to DNVGL-ST-0126 §4.5.1.2.

5.3.2. Local buckling analysis

As stated before, the cross-section is often classified in category 4, especially for guyed monopiles where extra slenderness is introduced. In this cross-section class, local buckling might occur over flexural (column) buckling. Local buckling is also referred to as shell buckling. This is the phenomenon where kinks or creases appear along the wall when the compression inside of the slender monopile wall is too high [2]. Therefore, a shell buckling analysis is performed for every used beam element in the model described in chapter 3. The buckling stress will be compared to the buckling strength. This is firstly done according to §3.4.2 of DNVGL-RP-C202 and afterwards according to Eurocode 1993-1-6.

Shell buckling analysis according to DNVGL-RP-C202

The curvature parameter is as follows:

$$Z_l = \frac{l^2}{r \cdot t} \cdot \sqrt{1 - v^2} \quad (5.20)$$

Where:

- l = shell length.
- r = radius of the monopile (=D/2).
- t = the thickness of the monopile.
- v = the Poisson ratio for steel, taken as 0.3.

The reduced buckling coefficients for axial stress, bending stress, and shear stress are as follows, respectively:

$$C_a = \sqrt{1 + (\rho_a \cdot 0.702 \cdot Z_l)^2} \quad (5.21) \quad C_M = \sqrt{1 + (\rho_M \cdot 0.702 \cdot Z_l)^2} \quad (5.22) \quad C_\tau = 5.34 \cdot \sqrt{1 + (0.09618 \cdot Z_l^{0.75})^2} \quad (5.23)$$

Where:

- ρ_a = $0.5 \cdot (1 + \frac{r}{150 \cdot t})^{-0.5}$.
- ρ_M = $0.5 \cdot (1 + \frac{r}{300 \cdot t})^{-0.5}$.
- r = radius of the monopile (= D/2).
- t = the thickness of the monopile.

The elastic shell buckling strengths for axial stress, bending stress, and shear stress are as follows, respectively:

$$F_{Ea} = C_a \cdot \frac{\pi^2 \cdot E}{12 \cdot (1 - \nu^2)} \cdot \left(\frac{t}{l}\right)^2 \quad F_{EM} = C_M \cdot \frac{\pi^2 \cdot E}{12 \cdot (1 - \nu^2)} \cdot \left(\frac{t}{l}\right)^2 \quad F_{E\tau} = C_\tau \cdot \frac{\pi^2 \cdot E}{12 \cdot (1 - \nu^2)} \cdot \left(\frac{t}{l}\right)^2 \quad (5.24) \quad (5.25) \quad (5.26)$$

Where:

- E = the elasticity modulus of steel, set to 210 GPa.
- ν = the Poisson ratio of steel, set to 0.3.
- t = the thickness of the monopile.
- l = shell length.

The final shell buckling criterion can be defined as:

$$\sigma_y \leq \frac{f_y}{\sqrt{1 + \lambda^4}} \quad (5.27)$$

Where:

- σ_y = yield distortion as described in equation 5.18.
- f_y = the characteristic yield stress of the steel.
- λ = $\sqrt{\frac{f_y}{\sigma_y} \cdot \left(\frac{\sigma_a}{f_{Ea}} + \frac{\sigma_M}{f_{EM}} + \frac{\tau}{f_{E\tau}}\right)}$.
- σ_y = yield distortion according to equation 5.18
- σ_a = axial stress according to equation 5.15
- σ_M = bending moment stress according to equation 5.16
- τ = shear stress according to equation 5.17

Stress-based local buckling analysis according to Eurocode 1993-1-6

Local buckling is also checked by the stress-based method which is described in §8.5.3 of Eurocode 1993-1-6 [19]. As this thesis assumes that two two buckling relevant membrane stress components are present, the interaction check is done as follows:

$$\left(\frac{\sigma_{x,Ed}}{\sigma_{x,Rd}}\right)^{k_x} + k_i \left(\frac{\sigma_{x,Ed}}{\sigma_{x,Rd}}\right) \left(\frac{\sigma_{\theta,Ed}}{\sigma_{\theta,Rd}}\right) + \left(\frac{\sigma_{\theta,Ed}}{\sigma_{\theta,Rd}}\right)^{k_\theta} + \left(\frac{\tau_{x\theta,Ed}}{\tau_{x\theta,Rd}}\right)^{k_\tau} \leq 1 \quad (5.28)$$

Where:

- $\sigma_{x,Ed}$ = the acting meridional buckling stress.
- $\sigma_{\theta,Ed}$ = the acting circumferential buckling stress.
- $\tau_{x\theta,Ed}$ = the acting buckling shear stress.
- $\sigma_{x,Rd}$ = the design meridional buckling stress.
- $\sigma_{\theta,Rd}$ = the design circumferential buckling stress.
- $\tau_{x\theta,Rd}$ = the design buckling shear stress.
- $k_x, k_\theta, k_\tau, k_i$ = buckling interaction parameters.

Monopiles consist of hollow cross-sections that are filled with seawater after the installation of the pile. Therefore, the pressure is equal at both the inside and the outside of the monopile. This results in relatively small stress due to circumferential buckling [25]. As a result, equation 5.28 can be rewritten as follows:

$$\left(\frac{\sigma_{x,Ed}}{\sigma_{x,Rd}}\right)^{k_x} + \left(\frac{\tau_{x\theta,Ed}}{\tau_{x\theta,Rd}}\right)^{k_\tau} \leq 1 \quad (5.29)$$

Where:

- $\sigma_{x,Ed}$ = $\sigma_a + \sigma_M$
the sum of the axial and bending stress as calculated in equations 5.15 and 5.16
- $\tau_{x\theta,Ed}$ = τ
the acting shear stress as calculated in equation 5.17.

Meridional buckling stress

The expressions used for calculating the meridional buckling stress are determined according to Annex D of EC1993-1-6. The meridional elastic imperfection reduction factor is determined as follows:

$$\alpha_x = \frac{0,62}{1 + 1,91 (\Delta w_k/t)^{1,44}} \quad (5.30)$$

where:

$$\begin{aligned} \Delta w_k &= \frac{1}{Q} \sqrt{\frac{F}{t}} \cdot t \\ &\quad \text{the characteristic imperfection amplitude.} \\ Q &= \text{a fabrication quality factor, taken as 25 (Class B).} \\ t &= \text{the thickness of the monopile's wall.} \end{aligned}$$

The plastic limit relative slenderness is then determined as follows:

$$\bar{\lambda}_{px} = \sqrt{\frac{\alpha_x}{1 - \beta}} \quad (5.31)$$

Where:

$$\beta = 0.60, \text{ the plastic range factor.}$$

The relative shell slenderness parameter for meridional buckling of the monopile's cross-section is determined as follows:

$$\bar{\lambda}_x = \sqrt{f_{yk}/\sigma_{x,Rcr}} \quad (5.32)$$

Where:

$$\begin{aligned} \sigma_{x,Rcr} &= 0,605 E C_x \frac{t}{r} \\ &\quad \text{the elastic critical meridional buckling stress.} \\ E &= \text{the elasticity modulus of the steel.} \\ C_x &= \text{taken as 1.0 for medium-length cylinders.} \\ r &= D/2, \text{ the radius of the monopile's cross-section.} \end{aligned}$$

The buckling reduction parameter χ_x is calculated as follows:

$$\begin{aligned} \chi_x &= 1 && \text{if } \bar{\lambda}_x \leq \bar{\lambda}_{x0} \\ \chi_x &= 1 - \beta \left(\frac{\bar{\lambda}_x - \bar{\lambda}_{x0}}{\bar{\lambda}_{px} - \bar{\lambda}_{x0}} \right)^\eta && \text{if } \bar{\lambda}_{x0} < \bar{\lambda}_x < \bar{\lambda}_{px} \\ \chi_x &= \frac{\alpha_x}{\bar{\lambda}_x^2} && \text{if } \bar{\lambda}_{px} \leq \bar{\lambda}_x \end{aligned} \quad (5.33)$$

where:

$$\begin{aligned} \bar{\lambda}_{x0} &= 0.20, \text{ the meridional squash limit slenderness of the monopile's cross-section.} \\ \eta &= 1.0, \text{ an interaction exponent.} \end{aligned}$$

The buckling interaction parameter due to meridional buckling is calculated as follows:

$$k_x = 1.25 + 0.75 \cdot \chi_x \quad (5.34)$$

The design meridional buckling stress is calculated as follows:

$$\sigma_{x,Rd} = \frac{\chi_x \cdot f_{yk}}{\gamma_{m,1}} \quad (5.35)$$

Where:

- χ_x = the buckling reduction parameter.
 f_{yk} = the characteristic design yield strength.
 $\gamma_{m,1}$ = the material factor, taken as 1.1.

Shear stress

A similar approach is used to calculate the shear stress. The expressions used for calculating the shear stress are determined according to Annex D of EC1993-1-6. The plastic limit relative slenderness is then determined as follows:

$$\bar{\lambda}_{p\tau} = \sqrt{\frac{\alpha_\tau}{1 - \beta}} \quad (5.36)$$

Where:

- α_τ = a factor following from the fabrication quality, taken as 0.65 (class B).
 β = 0.60, the plastic range factor.

The relative shell slenderness parameter for shear stress of the monopile's cross-section is determined as follows:

$$\bar{\lambda}_t = \sqrt{\left(f_{yk}/\sqrt{3}\right) / \tau_{x\theta, Rcr}} \quad (5.37)$$

Where:

- $\tau_{x\theta, Rcr}$ = $0,75EC_\tau\sqrt{\frac{1}{\omega}}\left(\frac{t}{r}\right)$
 the elastic critical shear stress.
 ω = $\frac{l}{r}\sqrt{\frac{r}{t}} = \frac{l}{\sqrt{rt}}$
 a dimensionless length parameter.
 E = the elasticity modulus of the steel.
 C_τ = taken as 1.0 for medium-length cylinders.

The shear reduction parameter χ_τ is calculated as follows:

$$\begin{aligned} \chi_\tau &= 1 & \text{if } \bar{\lambda}_\tau \leq \bar{\lambda}_{\tau 0} \\ \chi_\tau &= 1 - \beta \left(\frac{\bar{\lambda}_\tau - \bar{\lambda}_{\tau 0}}{\bar{\lambda}_{p\tau} - \bar{\lambda}_{\tau 0}} \right)^\eta & \text{if } \bar{\lambda}_{\tau 0} < \bar{\lambda}_\tau < \bar{\lambda}_{p\tau} \\ \chi_\tau &= \frac{\alpha_\tau}{\bar{\lambda}_\tau^2} & \text{if } \bar{\lambda}_{p\tau} \leq \bar{\lambda}_\tau \end{aligned} \quad (5.38)$$

where:

- $\bar{\lambda}_{\tau 0}$ = 0.40, the shear squash limit slenderness of the monopile's cross-section.
 η = 1.0, an interaction exponent.

The buckling interaction parameter due to shear stress is calculated as follows:

$$k_\tau = 1.75 + 0.25 \cdot \chi_\tau \quad (5.39)$$

The design shear stress is calculated as follows:

$$\tau_{x\theta, Rd} = \frac{\chi_\tau \cdot f_{yk}}{\sqrt{3} \cdot \gamma_{m,1}} \quad (5.40)$$

Where:

- χ_τ = the buckling reduction parameter.
 $\gamma_{m,1}$ = the material factor, taken as 1.1.

5.3.3. Column buckling analysis

According to Chakrabarti, column buckling (or Euler buckling or flexural Buckling) is a problem for fixed offshore structures consisting of circular hollow sections with large slenderness and axial loads [8]. In this phenomenon, a column deflects and forms an arc-shaped curve[2]. When this deflection grows too large, cracks can start to initiate in the monopile wall. A column buckling analysis is performed to ensure this is not happening.

Buckling length

The first step in this analysis is to determine the effective length. A conventional monopile can be seen as a cantilevered beam as in figure 5.3. Here, the length of the cantilever is equal to the distance between the top of the tower and the mudline and one diameter of the monopile at the mudline, according to DNVGL-RP-C202[13]:

$$L = z_{RNA} - z_{mudline} + D_{mudline} \quad (5.41)$$

Where:

- z_{RNA} = the elevation of the RNA (or top of the tower).
- $z_{mudline}$ = the elevation of the mudline.
- $D_{mudline}$ = the diameter of the monopile at mudline.

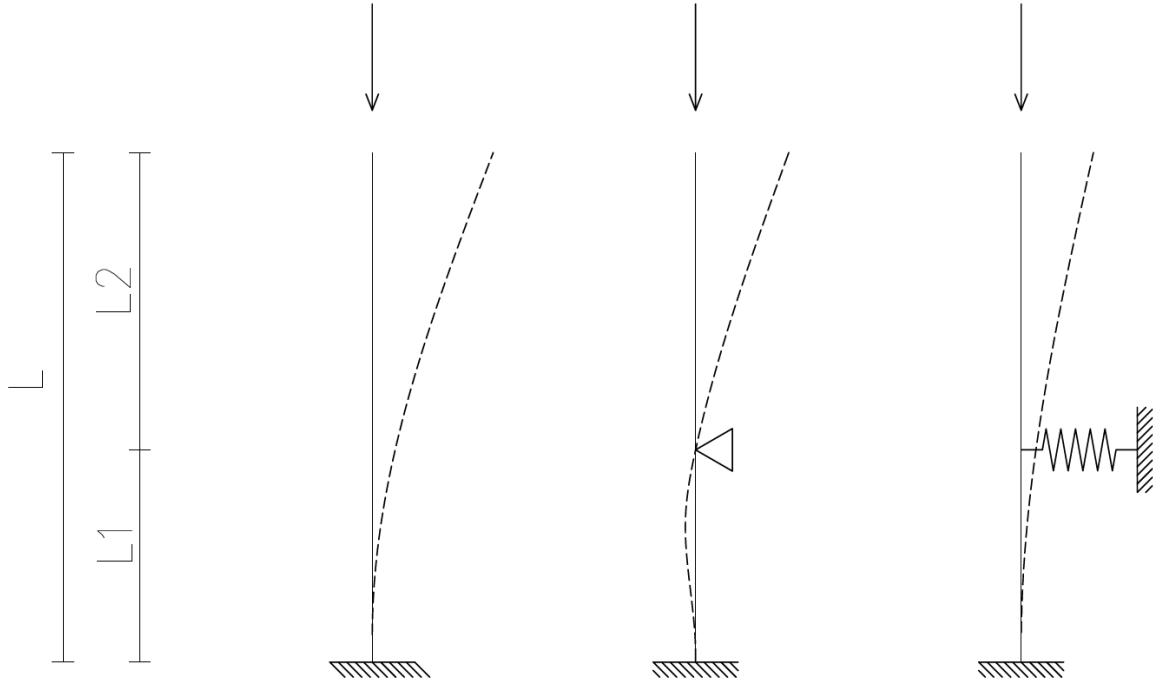


Figure 5.3: Buckling deformations of a cantilever, simply supported cantilever and guyed cantilever

In this case, the effective buckling length is equal to 2 times the cantilever length. For a guyed monopile, it is more complicated due to the range in which the actual effective length will be. Supposing a rather low stiffness gives the same deformation as for the cantilevered beam on the left of figure 5.3. However, supposing an infinite stiffness, the spring support will behave like a hinge where displacement in the horizontal direction is prevented and the beam is free to rotate. In this case, the effective length will be the maximum of the buckling length of the upper part above the mooring attachment or the lower part between the seabed (including one diameter below mudline [13]) and mooring attachment. As both are not the case for a guyed monopile, the actual stiffness will be somewhere in between and the effective buckling length will lie between the two cases. To prevent the occurrence of column buckling, the most conservative case is analyzed, this is when the stiffness is equal to 0 and the WTG is treated as if it is a

cantilevered beam. If the stress does not surpass the buckling strength, then it can also be ensured that column buckling will not occur when the moorings have been applied.

Buckling strength

The Euler buckling strength can be determined according to equation 3.8.3 of DNVGL-RP-C202:

$$f_E = \frac{\pi^2 E i_C^2}{(k L_C)^2} \quad (5.42)$$

Where:

- k = the effective length factor set conservatively to 2 for a guyed monopile, as described in section 5.3.3.
- L_C = total cylinder length, taken as the distance between the top of the monopile and 1 diameter below the mudline.
- i_C = radius of gyration of the monopiles cross-section.
- E = the elasticity modulus of steel.

Because a guyed monopile is an unstiffened shell, the characteristic local buckling strength, f_{ak} , is calculated as follows, according to equations 3.8.8 - 3.8.11 in DNVGL-RP-C202:

$$f_{ak} = \frac{f_{Ea} \cdot f_y}{\sqrt{f_{Ea}^2 + f_y^2}} \quad (5.43)$$

Where:

- f_{Ea} = the axial elastic buckling strength as defined in equation 5.24.
- f_y = the characteristic yield stress of the steel.

The characteristic column buckling strength, f_{kc} , is then calculated as :

$$f_{kc} = [1.0 - 0.28 \bar{\lambda}^2] f_{ak} \quad \text{for } \bar{\lambda} \leq 1.34 \quad (5.44)$$

$$f_{kc} = \frac{0.9}{\bar{\lambda}^2} f_{ak} \quad \text{for } \bar{\lambda} > 1.34 \quad (5.45)$$

Where:

$$\bar{\lambda} = \text{the reduced column slenderness } (= \frac{k \cdot L_c}{\pi \cdot i_c} \cdot \sqrt{\frac{f_{ak}}{E}})$$

The stability requirement for column buckling can then be described as follows:

$$\frac{\sigma_a}{f_{kcd}} + \frac{1}{f_{akd}} \cdot \frac{\sigma_m}{1 - \frac{\sigma_a}{f_E}} \leq 1.0 \quad (5.46)$$

Where:

- f_{akd} = the design local buckling strength ($= f_{ak} / \sigma_M$).
- f_{kcd} = the design column buckling strength ($= f_{kc} / \sigma_M$).
- σ_a = axial stress according to equation 5.15
- σ_M = bending moment stress according to equation 5.16

Buckling strength according to Eurocode 1993-1-1

Following the buckling analysis of the Eurocode [18], for members which are subjected to combined bending and axial compression gives:

$$\frac{N_{Ed}}{\frac{\chi_{y1} N_{Rk}}{\gamma_{M1}}} + k_{zy} \frac{M_{y,Ed} + \Delta M_{y,Ed}}{\frac{\chi_{LT} M_{y,Rk}}{\gamma_{M1}}} + k_{zz} \frac{M_{z,Ed} + \Delta M_{z,Ed}}{\frac{M_{z,Rk}}{\gamma_{M1}}} \leq 0.9 \quad (5.47)$$

$$\frac{N_{Ed}}{\chi_z N_{Rk}} + k_{yy} \frac{M_{y,Ed} + \Delta M_{y,Ed}}{\chi_{LT} M_{y,Rk}} + k_{yz} \frac{M_{z,Ed} + \Delta M_{z,Ed}}{M_{z,Rk}} \leq 0.9 \quad (5.48)$$

Where:

N_{Ed} , $M_{y,Ed}$ and $M_{z,Ed}$	=	the design axial force and bending moments
$\Delta M_{y,Ed}$ and $\Delta M_{z,Ed}$	=	the moments due to the shift of the centroidal axis.
χ_y and χ_z	=	reduction factors due to flexural buckling.
χ_{LT}	=	reduction factors due to lateral torsional buckling.
k_{yy} , k_{yz} , k_{zy} and k_{zz}	=	interaction factors.
N_{Rk}	=	$A_{eff} \cdot f_y$ Characteristic compression resistance.
A_{eff}	=	$\left[\left(\frac{80}{D/t} \right) \left(\frac{275}{f_y} \right) \right]^{0.5} \cdot A$ effective area for class 4 cross-section, according to BS5950-1 [27].
A	=	Cross-sectional area.
$M_{y,Rk}$	=	$W_{el,eff} \cdot f_y$ Characteristic elastic bending moment resistance.
$W_{el,eff}$	=	$\left[\left(\frac{140}{D/t} \right) \left(\frac{275}{f_y} \right) \right]^{0.25} \cdot W$ Effective elastic section modulus for class 4 cross-section according to BS5950-1, according to BS5950-1 [27].
W_{el}	=	elastic section modulus.
D	=	Outer diameter of the monopile's cross-section.
t	=	the thickness of the monopile's wall.
f_y	=	the yield strength of the steel material.

Equations 5.47 and 5.48 are simplified to a single unity check given by the previous equations. This is done because torsion moments are not taken into account ($\chi_{LT} = 1.0$) in this study, and bending moments are assumed to act in one direction, i.e. around the y-axis ($M_{z,Ed} = k_{yz} = k_{zy} = k_{zz} = 0$).

$$\frac{N_{Ed}}{\chi_z N_{Rk}} + k_{yy} \frac{M_{y,Ed}}{M_{y,Rk}} \leq 0.9 \quad (5.49)$$

The reduction factor due to flexural buckling is determined according to §6.3.1 of the Eurocode [18]:

$$\chi = \frac{1}{\Phi + \sqrt{\Phi^2 - \bar{\lambda}^2}} \leq 1.0 \quad (5.50)$$

Where:

Φ	=	$0.5 \cdot [1 + \alpha(\bar{\lambda} - 0.2) + \bar{\lambda}^2]$
$\bar{\lambda}$	=	$\sqrt{\frac{A \cdot f_y}{N_{cr}}}$
α	=	an imperfection factor, according to table 5.1.
N_{cr}	=	$\frac{\pi^2 \cdot EI}{(k \cdot L)^2}$ The elastic critical force for the relevant buckling mode .
k	=	the effective length factor set conservatively to 2 for a guyed monopile, as described in section 5.3.3.

Table 5.1: Imperfection factor α for buckling curve, source: EC1993-1-1 [18]

Buckling curve	a ₀	a	b	c	d
Imperfection factor, α	0.13	0.21	0.34	0.49	0.76

The interaction factor k_{yy} is determined according to Annex A of the Eurocode [18]. This is done according to table A.1, where the elastic cross-sectional properties are class 3 or class 4.

$$C_{my} C_{mLT} \frac{\mu_y}{1 - \frac{N_{Ed}}{N_{cr,y}}} \quad (5.51)$$

Where:

$$\begin{aligned} C_{my} &= 1 - \frac{N_{Ed}}{N_{cr}} \\ C_{mLT} &= 1.0 \\ \mu &= \text{an auxiliary term, as defined in equation 5.52} \end{aligned}$$

$$\mu_y = \frac{1 - \frac{N_{Ed}}{N_{cr,y}}}{1 - \chi_y \frac{N_{Ed}}{N_{cr,y}}} \quad (5.52)$$

5.3.4. Geotechnical capacity check

The soil needs to withstand the forces which are transferred to the ground. This is done by checking the lateral pile capacity of the soil, which needs to be larger than the internal acting forces at the mudline, where these forces and displacements in the buried section of the monopile are the largest. The lateral capacity is calculated according to the conventional statical approach described in chapter 7 of Poulos and Davis [41]. This is done by linearizing the soil resistance over the depth by linear regression of the $p_u(z)$ values. Here, it is assumed that the pile has no deformation. Hence it can be seen as a rigid pile.

$$F_{res} = \int_O^{z_r} p_u \, ddz - \int_{z_r}^L p_u \, ddz \quad (5.53)$$

$$M_{res} = H_u e = - \int_O^{z_r} p_u \, dzdz + \int_{z_r}^L p_u \, dzdz \quad (5.54)$$

The requirement for soil stability is as follows:

$$F_{res} \geq \gamma_{soil} \cdot V_{mud} \quad (5.55)$$

$$M_{res} \geq \gamma_{soil} \cdot M_{mud} \quad (5.56)$$

Where:

$$\begin{aligned} V_{mud} &= \text{the acting shear force at mudline.} \\ M_{mud} &= \text{the acting bending moment at mudline.} \\ \gamma_{soil} &= \text{the soil material factor, taken as 1.15 according to table 7.1 from DNVGL-ST-0126} \end{aligned}$$

6

Dynamic Analysis

As WTGs are mainly subjected to repeated cyclic loading, one of the main governing failure modes is fatigue. In this chapter, a dynamic analysis is conducted. By doing this, the risk of potential failure due to fatigue damage over the lifetime of the WTG is minimized. The damage is derived with a superimposed calculation approach of wind and wave Damage Equivalent Loads (DEL). To do this, the Damage Equivalent bending Moment range (DEM) is determined for every circumferential weld of the monopile. Then the cumulated damage over the structures' design life is calculated by multiplying with the appropriate SCFs, see section 2.8.1. This damage is eventually compared to the S-N curve for this connection type to estimate if the occurring damage does not surpass the fatigue life of the steel material.

6.1. Modal Analysis

The modal analysis is determined by calculating the eigenvalues and corresponding eigenvectors of the matrix $\underline{\underline{M}}^{-1} \cdot \underline{\underline{K}}$. This matrix is determined as follows:

$$\underline{\underline{M}} \cdot \ddot{\underline{Y}} + \underline{\underline{K}} \cdot \underline{Y} = 0 \quad (6.1)$$

Assumed an equation of motion of the form:

$$\underline{Y}_i(t) = \underline{\Phi}_i \cdot e^{j \cdot \omega_i \cdot t} \quad (6.2)$$

Where:

- i = the number of the mode of vibration.
- j = the imaginary unit.
- ω_i = the eigenvalue of the i-th mode of vibration.
- Φ_i = the eigenvector of the i-th mode of vibration.

The first and second time derivatives of equation 6.2 are:

$$\dot{\underline{Y}}_i(t) = j \cdot \omega_i \cdot \underline{\Phi}_i \cdot e^{j \cdot \omega_i \cdot t} \quad (6.3)$$

$$\ddot{\underline{Y}}_i(t) = -\omega_i^2 \cdot \underline{\Phi}_i \cdot e^{j \cdot \omega_i \cdot t} \quad (6.4)$$

Substituting equations 6.2 and 6.4 into equation 6.1 gives:

$$-\underline{\underline{M}} \cdot \omega_i^2 \cdot \underline{\Phi}_i \cdot e^{j \cdot \omega_i \cdot t} + \underline{\underline{K}} \cdot \underline{\Phi}_i \cdot e^{j \cdot \omega_i \cdot t} = 0 \quad (6.5)$$

This can be rewritten as:

$$\underline{\Phi}_i \cdot (\underline{\underline{M}}^{-1} \underline{\underline{K}} - \omega_i^2) = 0 \quad (6.6)$$

Calculating the eigenvalues and corresponding eigenvectors gives the natural frequencies of the guyed monopile.

6.2. Harmonic load response

If the structure is loaded harmonically, the EoM in equation 6.1 becomes as follows:

$$\underline{\underline{M}} \cdot \ddot{\underline{Y}} + \underline{\underline{C}} \cdot \dot{\underline{Y}} + \underline{\underline{K}} \cdot \underline{Y} = \underline{\hat{Q}} \cdot e^{j \cdot \Omega \cdot t} \quad (6.7)$$

Where:

- j = the imaginary unit.
- Ω = the frequency of the harmonic load.
- $\underline{\underline{C}}$ = the damping matrix.
- $\underline{\hat{Q}}$ = the amplitude vector of the harmonic load.

The transient solution of equation 6.7 will quickly damp away, therefore, only the particular solution will be considered. Such solution is:

$$\underline{Y}(t) = \underline{\hat{Y}} \cdot e^{j \cdot \Omega \cdot t} \quad (6.8)$$

Where:

- $\underline{\hat{Y}}$ = the amplitude of the harmonic displacement vector.

The first and second time derivatives of equation 6.8 are:

$$\dot{\underline{Y}}(t) = j \cdot \Omega \cdot \underline{\hat{Y}} \cdot e^{j \cdot \Omega \cdot t} \quad (6.9)$$

$$\ddot{\underline{Y}}(t) = -\Omega^2 \cdot \underline{\hat{Y}} \cdot e^{j \cdot \Omega \cdot t} \quad (6.10)$$

Substituting equations 6.9 and 6.10 into equation 6.7 gives the following:

$$\underline{Y}(t) = (-\Omega^2 \cdot \underline{\underline{M}} + j \cdot \Omega \cdot \underline{\underline{C}} + \underline{\underline{K}})^{-1} \cdot \underline{\hat{Q}} \quad (6.11)$$

Equation 6.11 will be solved in the eigenspace, where the matrices become diagonal and the dynamic system can be seen as a series of decoupled 1DOF harmonic oscillators. Only the contribution of the first h eigenmodes will be considered. The number of relevant eigenmodes is determined case by case by increasing it until a further increase does not produce significant changes in the result. The amplitude of the displacement is therefore calculated as follows:

$$\underline{\hat{Y}} = \sum_{i=0}^{h-1} \frac{\underline{\Phi}_i^T \cdot \underline{\hat{Q}}}{-\Omega^2 \cdot m_i + j \cdot \Omega \cdot c_i + k_i} \cdot \underline{\Phi}_i \quad (6.12)$$

Where:

- m_i = $\underline{\Phi}_i^T \cdot \underline{\underline{M}} \cdot \underline{\Phi}_i$
The generalized mass of the i-th eigenmode.
- k_i = $\underline{\Phi}_i^T \cdot \underline{\underline{K}} \cdot \underline{\Phi}_i$
The generalized stiffness of the i-th eigenmode
- c_i = $\xi \cdot c_{cr,i} = 2 \cdot \xi \cdot m_i \cdot \omega_i$
The damping coefficient of the i-th mode, expresses as the ratio of the critical damping.
- ξ = The damping ratio as described in section 2.8.2.

Solving the displacement vector of equation 6.12 gives the response amplitude. The corresponding internal forces amplitude vector can then be calculated as follows:

$$\underline{IF} = \underline{\underline{R}} \cdot \underline{Y} \quad (6.13)$$

Where:

- \underline{IF} = the internal force amplitude vector.
- \underline{Y} = the displacement amplitude vector.
- $\underline{\underline{R}}$ = Matrix having for i-th column the internal forces vector generated by a unit force applied to the i-th DOF. Each column can be calculated as shown in previous equations.

6.3. Damage equivalent bending moment

The fatigue damage is derived with a superimposed calculation approach where the Damage Equivalent Loads (DEL) are calculated. The combined damage equivalent bending moment range is calculated for both wind and waves at every circumferential weld within the monopile. The weld is checked at 12 points as shown in figure 6.1 of which the fatigue life is checked at both the inside and the outside of the monopile. Based on the weld detail, an S-N curve has been chosen after which the cumulated damage can be calculated and finally, the cumulated damage is then compared with the allowable damage.

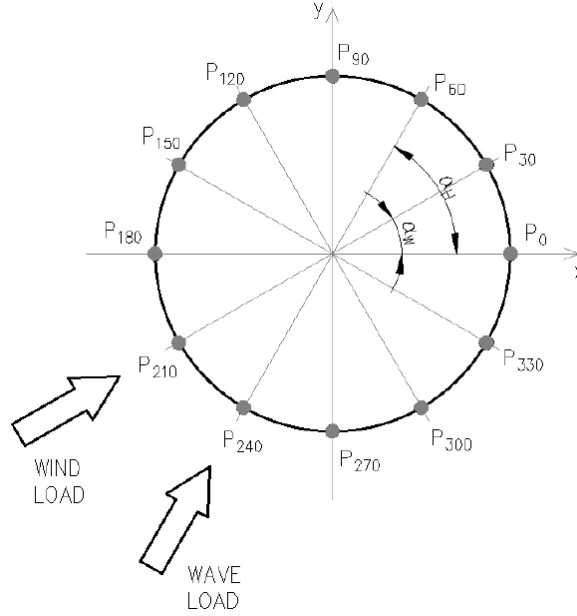


Figure 6.1: Cross section points where the damage is calculated

6.3.1. Damage equivalent bending moment for wind

The damage-equivalent wind loads for each wind direction are typically provided by the WTM and summarized in the BoD in terms of a horizontal force range (ΔF_W), a bending moment range (ΔM_W), the elevation (z_W) at which these loads are applied, the equivalent number of cycles ($n_{eq,W}$), and the inverse slope (m_W) of the (single-sloped) S-N curve used to calculate the DEL loads. Such data is shown in table 6.1.

Table 6.1: DEL data provided by WTM

Wind Direction	0°	30°	60°	90°	120°	150°	180°	210°	240°	270°	300°	330°
Direction probability	$p_{w,0}$	$p_{w,30}$	$p_{w,60}$	$p_{w,90}$	$p_{w,120}$	$p_{w,150}$	$p_{w,180}$	$p_{w,210}$	$p_{w,240}$	$p_{w,270}$	$p_{w,300}$	$p_{w,330}$
Damage equivalent force	$\Delta F_{w,0}$	$\Delta F_{w,30}$	$\Delta F_{w,60}$	$\Delta F_{w,90}$	$\Delta F_{w,120}$	$\Delta F_{w,150}$	$\Delta F_{w,180}$	$\Delta F_{w,210}$	$\Delta F_{w,240}$	$\Delta F_{w,270}$	$\Delta F_{w,300}$	$\Delta F_{w,330}$
Damage equivalent moment	$\Delta M_{w,0}$	$\Delta M_{w,30}$	$\Delta M_{w,60}$	$\Delta M_{w,90}$	$\Delta M_{w,120}$	$\Delta M_{w,150}$	$\Delta M_{w,180}$	$\Delta M_{w,210}$	$\Delta M_{w,240}$	$\Delta M_{w,270}$	$\Delta M_{w,300}$	$\Delta M_{w,330}$

For every wind direction, the loads provided in table 6.1 are then applied to the structural model at the top node of the location of the RNA. The cumulated DEM for wind in each point P_i of figure 6.1 over the elevation of the tower is then calculated with:

$$\Delta \underline{M}_{eq,W}^m(P_i) = \sum_{k=0}^{11} p_{W,k} \cdot \underline{M}_k \cdot |\cos(\alpha_{W,k} - \alpha_i)|^m \quad (6.14)$$

Where:

$\Delta M_{eq,W}^m(P_i)$	=	DEM vector which, when applied n_{eq} times in the O-P direction
\underline{M}_k	=	The bending moment vector from a static analysis as shown in section 5.
$\alpha_{W,k}$	=	The k-th wind direction.
α_i	=	Angular coordinate of the point P_i .
$p_{W,k}$	=	The probability of the k-th wind direction.
m	=	the inverse slope of the S-N curve.

6.3.2. Damage equivalent bending moment for waves

Every particular combination of a sea state (indicated as k), wave direction (indicated as j), and wind direction (indicated as i) gives a different load condition. The total hydrodynamic damage cumulated over the structures' design life is the sum of all these partial load conditions combined, using the wave scatter table provides all the directional sea states. First, the hydrodynamic loads are determined, this is done in the frequency domain. The JONSWAP (Joint North Sea Wave Project) spectrum is used, which is a mathematical model for the distribution of wind-generated ocean waves. An example of a JONSWAP spectrum is shown in figure 6.2. The spectrum describes the relation between the wave frequency and the distribution of energy within the waves. With the spectrum, the maximum amplitude of an Airywave can be calculated as follows:

$$S(f) \cdot \Delta f = \frac{h^2}{2} \quad (6.15)$$

Where:

$S(f)$	=	The energy density as a function of the wave frequency, following from the JONSWAP spectrum.
Δf	=	the constant difference between successive frequencies.
h	=	(H/2) The maximum amplitude of a sin wave.

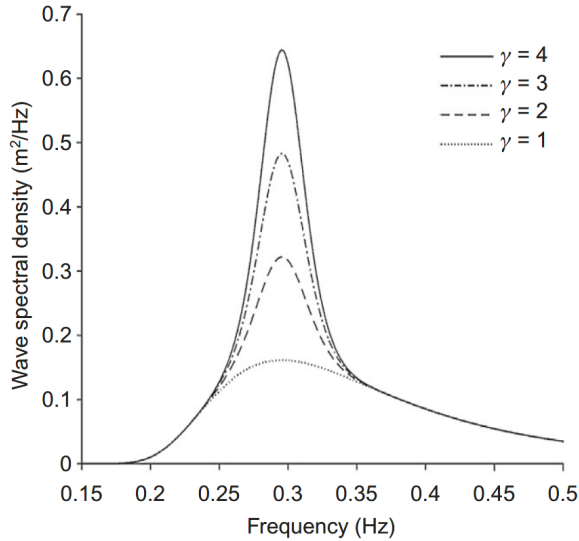


Figure 6.2: Example of a JONSWAP spectrum. Source:Ma et al.[33]

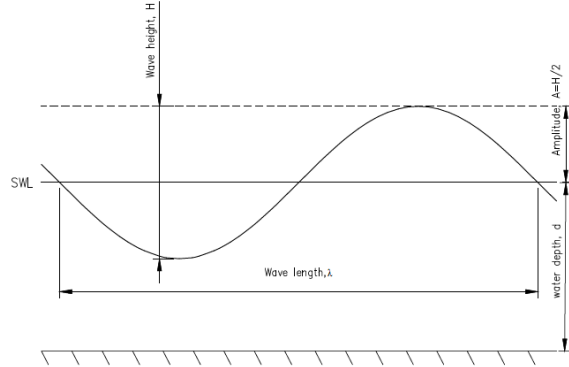


Figure 6.3: Example of an Airy wave

The spectrum is discretized in 1000 equidistant frequencies ranging between 0 Hz and 0.8 Hz. For every discretized frequency, a characteristic wave is modelled with the specific unit wave height according to the linear Airy wave theory, having a characteristic wave period $T_k = \frac{1}{f_k}$, see figure 6.3. The characteristic wave loads Q_k resulting from the theory are as follows:

$$Q_{k,i}(t) = \gamma_H \cdot [F_{d,i}(t) + j \cdot F_{m,i}(t)] \cdot \frac{z_{i+1} - z_{i-1}}{2} \quad (6.16)$$

Where:

γ_H	=	Fatigue load factor (=1)
z_i	=	elevation of the i-th node.
$F_{d,i}(t)$	=	$0.5 \cdot C_d \cdot \rho_W \cdot D_i \cdot v_i(t) \cdot v_i(t) $ Morison's drag force per unit length at depth z_i , due to the unit Airy wave with period T_k .
$F_{m,i}(t)$	=	$0.25 \cdot C_m(D_i) \cdot \pi \cdot D_i^2 \cdot a_i(t)$ Morison's inertia force per unit length at depth z_i and time t , due to the unit Airy wave with period T_k .
j	=	the imaginary unit.
ρ_w	=	the density of the sea water.
D_i	=	the outer diameter of the monopile at depth z_i .
C_d	=	Morison's drag coefficient.
$v_i(t_k)$	=	water velocity at depth z_i and time t_k , due to the unit Airy wave with period T_k .
$C_m(D_i)$	=	Morison's inertia coefficient.
$a_i(t_k)$	=	water acceleration at depth z_i and time t_k , due to the unit Airy wave with period T_k .

For every discretized wave, the corresponding bending moment is calculated using the harmonic load response of the structure as described in 6.2. Then, the moment spectrum, S_M , is obtained. With the moment spectrum, the Damage-Equivalent Moment is calculated by assuming a Rayleigh distribution of the stress ranges according to Barltrop and Adams [5] as follows:

$$\Delta M_{eq}(S_M) = \sqrt{8 \cdot m_0(S_M)} \cdot \sqrt[n_{eq} \cdot T_z(S_M)]{\frac{T_d}{\Gamma(1 + \frac{m}{2})}} \quad (6.17)$$

Where:

$\Delta M_{eq}(S_M)$	=	the DEM corresponding to a specific load condition.
S_m	=	$S \cdot [H_m(\alpha_w, \alpha_H, z)]^2$ Energy density spectrum of the bending moments at elevation z , as a result of a specific load condition (α_W, α_H, z) .
$H_M(\alpha_W, \alpha_H, z)$	=	Bending moment wave transfer function at elevation z , for wind direction α_W and wave direction α_H , as described in equation 6.16
T_d	=	the design life of the structure.
T_z	=	$\sqrt{\frac{m_0}{m_2}}$ zero-crossing period of the signal represented by the S_m spectrum.
n_{eq}	=	reference number of cycles.
m_0	=	variance of the S_m spectrum.
m_2	=	second moment of the S_m spectrum.
$\Gamma(x)$	=	Gamma function.
m	=	the inverse slope of the reference S-N curve.

The total damage due to waves cumulated during the entire lifetime of the structure is the sum of the partial damages produced by each possible load condition. A load condition is a combination of a sea state, wave direction, and wind direction:

$$LC_{i,j,k} = (\alpha_{W,i}, \alpha_{H,j}, S_k) \quad (6.18)$$

Where:

S_k	=	the energy density spectrum of the k-th sea state of the generic $H_s - T_p$ joint probability scatter table.
$\alpha_{H,j}$	=	j-th wave direction.
$\alpha_{W,i}$	=	i-th wind direction.

The total damage equivalent bending moment range due to waves is then expressed as follows:

$$[\Delta M_{eq,H}(z, \beta)]^m = \sum_{i=0}^{11} \sum_{j=0}^{11} \sum_{k=1}^N p_{i,j,k} \cdot [\Delta M_{eq}(\alpha_{W,i}, \alpha_{H,j}, S_k, z) \cdot |\cos(\beta - \alpha_{H,j})|]^m \quad (6.19)$$

$\Delta M_{eq,H}(z, \beta)$	=	The total damage-equivalent bending moment range due to waves.
$\Delta M_{eq}(\alpha_{W,i}, \alpha_{H,j}, S_k, z)$	=	The damage equivalent bending moment range at elevation z due to a specific load condition.
$p_{i,j,k}$	=	the joint probability of wind direction, wave direction, and sea state.
m	=	the inverse slope of the reference S-N curve.
β	=	the angular position of the point of the monopile wall where the damage is calculated.

6.3.3. Total damage equivalent bending moment

The total DEM depends on the simultaneous action between the wind and wave loads over the structure's lifetime. Assuming these are two stochastic processes, the total damage equivalent bending moment can be expressed as follows:

$$\Delta M_{eq}(P_i) = \sqrt{[\Delta M_{eq,wind}(P_i)]^2 + [\Delta M_{eq,wave}(P_i)]^2} \quad (6.20)$$

Where:

$\Delta M_{eq}(P_i)$	=	the total DEM.
$\Delta M_{eq,wind}(P_i)$	=	the total DEM due to wind as in equation 6.14.
$\Delta M_{eq,wave}(P_i)$	=	the total DEM due to wave, as in equation 6.19.

At each weld in the monopile, the damage-equivalent stress range for the inner circumferential weld as well as for the outer circumferential weld is calculated from the total damage-equivalent moment as follows, according to Kühn [31]:

$$\Delta \sigma_{eq,int}(P_i) = SCF \cdot \left(\frac{t}{t_{ref}}\right)^k \cdot \frac{\Delta M_{eq}(P_i)}{W_{int}} \quad (6.21)$$

$$\Delta \sigma_{eq,ext}(P_i) = SCF \cdot \left(\frac{t}{t_{ref}}\right)^k \cdot \frac{\Delta M_{eq}(P_i)}{W_{ext}} \quad (6.22)$$

Where:

SCF	=	Stress Concentration Factor, as described in section 2.8.1.
t	=	wall thickness of the monopile.
t_{ref}	=	reference thickness of 25mm.
k	=	Thickness exponent.
W_{in}	=	Section modulus of the cross-section at the inner surface of the monopile.
W_{out}	=	Section modulus of the cross-section at the outer surface of the monopile.

The cumulated damage is calculated for every point P_i with the maximum damage-equivalent stress:

$$D_{d,ext} = n_{eq} \cdot \frac{\Delta \sigma_{eq,ext}^m}{A_{ext}} \quad (6.23)$$

$$D_{d,int} = n_{eq} \cdot \frac{\Delta \sigma_{eq,int}^m}{A_{int}} \quad (6.24)$$

Where:

$\Delta \sigma_{eq,ext}$	=	the maximum damage-equivalent stress range at the external surface of the monopile.
$\Delta \sigma_{eq,int}$	=	the maximum damage-equivalent stress range at the internal surface of the monopile.
A_{ext}	=	Constant of the S-N curve applicable to the external surface.
A_{int}	=	Constant of the S-N curve applicable to the internal surface.
m	=	the inverse slope of the reference S-N curve.

Finally, the damage for each weld needs to be smaller than the allowed damage to ensure that fatigue failure is not occurring, as follows:

$$UC_{ext} = DFF \cdot D_{d,ext} \quad (6.25)$$

$$UC_{int} = DFF \cdot D_{d,int} \quad (6.26)$$

Where:

DFF = the design fatigue factor, taken as 3 for submerged surfaces.

7

Parametric case study: North Sea

In this chapter, a foundation for a WTG at a specific location is designed by optimizing the conventional monopile and a guyed monopile. This shows the differences between the two foundation methods on the structural - and dynamic response, fatigue damage, and total steel use. This method is repeated for different water depths to visualize the gains that can be made by using guyed monopiles. As this study focuses on deep water, assumed depths of 60, 80, 100, and 120 have been selected. In the chapter, one specific case is described in detail: a conventional monopile and a guyed monopile with six moorings applied for 80 meters of water depth. The results of the calculations made for the conventional monopile and the guyed can be found in appendices A and B, respectively. The case for 80 meters of water depth is described thoroughly, after which the other depths and mooring numbers are repeated.

7.1. Assumptions

First, the made assumptions for this case study are provided. The selected location is the new wind farm Hollandse Kust West (HKW) in front of the Dutch coast of the North Sea, which is planned to operate in 2026. The wind farm will have a total capacity of 2.1GW, according to data from the Dutch government [42]. Wind turbines with a capacity in the range of 14-15MW will be used. The wind farm zone of HKW does not have a water depth of the chosen field. However, this specific location was chosen because a lot of data is available on the Dutch website on the information of the North Sea, called Noordzeeloket. This data is reported and made public by the Netherlands Enterprise Agency. The structure is assumed to be used for 25 years. So that will also be the design life, which is governing the fatigue behaviour of the WTG foundation. Steel grade S355 has been chosen with a Poisson ratio of 0.3 and a modulus of elasticity of 205 GPA. Marine growth, scour, and corrosion are assumed to be out of the scope of this study. The interface between the tower and the monopile is assumed to be 16 meters above MSL to make sure that no waves impact at this elevation.

7.1.1. Wind turbine generator

The wind turbines used at HKW will be large utility-scale wind turbines. Hence, a 15MW reference turbine is chosen of which data is used that has been made available to the public by the International Energy Agency (IEA)[24]. This data has been made available for research purposes. Data of the selected WTG is shown in table 7.1

Table 7.1: Rotor nacelle assembly data, according to the IEA 15MW wind turbine generator[24]

Specification	Symbol	Value	Unit
Nominal Power	P_N	15,0	MW
Cut-in wind speed	V_{CI}	3,0	m/s
Cut-out wind speed	V_{CO}	25,0	m/s
Rotor diameter	D_{rotor}	240	m
Distance hub - tower interface	z_{hub}	4.88	m
x coordinate of the CoG relative to the interface flange	x_{CoG}	3.95	m
y coordinate of the CoG relative to the interface flange	y_{CoG}	0.00	m
z coordinate of the CoG relative to the interface flange	z_{CoG}	3.35	m
Mass RNA	m_{RNA}	1017	t
Moment of inertia RNA about x-axis	$J_{x,RNA}$	10681	tm ²
Moment of inertia RNA about y-axis	$J_{y,RNA}$	122478	tm ²
Moment of inertia RNA about z-axis	$J_{z,RNA}$	10046	tm ²
Minimum rotor angular speed	Ω_{min}	5.0	rpm
Maximum rotor angular speed	Ω_{max}	7.56	rpm

As described by the IEA, the tower of the WTG is assumed to consist of 10 hollow section cans whereof the diameter is tapered over the elevation of the tower. The length and tower wall thickness is taken according to the report of the IEA. The assumed geometry data is shown in table 7.2.

Table 7.2: Tower geometry

Top elevation [m]	Top diameter [m]	Bottom diameter [m]	Length [m]	thickness [mm]	Mass [t]
129.58	6.5	6.572	12.58	24	48.49
117.00	6.572	6.748	13.00	20.83	44.33
104.00	6.748	6.909	13.00	24.01	52.83
91.00	6.909	7.390	13.00	27.21	62.14
78.00	7.390	8.151	13.00	29.10	72.23
65.00	8.151	8.833	13.00	30.71	83.3
52.00	8.833	9.443	13.00	32.19	93.98
39.00	9.443	9.926	13.00	33.78	104.51
26.00	9.926	10.000	13.00	36.46	116.02
13.00	10.000	10.000	13.00	39.50	126.12

7.1.2. Environmental data

In 2020, the Netherlands Enterprise Agency launched a report of a metocean desk study that has been done for the wind farm zone HKW [22]. All site-specific data can be found in the report, therefore it is used as a basis for the environmental data used in this study. It provides detailed information on meteorological and oceanographic conditions. wind and wave scatter tables are used just as current data and significant water levels. The water levels are, in reality ranging between 22 and 32 meters [22]. but as stated before in this study, it is set at 80 meters. In table 7.3, the extreme oceanographic data, including the return periods, are shown.

Table 7.3: Extreme oceanographic data including return period, source: Lohmann, Hunt, and Redanz [32]

Specification	Symbol	1yr	50yr	unit
Significant wave height	H_s	5,60	7,50	m
Peak wave period	T_p	10,30	12,20	s
Extreme wave height	H_{max}	10,50	14,10	m
Period of extreme wave	T_{max}	8,90	10,50	s
Highest sea water level	$HSWL$	2,80	3,50	m
Lowest sea water level	$LSWL$	-0.30	-0.90	m
current velocity at still water level	v_{c0}	1,14	1,26	m/s
Morison's drag coefficient	C_d	1.1	-	
Morison's inertial coefficient	C_m	2.1	-	

Also, the wind and wave scatter tables are obtained from §8.4.3 of the report of the Netherlands Enterprise Agency [22].

7.1.3. Soil characteristics

The soil characteristics are obtained according to another report of the Netherlands Enterprise Agency prepared by geo-engineering company Fugro [23]. The report contains a geological site investigation to provide an overview of the geological ground of the HKW wind farm zone. A soil selection has been extracted from the document. This can be seen in table 7.4.

Table 7.4: Soil characteristics, source: Fugro

Soil type	Thickness, t	Internal angle of friction, ϕ	Elastic Shear modulus G_{max}	Density, γ
Unit:	[m]	[deg]	[MPa]	[kN/m ³]
Sand	1,00	35,0	30,00	20,00
Sand	3,40	36,0	67,50	20,00
Sand	5,30	36,0	67,50	20,00
Sand	1,80	37,5	104,00	20,00
Sand	2,50	35,0	160,00	19,50
Sand	8,80	32,0	120,00	19,50
Sand	4,00	31,0	90,00	19,50
Sand	4,30	31,0	115,00	19,50
Sand	4,10	31,0	95,00	19,50
Sand	6,00	31,5	105,00	19,50
Sand	3,90	33,0	105,00	19,50
Sand	25,00	33,0	155,00	19,50

7.2. Structural design

The foundation for the WTG is both designed using a CM as well as for a GM. The diameters used for the monopiles are shown in figure 7.1. It can be seen that the CM consists of 2 tapered sections to overcome the stiffness. The GM is stiffened using a six-mooring layout. The moorings consist of 200mm chains. The result of this is that it does not need an increase in diameter, i.e. a tapered section. The embedded length is set at 45 meters for the CM and 20 meters for the GM. In figure 7.1b, it can be seen that the total thickness used for all cans is less for the GM.

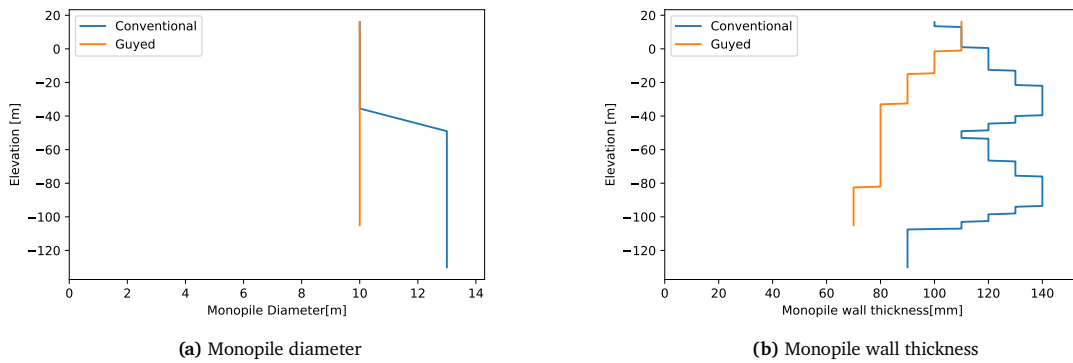


Figure 7.1: Monopile geometry

The mooring system of the GM consists of six chains, having a diameter of 200 millimeters. According to table 4.1, this gives a minimum breaking strength of 35840 kN, a submerged weight of 7480 N/m, and axial stiffness of 4040 MN. The mooring stiffness is as follows, according to chapter 4:

$$K_{moor,i} = \frac{1}{K_{pp}} + \frac{1}{K_{chain}} + \frac{1}{K_{mp}} = 5.09 MN/m \quad (7.1)$$

The pinpiles which are used are 20 meters long and have a diameter of 1.5 meters. The wall thickness that is used is equal to 70 millimeters. The stiffness that the pinpiles provide is equal to 71.3 MN/m. The GM has a thickness of 90 millimeters and a diameter of 7.5 meters at IFC. According to chapter 4 the total mooring system stiffness is then equal to:

$$K_{sys} = \sum_{i=1} k_i = 14.5 \text{ MN/m} \quad (7.2)$$

7.3. Modal Analysis

A modal analysis has been performed for the reference WTG for both the CM and GM and the results are shown in figure 7.2. Here, it can be seen that the first(ω_0) and second(ω_1) natural frequencies of the structure are of importance. The higher-order frequencies are larger and will not interfere with the 1P and 3P frequencies. Hence, these are not significant for the modal analysis. As the first natural frequency lies between the 1P-maximum and 3P-minimum and the second natural frequency is larger than the 3P-maximum, which corresponds with equation 6.6. Therefore, it can be concluded that the monopiles' design is sufficient for the modal analysis.

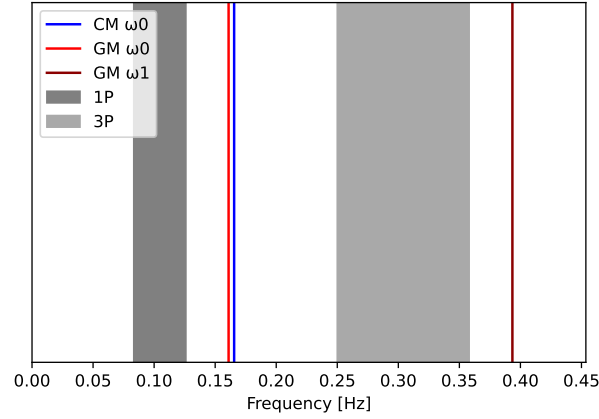


Figure 7.2: 1P and 3P Frequencies check for reference WTG for CM and GM

7.4. Static Analysis

7.4.1. Wind loads

The wind force is hypothetically but realistically taken as can be seen in table 7.5. These loads are calculated as described in chapter 5.

Table 7.5: Wind loads

Load	Symbol	Value	Unit
1 yr gust wind force	F_{wind}	2,00	MN
1 yr gust wind moment	M_{wind}	370	MNm
Elevation of load applied	z_{wind}	16	m

7.4.2. Hydrodynamic loads

The current loads are calculated as described in section 5.1.3. The profile can be given as shown in figure 7.3.

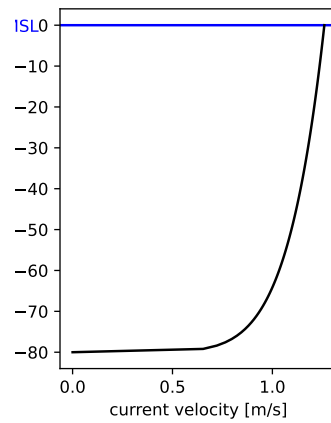


Figure 7.3: Current velocity for 80m water depth

The wave loads are calculated as described in section 5.1.3, by making use of the stream function wave theory with an 11th-order and an extreme wave height of $H_{max,50yr} = 14.1m$ and a corresponding wave period of $T_{max,50yr} = 10.5m$. The applied wave is shown in figure 7.4 and the separate stream function waves of all orders are visualized in appendix F.

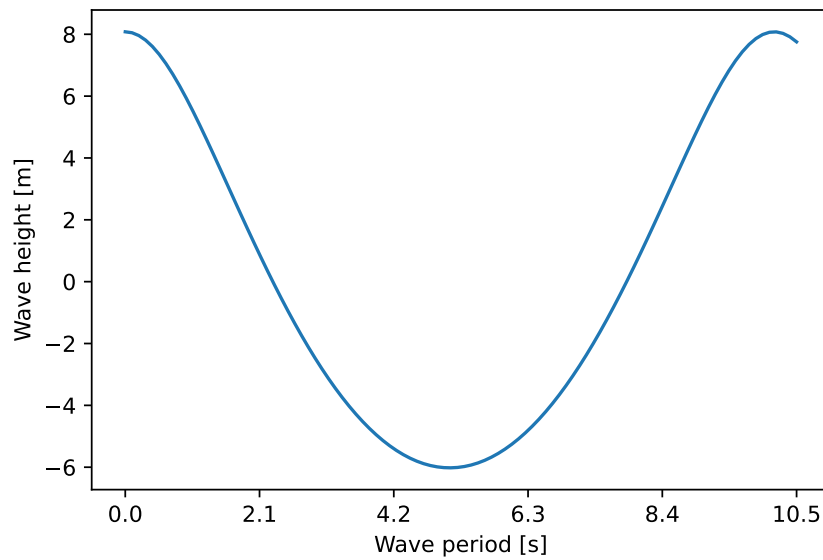


Figure 7.4: Applied stream function wave

The wave is then discretized in 72 steps whereof every different step, the loads onto the system are calculated. The resulting load envelopes are shown in figures 7.5.

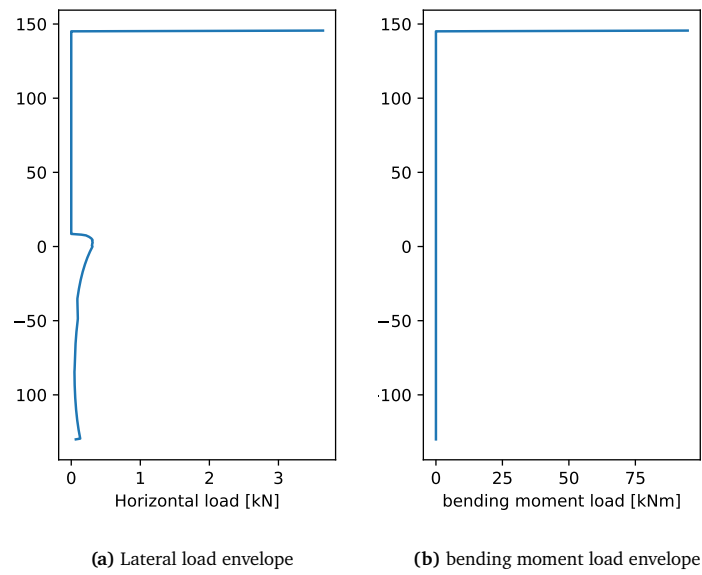


Figure 7.5: Applied static force envelopes

7.4.3. Internal forces

In figure 7.6, the internal shear force and an internal bending moment of the two monopile foundation designs are visualized.

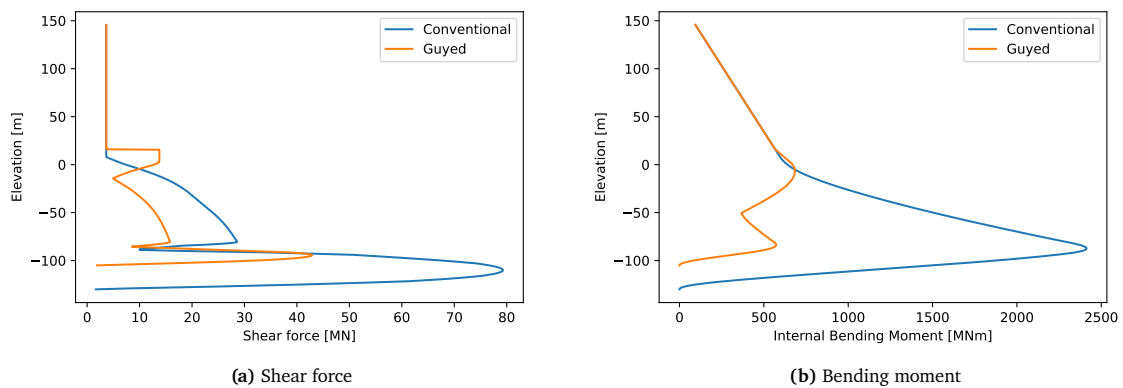


Figure 7.6: Internal forces

As can be seen in the figure, a great reduction of both internal forces is achieved for the GM. Also, the maximum forces at the seabed have experienced a significant reduction. This leads to a significant decrease in the needed embedded length.

7.4.4. Internal stresses

As the cross-section of the guyed monopile is smaller, the stresses in the cross-section are larger. However, as described in the previous section, the internal forces are decreased which leads to a smaller internal stress. The result of the internal stresses, following from a static response analysis as described in chapter 5, gives the internal stresses as shown in figure 7.7, for both the conventional as the guyed monopile.

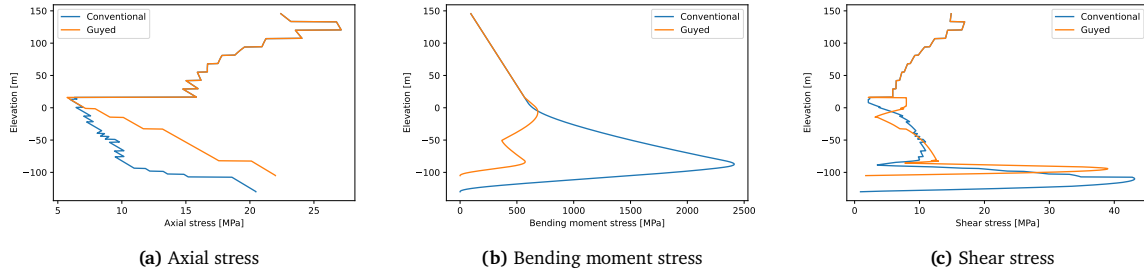


Figure 7.7: Internal Stresses

In figure 7.8, the requirements for the CM and GM are visualized. Maximum utilization is seen beneath the mudline for the conventional monopile. While it is found at the mooring attachment at the interface for the guyed monopile.

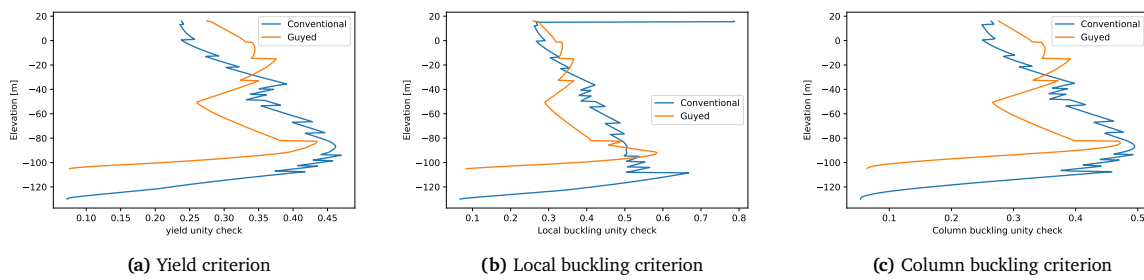


Figure 7.8: Unity Checks

In figure 7.9, the results of the envelope on the unity checks can be seen. Here, it can be seen that for both the CM as GM, the unity checks at all nodes are below 1.0. Consequently, the monopiles are sufficiently designed. Compared to the fatigue design shown in the next section, the utilization of the ULS is rather low. This makes that the ULS requirements are not governing the design steps

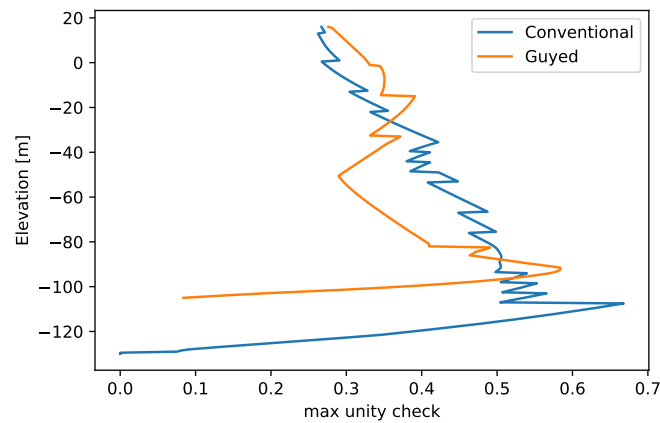


Figure 7.9: Maximum of the criteria of every node

7.5. Dynamic analysis

As stated before, the design life of the WTG foundation is set at 25 years. Therefore, the fatigue design needs to be able to withstand 25 years of forces acting on the structure.

7.5.1. Damage-equivalent loads

The wind damage equivalent loads are taken hypothetically but realistically as can be seen in table 7.6. The DEM loads are applied at the interface between the tower and monopile.

Table 7.6: Assumed DEL data

Wind Direction	0°	30°	60°	90°	120°	150°	180°	210°	240°	270°	300°	330°
Direction probability	6,64%	6,35%	6,42%	6,37%	5,29%	4,97%	7,25%	13,46%	15,20%	11,33%	8,87%	7,84%
Damage equivalent force [MN]	0.36	0.38	0.39	0.38	0.37	0.36	0.36	0.38	0.39	0.38	0.37	0.36
Damage equivalent moment [MNm]	26.52	25.39	24.61	25.09	26.36	27.01	26.52	25.39	24.61	25.09	26.36	27.01

The wave-damage equivalent loads are calculated as described in chapter 6. Given the wave as described in the load. Together with the wave scatter diagrams given by Fery et al. [22], a probabilistic analysis is performed to calculate the total damage-equivalent loads onto the structure.

7.5.2. Damage-equivalent moment

The results of the dynamic analysis can be seen in figure 7.10c. The largest damage equivalent moments are shown due to the wave DEM. This can be concluded due to figures 7.10b and 7.10c, which are similar. This is due to the way the total DEM is calculated, as in equation 6.20. This results in relatively small damage equivalent due to wind. Therefore a small amount of total damage is found. Hence, the wave damage equivalent is governing the monopile design of fatigue, and thus the design of monopiles.

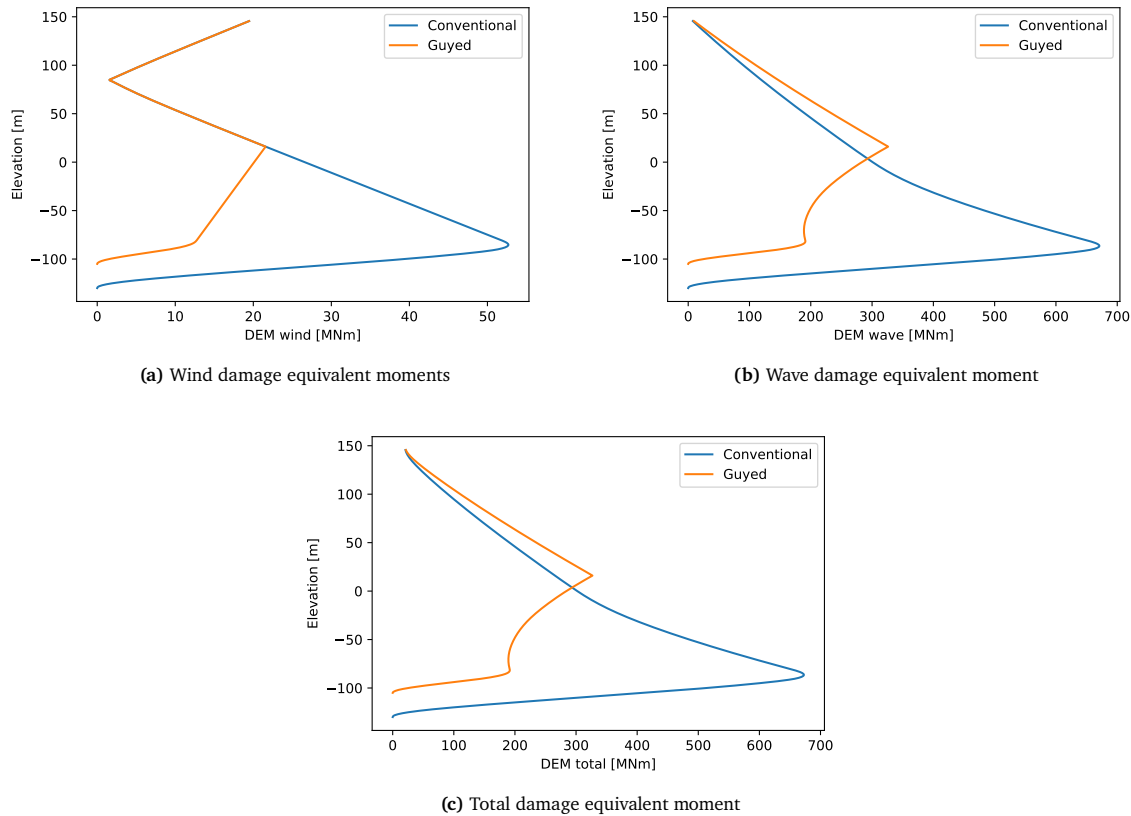


Figure 7.10: Damage equivalent bending moments

7.5.3. Fatigue criteria

Both monopiles are sufficiently designed. Combining the fatigue unity checks with the requirements for ULS gives that the design is highly influenced by the fatigue failure mode. This is also in line with expectations because fatigue will play a higher role when WTGs are placed in deep water. Calculating the total weight of the foundation gives the conventional monopile a total weight of 4610 tonnes. The total foundation weight for the guyed monopile, including pinpiles and moorings, is 2238 tonnes. It can

be concluded that for this specific case, the used model and the made assumptions, the decrease of the total steel used for a guyed monopile, can be halved in comparison to a conventional monopile.

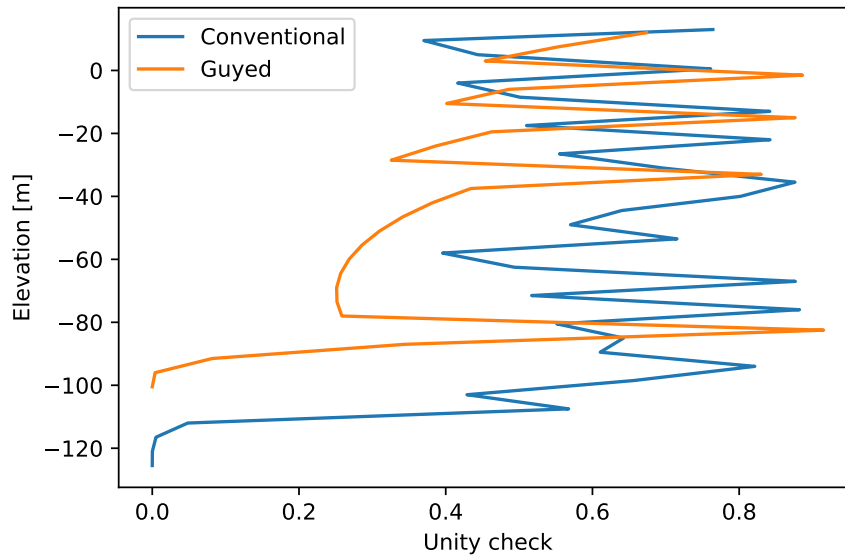


Figure 7.11: Fatigue damage utilization for the conventional and guyed monopile

7.6. Parametric study

The design for the WTG foundation on a CM and a GM as described in the previous section is repeated for varying water depths; 60, 100, and 120 meters, and a varying amount of moorings; 3, 6, 9. By doing this, the effect of the moorings on the total foundation weight is determined. The geometry used for the designs can be found in appendix C. All calculations are made following the same steps as described in the previous section for the 80-meter case. The results of this analysis can be seen in appendix E. The designs are all passing the ULS and FLS criteria. In the results, a maximum ULS utilization of 67%, while the FLS is utilized up to 100%. For every design made, the FLS or resonance were governing the design for both guyed and conventional monopiles. Therefore, it is concluded that the design for monopiles in deep water is not governed by ULS. For deeper waters, the structure is becoming more slender as the length of the monopile increases. As a result, the second natural frequency is decreasing, and eventually, for 120 meters of water depth, the frequency starts to interfere with the 3P frequency of the turbine. All results for the modal analysis are shown in figure D. Here, it is visualized that the resonance criteria are surpassed for all designs below 120 meters. The designs for the conventional and guyed monopiles in 120-meter water depth are, however, not sufficiently designed for the modal analysis. A way to overcome this is to add or subtract the mass of the structure to decrease or increase the second natural frequency. However, after multiple iterations, the second natural frequency constantly interferes with the 3P frequency. Another way to overcome this is to increase the damping of the structure or avoid the specific frequencies by tweaking the angular speed of the wind turbine generator. However, certain analysis is assumed to be out of scope for this thesis. Therefore, it is concluded that resonance issues occur when approaching deeper waters larger than 100 meters. The total foundation weight is calculated for all different designs. The result of this analysis is shown in figure 7.12. In the figure, the amount of mooring is indicated using GM_i , where i stands for the number of moorings that have been used in the design.

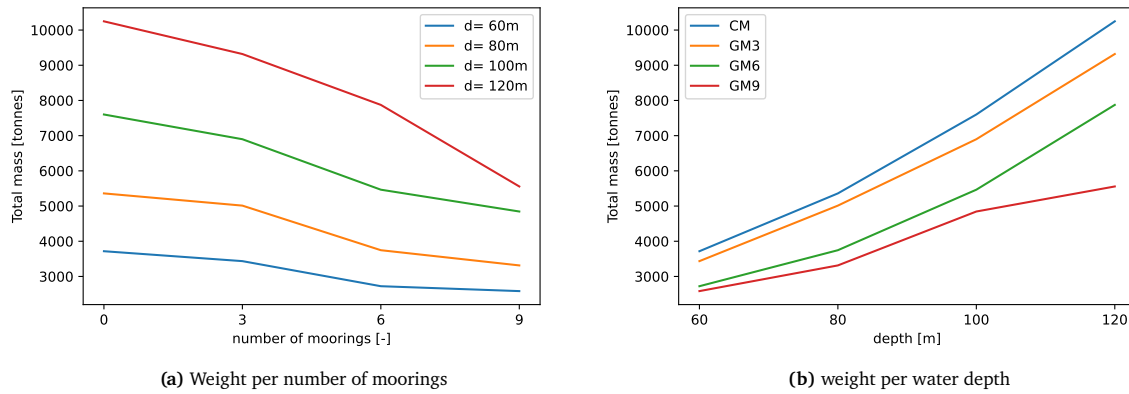


Figure 7.12: Total foundation mass resulting from the parametric study

For every water depth, there is a number of moorings that gives such stiffness that a tapered section is not necessary anymore. Applying moorings, therefore, gives great benefits for application in larger water depths. The total weight can be reduced up to 45% when a guyed monopile having 9 moorings is used instead of a conventional monopile. Applying a guyed monopile with a lower number of moorings gives less benefit in deeper waters. The same applies to a GM9 over a GM6 for relatively smaller water depths. Therefore, it can be concluded that for every water depth the mooring system has to be chosen such that the mooring stiffness is great enough to provide the stability which is necessary for the structure. The total weight of the foundation structure is mainly governed by the weight of the monopile. This total weight exponentially increases over the depth when a CM is used. The weight of the moorings also increases exponentially for an increasing water depth. However, the share of the total foundation weight is significantly smaller in comparison to the monopile. For a GM, only moorings can be used to provide the needed stiffness necessary to overcome the growing water depth. The monopile only has to be extended to overcome the extra depth, which gives a linear weight. Therefore, the guyed monopile has a more linear distribution over the water depth.

8

Ansys validation

To make sure that the structural model made in chapter 3 is correct, the finite element model is recreated in Ansys Workbench. An 80-meter GM foundation is built in the software by using a 3D model with 2D beam elements. The model is based on the case study of chapter 7.6, having the same assumptions made in the case study. The validation is based on 4 different aspects: Internal forces, deformation, natural frequencies, and harmonic response.

8.1. Geometry

First, the geometry of the whole structure is modelled, as shown in figure 8.1. In the numerical model, tapered cans have been applied. However, this is not possible in Ansys. Therefore, the Ansys model contains cans consisting of the averaged diameter between the top and bottom can diameter. By doing this, the weight of the tower is exactly similar to the numerical model. On top of the structure, the weight of the RNA is modelled as an added mass of 1017 tonnes, as described for the reference turbine of the IEA [24]. The Center of Gravity (CoG) of the RNA is not exactly located above the centre of the tower. The added mass has an offset that is equal to the numerical model, given in table 7.1. The sea has been modelled using an ocean environment within the offshore component of Ansys. Ansys's component allows it to select a specific water depth and model the current characteristics. Also, a wave theory can be selected to create the wave forces onto the structure according to the stream function wave theory as used in the case study. The added mass following from the water around the can also be selected within the environment.

8.2. Supports

The moorings are modelled as springs, as shown in figure 8.2. These springs have the same stiffness as follows out of the mooring stiffness analysis. Therefore, the same stiffness is provided as in the numerical model. The other support component is the soil. For simplification of the model, rigid soil has been used. In the numerical model, this is done by applying infinitely stiff soil, or $k = \infty$, for every node beneath the mudline. In Ansys, this is done by modelling clamped supports at all nodes beneath the mudline.

8.3. Modal analysis

A modal analysis is performed in Ansys for the structure as described above. The resulting natural frequencies of both the numerical and the

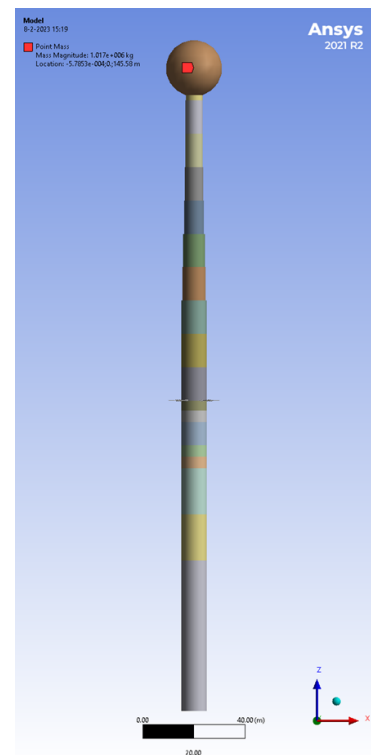


Figure 8.1: Geometry of the beam model in Ansys

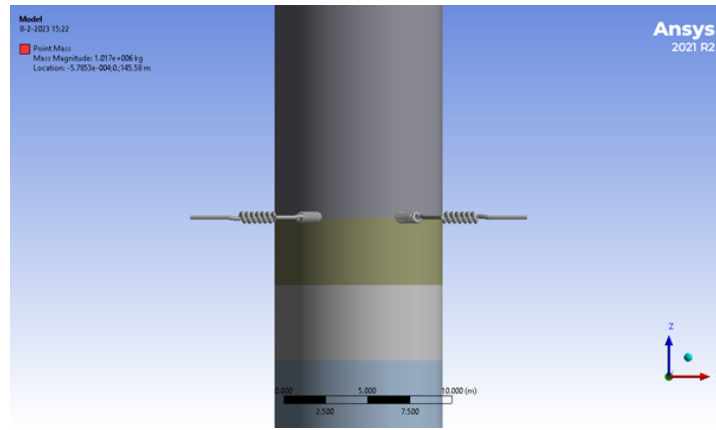


Figure 8.2: Springs representing the moorings

Ansys models can be seen in table 8.1. The results are similar. However, slight differences can be seen. As the Ansys model is a 3D model, the modal analysis gives results in both x and y directions, while the numerical model is a 2D model where the results can only be found around the y-axis (in the x-direction). As can be seen, the results for the first and second-order eigenfrequencies are similar. There is a slight difference between the two directions in which the 3D model deforms. This difference can be explained by the differences in CoG for the two directions. For a higher order of natural frequency, the divergence grows. This may be due to the non-tapered sections of the tower for the Ansys model, where the beam elements of the tower in the numerical model are tapered. The first two natural frequencies are mainly important for the structure as they lie within the 1P and 3P frequencies of the WTG. As these divergences are rather small, the modal analysis done for the structure is assumed to be justified. In figure 8.3, the deformed shapes of the first, second and third natural frequencies are shown,

Table 8.1: Natural frequencies Ansys vs. numerical model

Natural frequency	Ansys	Numerical model
First, around x-axis [Hz]	0.1778	-
First, around y-axis [Hz]	0.1787	0.1785
Second, around x-axis [Hz]	0.6167	-
Second, around y-axis [Hz]	0.6263	0.6216
Third, around x-axis [Hz]	1.4258	-
Third, around y-axis [Hz]	1.6524	1.4641

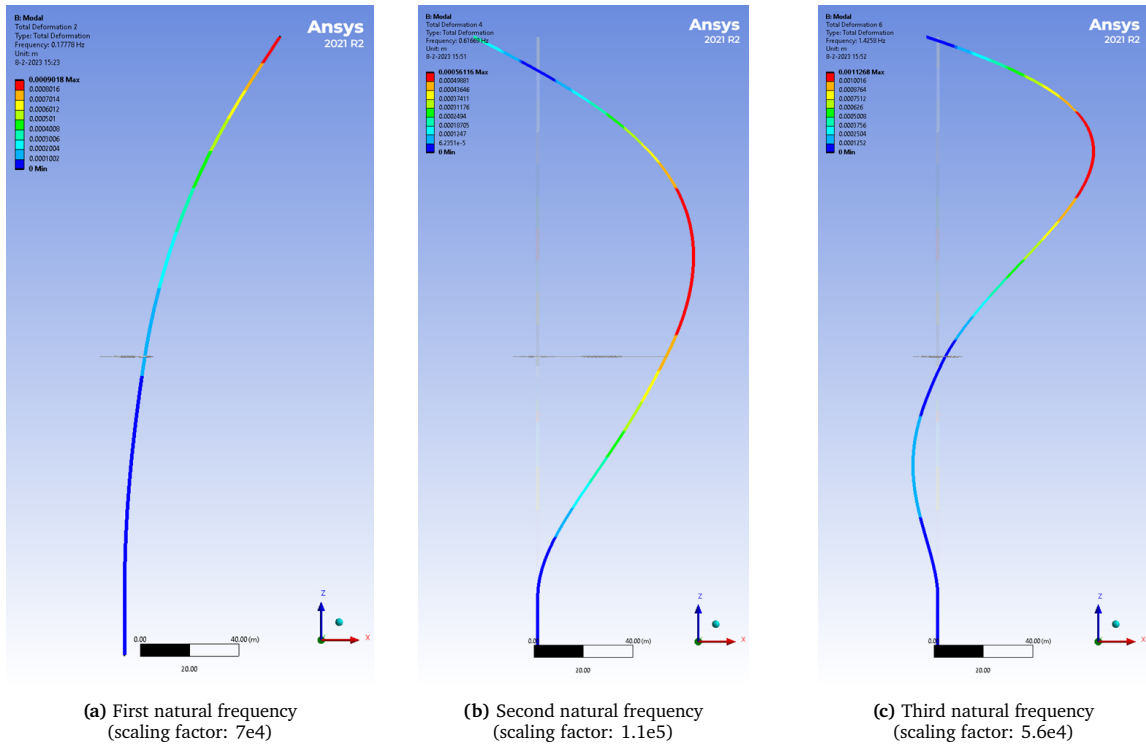


Figure 8.3: Modal analysis results from Ansys

8.4. Static analysis

As stated before, in the ocean environment used in Ansys the current forces are modelled by applying a current velocity to the structure. Here, the current also has a non-linear distribution over the depth of the seawater. Where the velocity at the surface is equal to the value used in the numerical model. Within the ocean environment, a wave load is also calculated based on the stream function theory to the 11th order. The wind force is modelled as a horizontal force, and a bending moment is applied at the tip of the tower (or the top node of the model), where the RNA is located as a point mass. For these loads, a static analysis is performed. The results of this analysis of both the numerical and the Ansys models can be seen in figure 8.4. The result of the deformed Ansys model can be seen in figure 8.5. The results are quite similar. However, the shear stress found at the mudline is for the numerical model larger than for the Ansys model. This is due to the modelling of the soil as springs, where the number chosen to model the stiffness is not high enough. Consequently, the resulting internal shear force is larger and to a smaller extent also, the bending moment at the mudline is increased in comparison to the Ansys model. However, as the rest of the results are similar, and the numerical model gives more conservative results, it is assumed that this behaviour is neglected. Lastly, the deformation due to the static analysis is compared, shown in figure 8.6a. Here, no relevant differences are seen. Therefore, the static analysis of the numerical model is assumed to be justified.

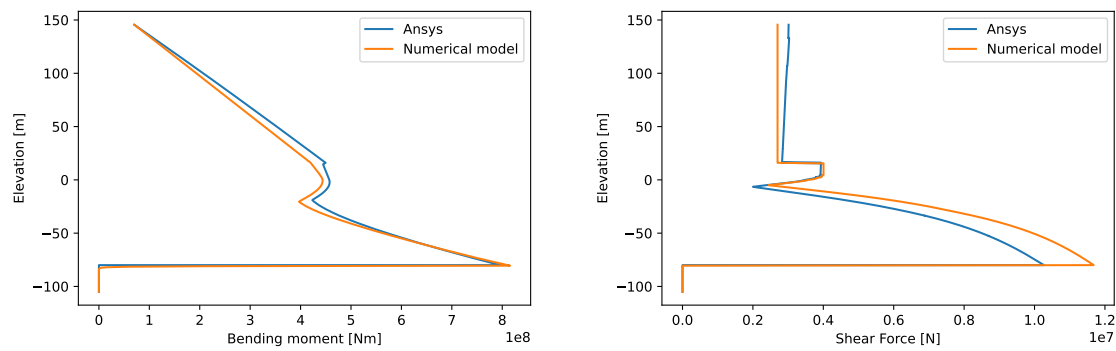
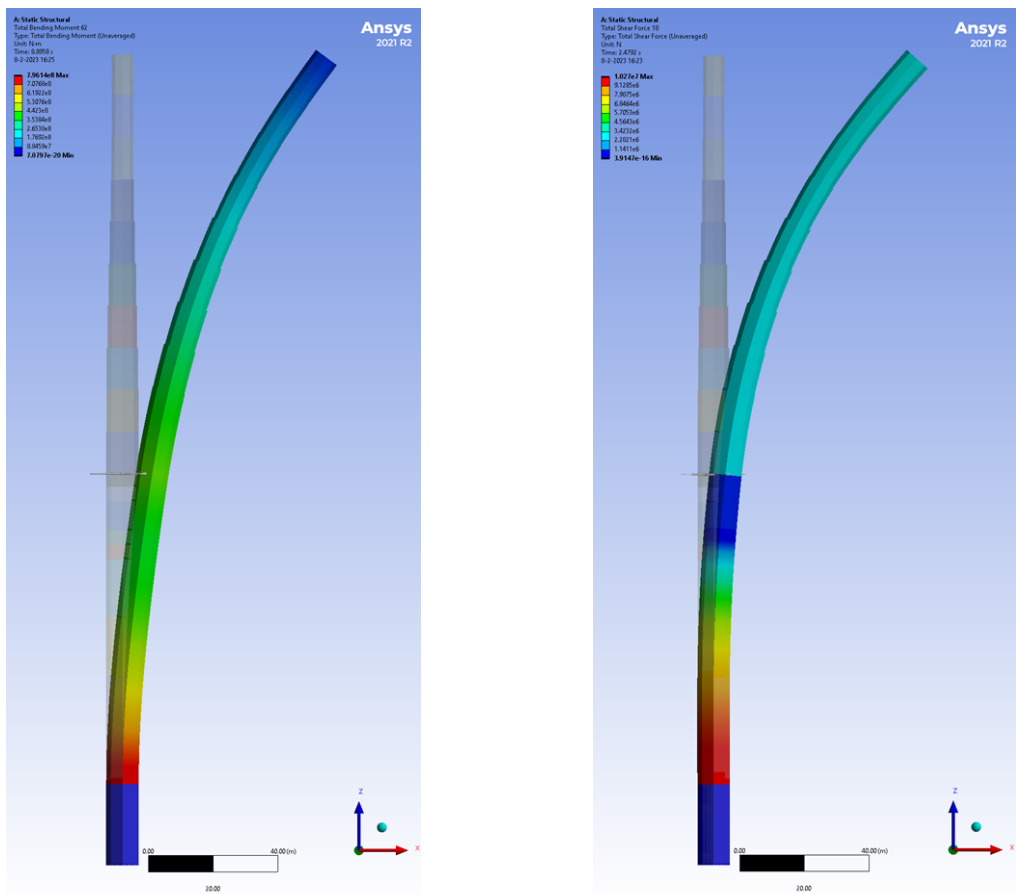


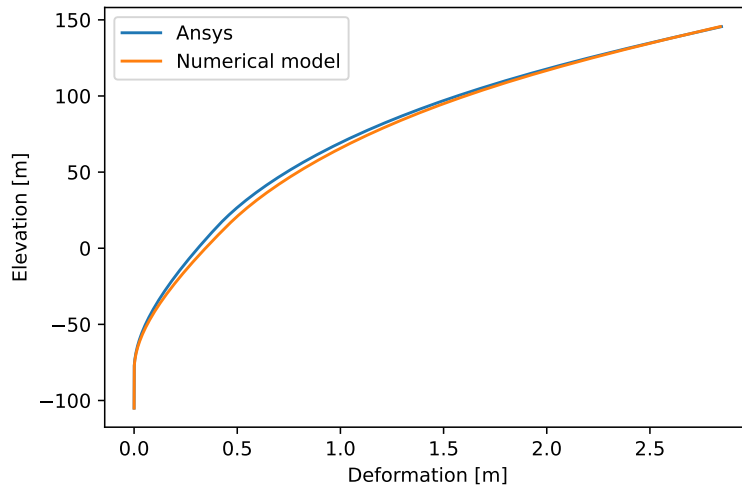
Figure 8.4: Comparison internal forces: bending moment (left) and shear force (right)



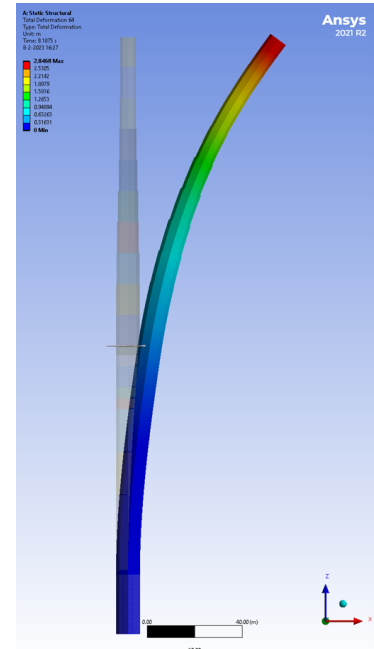
(a) Bending moment, scale=22

(b) Shear force, scale=25

Figure 8.5: Ansys deformed internal force results



(a) Comparison total deformation due to static forces

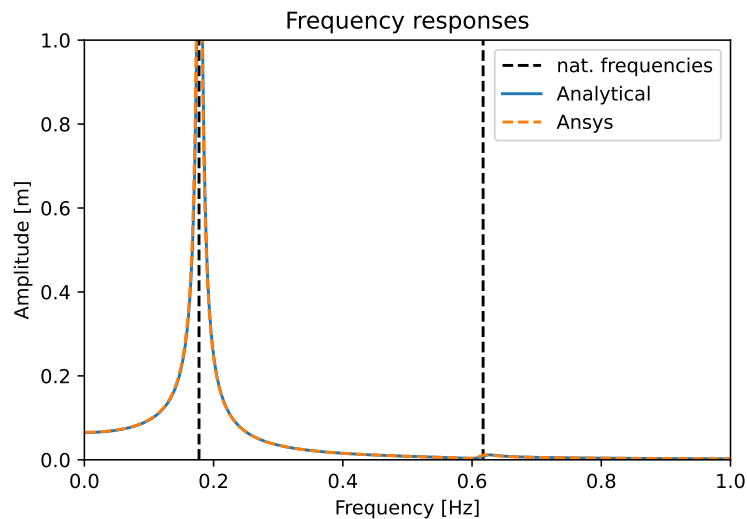


(b) Deformation result from Ansys (scaling factor: 22)

Figure 8.6: Deformations of Ansys-Numerical model validation

8.4.1. Dynamic response

The fatigue analysis is based on the harmonic response of the structure due to the waves, which are assumed to be harmonic loads. This response is validated by using a harmonic response in Ansys. The results of the analysis are shown in figure 8.7. As can be seen in the figure, In the model, large amplitudes are shown at 0.18 Hz. Also, a small deflection is present in the graph at a frequency of 0.62 Hz. This makes sense due to the eigenfrequencies, which have the same value out of section 8.3. Another conclusion of this graph is that the amplitudes as a result of the frequency response of the structure are similar for the numerical model and Ansys. So it can be concluded that the numerical model is correct regarding the harmonic response.

**Figure 8.7:** Harmonic responses Ansys and Numerical model

9

Sensitivity Analysis

This chapter analyses the design parameters' influence on the structures' responses. Arany et al. elaborated a method to design monopiles for offshore wind turbines in 10 steps [3]. The paper also performs a parametric analysis in which the key design monopile dimensions are changed for a typical baseline design. By following this methodology, the pile dimensions can be selected, and a design optimization approach is composed. It is stated in the paper that the pile diameter, wall thickness, and embedded length mainly influence the bending stiffness, natural frequency, pile head deflection, and rotation at the mudline in the design of conventional monopiles. In the design of guyed monopiles, the mooring stiffness will also influence these aspects. One of the questions is how big the impact of changing this stiffness parameter is on the structure's stiffness. To answer this question, a similar parametric analysis as in the previous section has been performed for a guyed monopile design. Here, the model is taken following the described design for the guyed monopile with 80-meter water depth. The initial values for this analysis have been set at the values which are found for the guyed monopile designed in the case study as in chapter 7.6: (1) a constant monopile diameter of $D = 10.0m$, which is equal to the bottom diameter of the tower, (2) a constant monopile thickness of $t = 80mm$, which is equal to the monopile thickness of the top can of the monopile. (3) an embedded length of $L_e = 20m$. a 6-mooring chain layout is used where the angle between the seabed and unstretched chain length is set at $\alpha = 35^\circ$, as described in section 4.1.2. The diameter of the chain is set at an initial value of 200 mm. This gives a (4) total mooring system stiffness of $K = 15.3MN/m$. Subsequently, the sensitivity is determined by changing each parameter separately by taking a linearly spaced range between the minimum and maximum values. These values are based on the design parameters as described in section 2.4. The selected ranges can be found in table 9.1. The minimum for the design is set at half of the initial diameter, and the maximum is set at 2 times the initial diameter. The thickness is set at the minimum value, resulting from the maximum D/t ratio for the initial diameter. The maximum thickness is chosen as described in section 2.4. The embedded length ranges between a minimum of 20 meters, which is equal to the initial design, and 4 times the initial depth, 80 meters. The mooring stiffness ranges between having no moorings and having 9 moorings with a maximum diameter of 200 mm.

Table 9.1: Design parameter ranges

Parameter	Minimum value	Maximum value
Diameter	5 m	20 m
Thickness	70 mm	150 mm
Embedded depth	20 m	80 m
Mooring stiffness	0 moorings 0 MN/m	9 moorings, d=200 mm 23.0 MN/m

9.1. Natural frequencies

First, the sensitivity of the parameters is determined by the system's natural frequencies. To do this, modal analysis has been performed as described in chapter 6 to obtain the natural frequencies of the

initial structure. Modal analysis is repeated for every design case, and the natural frequencies within the monopile are determined. The results of the first two eigenfrequencies are plotted on a dimensionless y-axis, given as a ratio between the natural frequency of the changed design onto the initial design. The first natural frequency is shown in figure 9.1.

9.1.1. First natural frequency

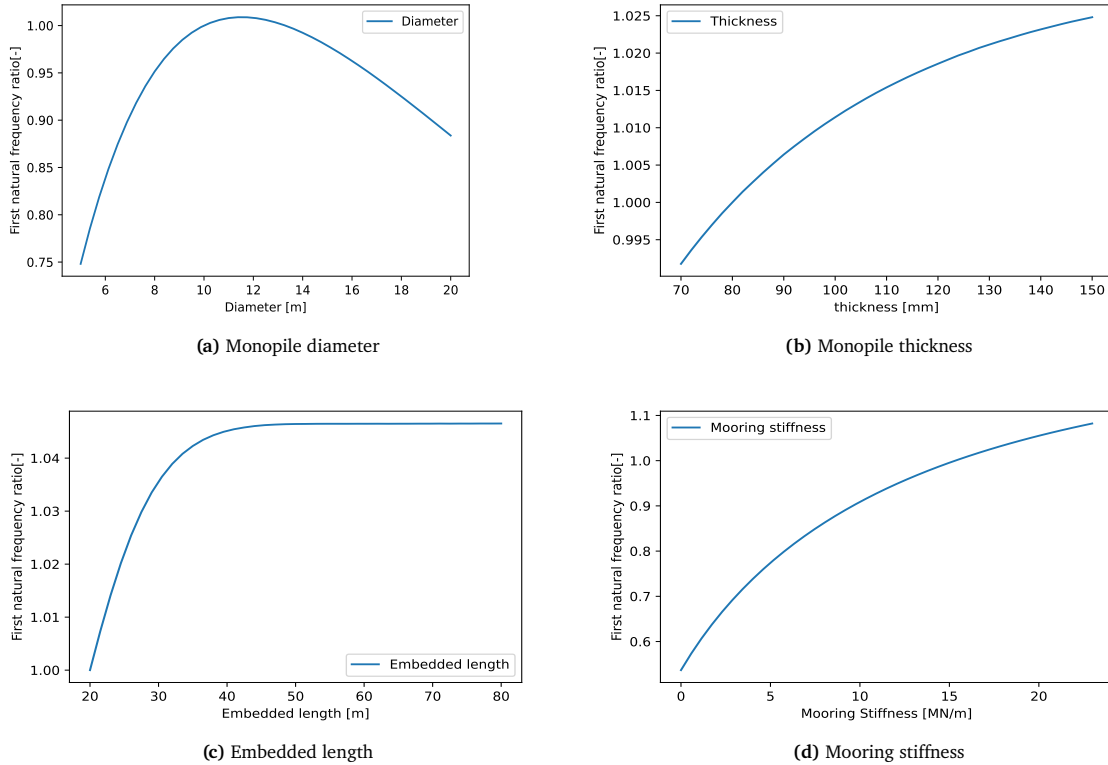


Figure 9.1: Influence of the mooring stiffness in comparison to other main design parameters on the first natural frequency

It can be seen that the monopile thickness, embedded length, and mooring stiffness have a non-linear increasing effect on the first natural frequency of the structure, with an increase of 2.5%, 4.5%, and 10%, respectively. Similar behaviour is found for the monopile's diameter. However, a maximum is found for a diameter of 11 meters. While the diameter increases, the embedded depth is kept equal, which is rather low for the initial case. The soil stiffness is, therefore, also rather low. The structural stiffness is also quite low for a relatively small diameter, and the soil and structural stiffness ratio is high. The soil will act as a clamped support. Therefore, the natural frequency grows when the diameter also increases. However, the soil's stiffness is relatively low for a certain diameter compared to the structural stiffness. As a result, the soil starts reacting as if it is simply supported, where more rotation at the mudline is allowed, and the 1NF will decrease. The tipping point is for this particular design found at 11 meters for the 1NF. This also explains why an increasing embedded depth does not grow the 1NF after approximately 50 meters. The maximum stiffness is reached, the minimum amount of rotation is achieved, and the monopile will act as if it is clamped at the mudline. Increasing the embedded depth further will not have an impact on the rotation of the monopile. For the thickness, similar behaviour as for the diameter is expected. An increasing thickness also results in a higher stiffness of the monopile. However, a maximum is not found in the figure. That is because the tipping point will not be found by increasing the thickness between the selected range. The mooring stiffness will also have a maximum value for the increase in the first natural frequency. If the stiffness is set great enough, the support will act as laterally hinged support where no displacement is allowed, and the beam is free to rotate. If the mooring stiffness is set to zero, then the 1NF will decrease in comparison to the initial design but will not go to zero because the soil does provide stiffness to the structure.

9.1.2. Second natural frequency

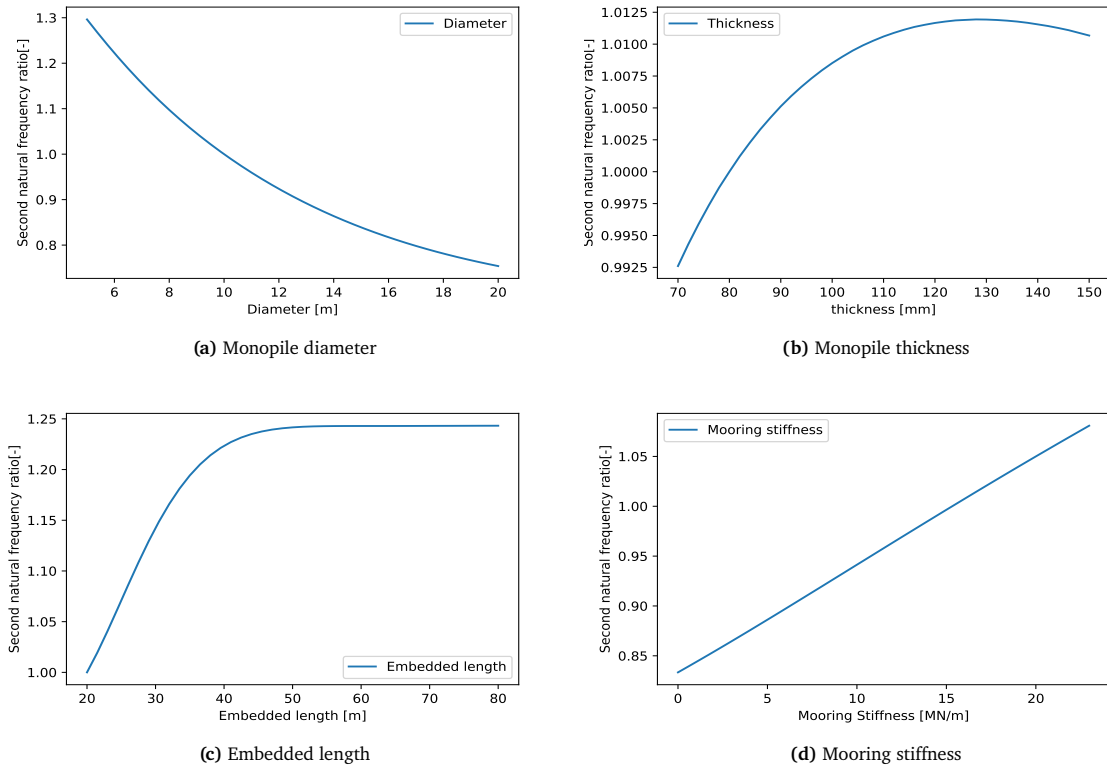


Figure 9.2: Influence of the mooring stiffness in comparison to other main design parameters on the second natural frequency

The results for the second natural frequency can be seen in figure 9.2. The 2NF for a varying diameter is decreasing. This is due to the same behaviour as described for the first natural frequency. The ratio between the soil stiffness and structural stiffness is rather low; therefore, the soil allows the monopile to rotate. At a certain diameter, an asymptote will be found for the second natural frequency where the soil stiffness is totally behaving like hinged support, and the stiffness of the moorings is great enough to provide the needed stability for the structure. The second natural frequency also grows to a certain point for a growing thickness. When the monopile thickness is larger than 130 millimeters the tipping point of the soil, and structural stiffness ratio is achieved, and also rotations will occur. Afterwards, the second natural frequency decreases. Increasing the embedded depth provides similar results as for the 1NF. After a depth of 50 meters, the soil will act as if it is a clamped support. If so, the second natural frequency increases by a maximum of 25%. For the selected range, the mooring stiffness has a linear increasing effect on the second natural frequency. If the stiffness is increased beyond the selected range, a maximum will be found where the horizontal spring acts as a hinged support where no displacements are allowed, and the second natural frequency will not increase any further.

9.2. Internal Stresses

For the initial design, the loads are applied, and static analysis has been performed according to chapter 5 to obtain the internal stresses of the initial structure. Subsequently, the sensitivity is determined by changing each parameter separately in the same way as in the previous section. Static analysis is repeated for every design case, and the maximum value for the stresses within the monopile is determined. The results are plotted on a dimensionless y-axis, given as a ratio from the initial design, shown in figures 9.3 - 9.5.

9.2.1. Axial stress

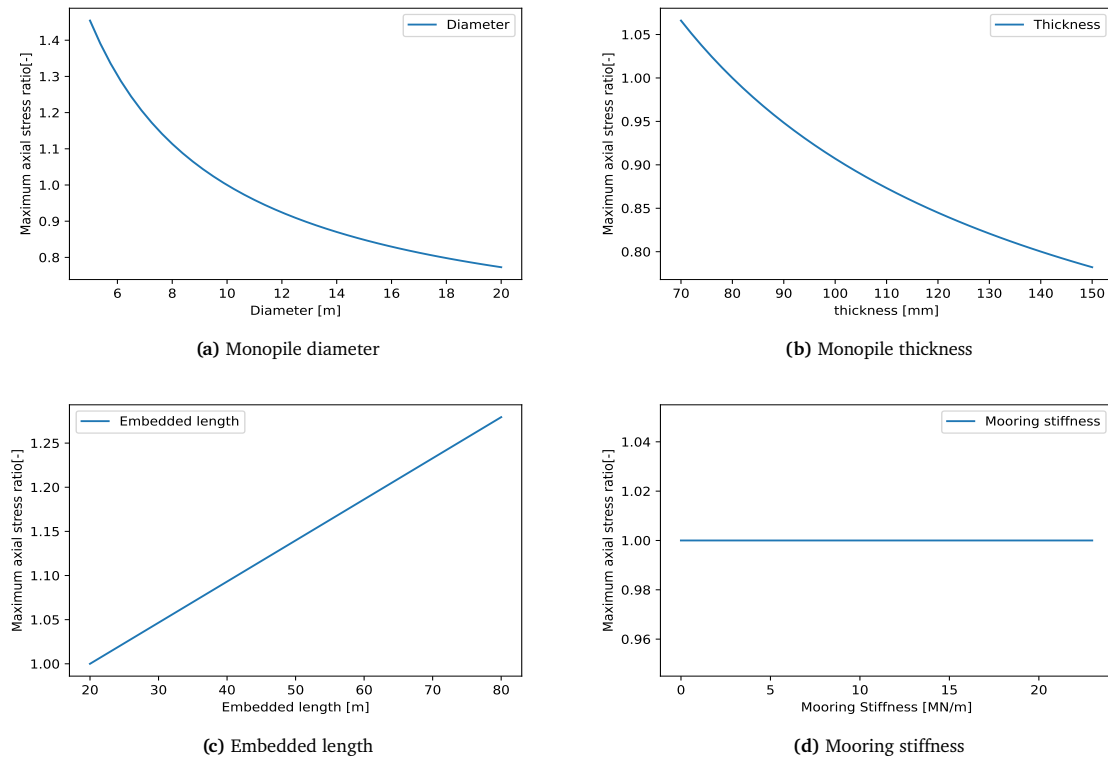
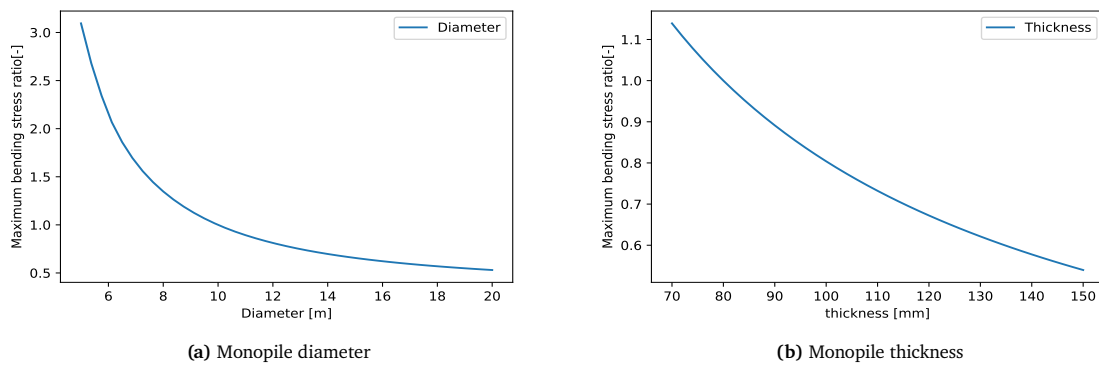


Figure 9.3: Influence of the mooring stiffness in comparison to other main design parameters on the axial stress

The axial stress within the monopile is determined by dividing the axial force over the cross-sectional area of the monopile, i.e. $\sigma = \frac{N}{A}$. As the area is a function of both the diameter and the thickness, these are the main parameters influencing the axial stress. When the diameter or thickness increases, the cross-sectional area also increases. This results in lower axial stress. This can also be concluded from the figure, where both the diameter and thickness give a reduction of approximately 20%. Because it is assumed that the moorings only provide horizontal lateral stiffness, no difference can be found for the axial force, and thus the axial stress does not change. The same applies to the soil, which is also modelled as horizontal springs. By doing this, the friction of the soil onto the monopile wall is neglected. Consequently, the axial stress does not change within the soil. Having a higher embedded depth results in a larger pile length and, thus, a higher total mass. Therefore, the total axial force in the monopile increases for a larger embedded depth.

9.2.2. Bending stress



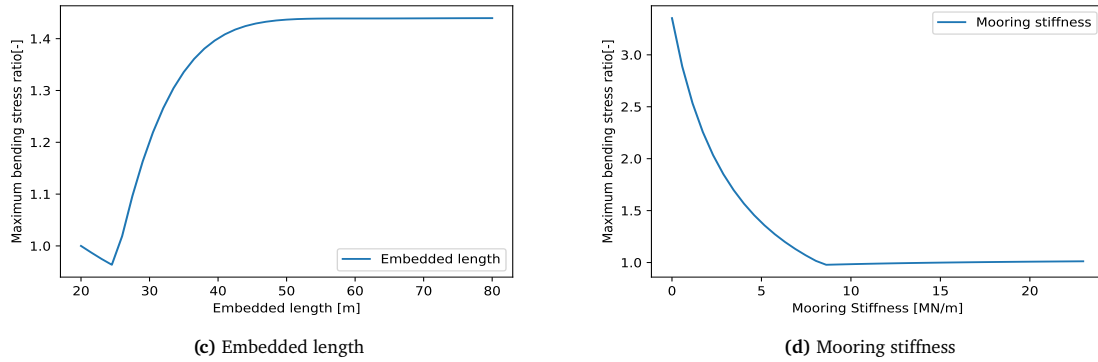
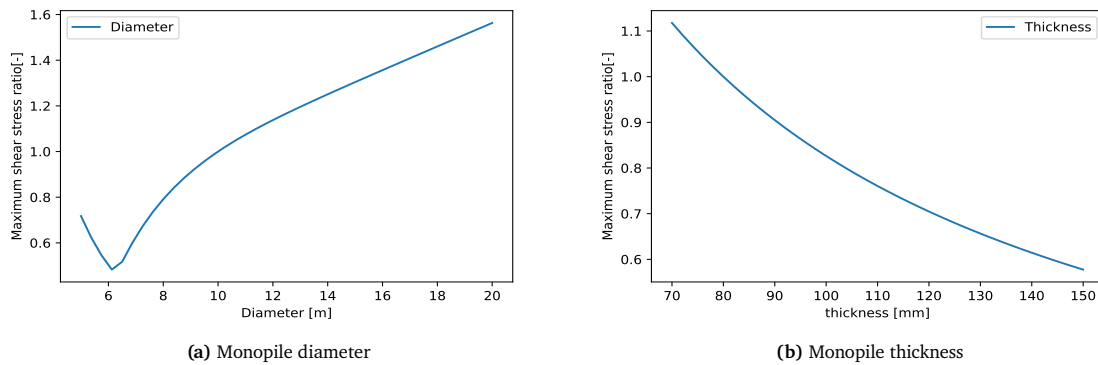


Figure 9.4: Influence of the mooring stiffness in comparison to other main design parameters on the bending stress

The bending stress is also mainly influenced by the diameter and thickness as it is calculated by dividing the internal bending moment over the diameter squared and the thickness, i.e. $\frac{4 \cdot M}{\pi \cdot D^2 \cdot t}$. Increasing the diameter or thickness results in lower bending stress. The diameter has a higher effect than the thickness due to the exponent. Hence, the slope of the found curve is higher for the diameter than for the thickness. The maximum bending stress in the monopile, Increasing the embedded length, first decreases the maximum bending stress within the monopile as more as the maximum bending stress is first located at the mooring attachment. Increasing the embedded length beyond this point increases the stiffness of the soil. As a result, the bending stress in the soil increases as well and the maximum stress shifts towards the soil. Again, for a depth of 50 meters, the maximum stress ratio is achieved, and the bending stress does not increase any further. The mooring stiffness reduces the bending stress within the monopile up to a certain point where the maximum stress is found at the interface and does not decrease any further. Therefore, it is most beneficial if the mooring stiffness has a value of more or equal to this tipping point.

9.2.3. Shear stress



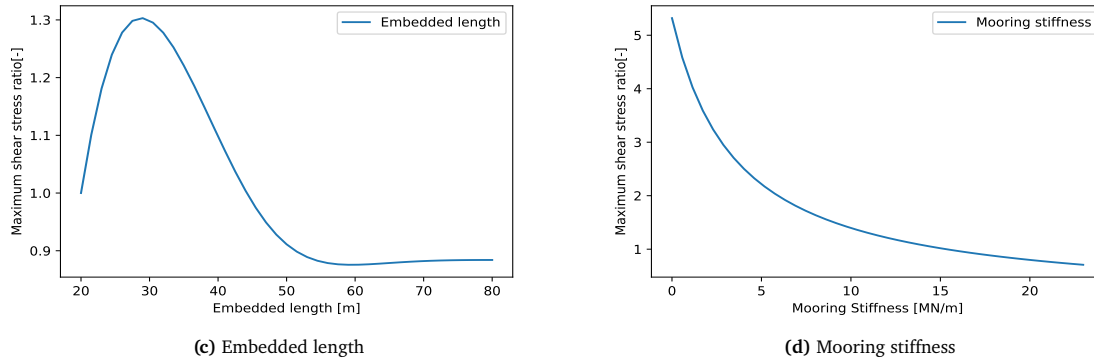


Figure 9.5: Influence of the mooring stiffness in comparison to other main design parameters on the shear stress

The shear stress is calculated by dividing the internal shear force over the multiple of the diameter and thickness, i.e. $\tau = \frac{2 \cdot V}{\pi \cdot D \cdot t}$. The expected effect due to a changing diameter and thickness is expected to be similarly decreasing for a growing parameter, as both decrease the shear stress by the power of 1. However, out of the figures, the opposite behaviour can be seen for the diameter. This is a consequence of the response of the soil due to a higher diameter. A higher diameter increases the soil stiffness due to the fact that more surface of the monopile is embedded. As a result of the growing stiffness, the shear stress beneath the mudline also increases. For lower diameters, the maximum is found at the location of the moorings. Higher diameters result in the maximum shear stress beneath the mudline. The embedded length increases first when increased from the initial design. This makes sense as the stiffness of the soil is more activated. After 32 meters of embedded depth, the maximum shear stress in the monopile starts decreasing. That is because more material is activated to transfer the shear force into the soil. After a certain depth, the maximum shear stress does not decrease further. This is due to the fact that no deformation will occur for further depths. If no mooring system is present and the mooring stiffness equals zero, all shear force within the monopile must be transferred to the soil. Therefore, the highest shear stress will also be found then. If the mooring stiffness increases, the deformation of the monopile within the soil decreases, and the shear stress will decrease beneath the mudline. Therefore, the higher the mooring stiffness, the lower the maximum stress ratio.

10

Conclusions & Recommendations

In this chapter, the conclusions of this research are presented. This study investigates the limitations of a guyed monopile and elaborates that a guyed monopile is favourable over a conventional monopile for deepwater when applied as a foundation for large wind turbine generators. Recommendations for further research and the limitations of this research are discussed afterwards. Overall, the chapter will provide a comprehensive overview of the research's key takeaways and potential impact.

10.1. Conclusions

The availability of the most favourable locations for wind farms is shrinking, while the demand for off-shore wind has never risen faster. Therefore, the wind turbines get positioned in deep waters. As the industry is not yet able to upscale the production of floating foundations for WTGs, the industry is looking for opportunities of applying offshore wind in deep water. This is one of the reasons why the extension of monopiles is researched thoroughly. Deep water results in higher loads, and to overcome this problem, the structure's stiffness needs to be increased. For conventional monopiles, this is usually done by increasing the diameter over the depth and applying higher thicknesses. The stiffness problems can also be overcome by applying a mooring system to the monopiles, i.e. guyed monopiles. Overall, the optimized guyed monopile concept described in this study is proven to be a good solution for the application in deep water. It is confirmed that a mooring system can extend the use of monopiles into deeper waters. But also highlights the obstacles that occur when wind farms are placed in greater water depths.

Research question 1: What order of magnitude of stiffness can the mooring system for a guyed monopile provide?

This study uses a 1D finite element method to model a wind turbine generator supported by a guyed monopile. The model consists of beam elements which are supported by springs representing the soil. The spring stiffness for the soil is determined by making use of the p-y method. The fem model contains an extra horizontal spring representing the mooring stiffness modelled by using a non-linear approach for suspended mooring lines. Also, the stiffness of an anchor and the stiffness due to the ovalization of the monopile is modelled. Dyneema, steel chains and steel wire are compared by their stiffness. It is concluded that steel chains provide the highest stiffness for the three mooring types having the same diameter. Also, the influence of the extra weight due to marine growth is determined whereof it results that the influence of marine growth is minimal and the stiffness will not decrease. When implementing a mooring system with a minimum of three moorings evenly distributed over the cross-section, the stiffness in all horizontal directions is equal. also, more moorings lead to higher stiffness. The relationship between the total stiffness of a mooring system is found to be linearly distributed over the total number of moorings applied. To increase the stiffness of a mooring, mainly the diameter is important. Increasing it gives an exponential increase in the stiffness per mooring. Also, the ideal angle between the seabed and a mooring is found to be 35°. Increasing the number of moorings gives a linear growth of the total system stiffness applied to a guyed monopile. This study assumes a maximum of 9 moorings, which gives a maximum system stiffness of 35.5 MN/m. Overall, This mooring system provides enough stiffness to be used in a guyed monopile.

Research question 2: Given a case of environmental conditions, what would be the weight reduction of a monopile foundation that can be achieved by the application of moorings for different water depths?

Guyed and conventional monopile structures are designed for a reference wind turbine provided by the International Energy Agency. The wind farm zone Hollandse Kust West in the North Sea is taken as a location where multiple water depths are assumed at 60, 80, 100 and 120 meters. A realistic load case is taken where the structure is loaded by a stream function wave, current waves, and wind loads. It is proven that the design is not governed by the ultimate limit state requirements. The yield stress, column buckling and local buckling were in no circumstances the determining factor and were maximally utilized for 67%. Fatigue and resonance, however, have been governing for all cases treated in this study. Offshore wind turbines are constantly loaded by cyclic forces, and therefore fatigue greatly impacts the failure of the WTG foundation. These problems can only be overcome by applying a larger diameter for a conventional monopile, leading to a great increase in the total steel used for a foundation. However, the fatigue and resonance issues can also be solved for monopiles in deep waters by applying moorings. Applying moorings gives a reduction in the total weight as the anchors and moorings used in this model make up a small portion of the total weight. An increase due to stiffer moorings leads to a smaller increase in the total weight than an increase in the monopile diameter or its thickness. This reduction could be up to 45% of the overall foundation weight.

Research question 3: What is the influence of the mooring stiffness compared to other design variables and how does it affect the response of the structure?

The mooring stiffness has been compared to key design parameters by the natural frequencies and internal stresses. For an initial design case with a given water depth, the influence of the monopile diameter, monopile thickness, embedded length and mooring stiffness is determined by changing each parameter separately. The natural frequencies are mainly influenced by the ratio between the soil stiffness and the structural stiffness of the monopile. Increasing the diameter and thickness will increase the structural stiffness and thus increase the eigenfrequency. However, if structural stiffness is high compared to soil stiffness, the first and second natural frequencies reduce. As both might interfere with the 1P and 3P frequencies of the offshore wind turbine, this behaviour is undesirable. The mooring stiffness has a favourable effect on both the first and second eigenfrequencies. When the mooring stiffness increases, the first and second natural frequencies also increase. Therefore, applying moorings onto a monopile can solve the resonance issues which occur for larger water depths. The axial stress can be reduced by applying a greater cross-section, thus, increasing the diameter or thickness. The shear stress is mainly affected by the monopile diameter. The mooring stiffness has less influence on the internal stresses, and the other design parameters are preferred to be changed when problems occur.

10.2. Recommendations

The results of this research are promising. Guyed monopiles can replace jackets or XXL monopiles in waters between 60 and 120 meters. The results show that such a WTG foundation is able to resist all the realistically assumed loads that future wind turbines might bring. Before one realistically can consider the implementation of a guyed monopile, further research is required. Technical and non-technical issues still need to be addressed before a guyed monopile concept can be proven innovative, reliable, and profitable. This section will present recommended topics.

- Due to the application of the moorings, higher stress concentrations will occur at the top end of the mooring. the attachment of the moorings at the monopile needs to be carefully designed. To compensate for the growing stresses, stiffeners might be necessary, which leads to higher steel use. The fatigue damage that occurs here might govern the design of a guyed monopile. A detailed design of the stress concentration factor of such details is necessary to improve the concept.
- As this study focuses on the structural response of a guyed monopile, an economic feasibility study is advised to determine if the concept is achievable. The steel weight reduction found is excellent, which also gives an economic advantage. But, attaching the moorings brings more costs, e.g. the anchors need to be installed, the used chains may be a lot more expensive than adding weight to the monopile, and the costs of the mooring attachment as described in the previous item could be substantial.
- Because the internal forces beneath the mudline can be significantly reduced, a GM could also

be suitable for locations where the seabed is relatively weak, e.g. soft clay, silt, or loose sands. These soils often have a low shear strength and a low bearing capacity. More thorough research is recommended to find a GM's dynamic and static response when applied in weak soil. Also, the soil model used is relatively conservative, and a linear displacement distribution over the depth is assumed, i.e. rigid pile motion is assumed. However, this will not be the case in reality, and the pile will also deform slightly beneath the mudline. Therefore, a more precise geotechnical analysis is advised.

- The damping ratio needs to be determined for deep waters as the damping increases. The damping ratio is now taken as 0.02, which is a good assumption for shallow waters. For deep waters, more mass needs to be replaced for a displacement of the pile. Thus, the inertia is higher. Consequently, the damping ratio increases as well. A thorough damping analysis is recommended.
- As stated in this study, the weight of the structure is not considered to be of importance for the design. The shift into deepwater will also require that the boundaries of the monopile industry need to be pushed. For example, installing a guyed monopile might require larger boats with even larger lifting capabilities. This might also be a problem for the manufacturers of monopiles, as they might require new cranes to lift the larger monopiles. The extra slenderness of a guyed monopile might require new lifting methods, as local deformation might occur. However, this is the case for a more slender monopile as well as for a heavier conventional monopile. Still, more research is recommended.
- In this study, the moorings are modelled as a linear horizontal spring. Also, dynamic analysis of the moorings is recommended as this might bring extra stresses onto the monopile. The moorings can, for example, also start to resonate under certain circumstances. It needs to be made sure that this does not result in the failure of the foundation. Next to that, a breaking analysis of the moorings is of importance. If a mooring breaks, the stiffness of the structure differs, and the structure might fail due to too little overall stiffness. In addition, Fatigue behaviour might also play a role in the moorings. Chains are known to have good resistance against creep. However, fatigue might play a role in the moorings themselves. The overall stiffness of the structure might decrease over time. It is assumed in this study that the pretensioning is large enough at all times. There is a possibility that this
- Second-order effects are not considered. This effect may lead to additional stresses, which can significantly affect the structural behaviour of the guyed monopile, which might result in a reduction of the structural capacity. A second-order analysis, e.g. using FEM, can be performed to show the influence of this behaviour.
- Other load cases might bring larger stresses in the WTG foundation. This study focused on the case in which the 1-year gust wind together with a 50-year wave occurs. This is conservative and not what the offshore standards advise. Also, ice- and earthquake loads may be site-specific but are not taken into account in this research. Further research is recommended if both or one of these load cases is of importance. A more thorough study into the multiple load cases which are stated in the DNV standards might bring slight differences in the results of this research.
- Secondary steel of the monopile is not taken into account. The mass of the steel brings extra stresses into the stiffness, and extra hydrodynamic forces occur when a wave hits the secondary steel. This results in extra (local) stresses in the material. On top of that, marine life is neglected in this thesis, as described in chapter 4, which will grow on the monopile and moorings. This results in extra weight onto the monopile, and the axial stresses increase as well. This has a negative effect on the hydrodynamic loads. The diameter of the affected surface of the monopile increases, and therefore the hydrodynamic forces grow as well, according to Morison's equation.
- In this study, it is assumed that scour protection is in place. Due to scour, the soil around a structure placed in the seabed erodes due to waves and currents which occur at the mudline. This potentially decreases the stability of the structure. Also, this might not only happen for the monopile but also for the pinpiles. Measures might be necessary to prevent this behaviour.
- In the research, the splash zone coating is considered to be sufficient during the whole lifetime of the monopile. In reality, the coating might not be sufficient, after which free corrosion might happen. This has a negative effect on the fatigue life of the structure. The fatigue damage will increase over time as a result.

- Fatigue damage due to transport and installation is not taken into account. Realistically, more damage will be done due to hammering the monopile into the seabed. This is often taken as 10% of the total life of the structure, according to DNV standards. However, as this is similar for both a conventional and for a guyed monopile, this is assumed to be out of the scope of this research.
- When multiple guyed monopiles are placed in a wind park. There is the possibility to anchor more cables of other WTGs to the same anchors. Then, only one anchor is needed for having 3 or 4 moorings. This might reduce the costs of the total foundation even more.

References

- [1] NEN-EN-ISO 19901. *Petroleum and natural gas industries - Specific requirements for offshore structures - Part 1: Metocean design and operating considerations*. Nederlands Normalisatie-instituut, 2015.
- [2] David E. Alexander. *Nature's Machines*. 2017.
- [3] Laszlo Arany et al. "Design of monopiles for offshore wind turbines in 10 steps". In: *Soil Dynamics and Earthquake Engineering* 92 (Jan. 2017), pp. 126–152. ISSN: 02677261. DOI: 10.1016/j.soildyn.2016.09.024.
- [4] T. Ashuri et al. "Aeroservoelastic design definition of a 20 MW common research wind turbine model". In: *Wind Energy* 19 (11 Nov. 2016), pp. 2071–2087. ISSN: 10954244. DOI: 10.1002/we.1970.
- [5] N.D.P. Barltrop and A.J. Adams. *Dynamics of Fixed Marine Structures*. 3rd ed. Elsevier, 1991. ISBN: 9780750610469. DOI: 10.1016/C2013-0-04571-9.
- [6] J Bunce and J Carey. "A Guyed Support Structure Design for Large Megawatt Offshore Wind Turbines in Deep Waters". In: (Jan. 2002), pp. 10–12.
- [7] Tony Burton et al. *Wind Energy Handbook*. 3rd ed. John Wiley & Sons Ltd., 2021.
- [8] Subrata K. Chakrabarti. *Handbook of Offshore Engineering*. Vol. 2. Elsevier, 2005.
- [9] *DeepRope manual 2004*. BEXCO, 2004.
- [10] Dillinger. *Delivery program - heavy plate*. Brochure. 2018. URL: <https://www.dillinger.de/d/downloads/download/13440>.
- [11] DNV. *Floating offshore wind: The next five years*. 2022. URL: <https://www.dnv.com/focus-areas/floating-offshore-wind/floating-offshore-wind-the-next-five-years.html>.
- [12] DNVGL-CG-0127. *Finite element analysis*. 2020.
- [13] DNVGL-RP-C202. *Buckling strength of shells*. 2019.
- [14] DNVGL-RP-C203. *Fatigue design of offshore structures*. 2019.
- [15] DNVGL-RP-C205. *Environmental conditions and environmental loads*. 2019.
- [16] DNVGL-ST-0119. *Floating wind turbine structures*. 2018.
- [17] DNVGL-ST-0126. *Support structures for wind turbines*. 2019.
- [18] part 1-1 Eurocode 3. "Design of steel structures: General rules and rules for buildings". In: (2005).
- [19] part 1-6 Eurocode 3. "Design of steel structures: Strength and stability of Shell structures". In: (2007).
- [20] European Commission. *REPowerEU: A plan to rapidly reduce dependence on Russian fossil fuels and fast forward the green transition*. 2022. URL: https://ec.europa.eu/commission/presscorner/detail/en/IP_22_3131.
- [21] Eurostat: statistics explained. *Renewable energy statistics*. 2022. URL: https://ec.europa.eu/eurostat/statistics-explained/index.php?title=Renewable_energy_statistics#Wind_and_water_provide_most_renewable_electricity.3B_solar_is_the_fastest-growing_energy_source.
- [22] Natacha Fery et al. *Metocean desk study and database for Dutch Wind Farm Zones Hollandse Kust (west)*. Netherlands Enterprise Agency (RVO), Dec. 2020.
- [23] Fugro. *Hollandse Kust (west) Wind Farm Zone: Geological Ground Model*. Netherlands Enterprise Agency (RVO), May 2020.

- [24] Evan Gaertner et al. *Definition of the IEA 15-Megawatt offshore Reference Wind Turbine*. International Energy Agency Wind, Mar. 2020.
- [25] Thijs de Haan. “Buckling monopiles: The stability of a monopile-based offshore wind turbine”. Delft University of Technology, Jan. 2020.
- [26] Christian Hoffmann, Michel van Hoey, and Benedikt Zeumer. *Decarbonization challenge for steel*. 2020. URL: <https://www.mckinsey.com/industries/metals-and-mining/our-insights/decarbonization-challenge-for-steel>.
- [27] British Standard Institute. “British Standard 5950: Structural use of steelwork in buildings - Part 1: Code of practice for design —Rolled and welded sections”. In: (2000).
- [28] International Energy Agency. *Offshore Wind Outlook 2019*. 2019. URL: <https://www.iea.org/reports/offshore-wind-outlook-2019>.
- [29] Hermans K.W. and Peeringa J.M. *Future XL monopile foundation design for a 10 MW wind turbine in deep water*. Stichting Energieonderzoek Centrum Nederland, Dec. 2016.
- [30] D. Kallehave et al. “Optimization of monopiles for offshore wind turbines”. In: *The Royal Society Publishing* 373.2035 (2015).
- [31] Martin Kühn. *Dynamics and design optimisation of offshore wind energy conversion systems*. Jan. 2001.
- [32] Iris Lohmann, Helena Jane Hunt, and Pia Redanz. *Hollandse Kust (west) Wind Farm Zone: Certification Report Metocean Conditions*. Netherlands Enterprise Agency (RVO), Dec. 2020.
- [33] Kai-Tung Ma et al. *Mooring System Engineering for Offshore Structures*. Elsevier, 2019. ISBN: 9780128185513. DOI: 10.1016/C2018-0-02217-3.
- [34] Kai-tung Ma et al. “Mooring Designs for Floating Offshore Wind Turbines Leveraging Experience From the Oil and Gas Industry”. In: American Society of Mechanical Engineers, June 2021. ISBN: 978-0-7918-8511-6. DOI: 10.1115/OMAE2021-60739.
- [35] Abdollah Malekjafarian et al. “Foundation damping for monopile supported offshore wind turbines: A review”. In: *Marine Structures* 77 (May 2021), p. 102937. ISSN: 09518339. DOI: 10.1016/j.marstruc.2021.102937.
- [36] Alan Marson. *How far can we push D/t ratios?* July 2021. URL: <https://www.empireengineering.co.uk/how-far-can-we-push-d-t-ratios/>.
- [37] Benjamin Pakenham, Anna Ermakova, and Ali Mehmanparast. “A review of life extension strategies for offshore wind farms using techno-economic assessments”. In: *Energies* 14 (7 Apr. 2021). ISSN: 19961073. DOI: 10.3390/en14071936.
- [38] F. Papi and A. Bianchini. “Technical challenges in floating offshore wind turbine upscaling: A critical analysis based on the NREL 5 MW and IEA 15 MW Reference Turbines”. In: *Renewable and Sustainable Energy Reviews* 162 (July 2022), p. 112489. ISSN: 13640321. DOI: 10.1016/j.rser.2022.112489.
- [39] Patrik Passon. “Offshore Wind Turbine Foundation Design: Selected Topics from the Perspective of a Foundation Designer”. Technical University of Denmark, Mar. 2015.
- [40] Eric Paya and Aaron Zigeng Du. *The frontier between fixed and floating foundations in offshore wind*. Oct. 2020. URL: <https://www.empireengineering.co.uk/the-frontier-between-fixed-and-floating-foundations-in-offshore-wind/>.
- [41] Harry G. Poulos and Edward H. Davis. *Pile Foundation Analysis and Design*. 1980, pp. 163–225.
- [42] Rijksoverheid. *Shell and Eneco win tender on offshore wind farm Hollandse Kust (West)*. Dec. 2022. URL: <https://www.rijksoverheid.nl/actueel/nieuws/2022/12/15/shell-en-eneco-winnen-tender-windpark-op-zee-hollandse-kust-west>.
- [43] Mohammed Khair Al-Solihat and Meyer Nahon. “Stiffness of slack and taut moorings”. In: *Ships and Offshore Structures* 11 (8 Nov. 2016), pp. 890–904. ISSN: 1744-5302. DOI: 10.1080/17445302.2015.1089052.

- [44] Carlos Eduardo Silva de Souza and Erin E. Bachynski-Polić. “Design, structural modeling, control, and performance of 20 MW spar floating wind turbines”. In: *Marine Structures* 84 (July 2022), p. 103182. ISSN: 0951-8339. DOI: 10.1016/J.MARSTRUC.2022.103182.
- [45] T.W. Taconis. “Guyed tower offshore windmill”. Delft University of Technology, June 1984.
- [46] Eize de Vries. “Beyond XXL Monopiles: Slim monopiles for deep water windfarms”. In: *Offshore wind magazine* (Nov. 2019), pp. 20–25.
- [47] Wind Europe. *Offshore Wind in Europe - Key trends and statistics 2020*. 2021. URL: <https://windeurope.org/intelligence-platform/product/offshore-wind-in-europe-key-trends-and-statistics-2020/>.
- [48] Renqiang Xi et al. “Dynamic analysis of 10 MW monopile supported offshore wind turbine based on fully coupled model”. In: *Ocean Engineering* 234 (Aug. 2021), p. 109346. ISSN: 00298018. DOI: 10.1016/j.oceaneng.2021.109346.
- [49] Y.E. Liu. “Monopile Forever: Overcoming the Technical Boundaries of Monopile Foundations in Deep Waters”. 2021. URL: <http://resolver.tudelft.nl/uuid:5526ed6b-6a40-43b5-b96d-563c6891ae3f>.
- [50] Y. B. Yang and Jiunn-Yin Tsay. “Geometric nonlinear analysis of cable structures with a two-node cable element by generalized displacement control method”. In: *International Journal of Structural Stability and Dynamics* 07 (04 Dec. 2007), pp. 571–588. ISSN: 0219-4554. DOI: 10.1142/S0219455407002435.



Results Conventional Monopile

A.1. Geometry

Geometry			Geometric design criteria												
Cans	Diameter [m]	thickness s [mm]	Length [m]	Top elev.[m]	Bottom elev.[m]	Area [m²]	Section Modulus [m³]	Moment of inertia	Slenderness s [-]	Cross section class[-]	D/t ratio [-]	thickness length [-]	Δthickness[-] slope [-]		
1	10	0,1	3	16	13	3,11	7,62	38,11	100,00	4	0,63	0,00	0,67	0,50	0,00
2	10	0,11	3,5	13	9,5	3,42	8,36	41,79	90,91	4	0,57	0,00	0,78	0,00	0,00
3	10	0,11	4,5	9,5	5	3,42	8,36	41,79	90,91	4	0,57	0,00	1,00	0,00	0,00
4	10	0,11	4,5	5	0,5	3,42	8,36	41,79	90,91	4	0,57	0,00	1,00	0,50	0,00
5	10	0,12	4,5	0,5	-4	3,72	9,09	45,45	83,33	4	0,52	0,00	1,00	0,00	0,00
6	10	0,12	4,5	-4	-8,5	3,72	9,09	45,45	83,33	4	0,52	0,00	1,00	0,00	0,00
7	10	0,12	4,5	-8,5	-13	3,72	9,09	45,45	83,33	4	0,52	0,00	1,00	0,50	0,00
8	10	0,13	4,5	-13	-17,5	4,03	9,82	49,09	76,92	4	0,48	0,00	1,00	0,00	0,00
9	10	0,13	4,5	-17,5	-22	4,03	9,82	49,09	76,92	4	0,48	0,00	1,00	0,50	0,00
10	10	0,14	4,5	-22	-26,5	4,34	10,54	52,71	71,43	4	0,45	0,00	1,00	0,00	0,00
11	10	0,14	4,5	-26,5	-31	4,34	10,54	52,71	71,43	4	0,45	0,00	1,00	0,00	0,00
12	10	0,14	4,5	-31	-35,5	4,34	10,54	52,71	71,43	4	0,45	0,00	1,00	0,00	0,91
13	11	0,14	4,5	-35,5	-40	4,78	12,81	70,43	78,57	4	0,49	0,00	1,00	0,50	0,91
14	12	0,13	4,5	-40	-44,5	4,85	14,23	85,39	92,31	4	0,58	0,00	1,00	0,50	0,91
15	13	0,12	4,5	-44,5	-49	4,86	15,49	100,70	108,33	4	0,68	0,00	1,00	0,50	0,00
16	13	0,11	4,5	-49	-53,5	4,45	14,23	92,52	118,18	4	0,74	0,00	1,00	0,50	0,00
17	13	0,12	4,5	-53,5	-58	4,86	15,49	100,70	108,33	4	0,68	0,00	1,00	0,00	0,00
18	13	0,12	4,5	-58	-62,5	4,86	15,49	100,70	108,33	4	0,68	0,00	1,00	0,00	0,00
19	13	0,12	4,5	-62,5	-67	4,86	15,49	100,70	108,33	4	0,68	0,00	1,00	0,50	0,00
20	13	0,13	4,5	-67	-71,5	5,26	16,74	108,84	100,00	4	0,63	0,00	1,00	0,00	0,00
21	13	0,13	4,5	-71,5	-76	5,26	16,74	108,84	100,00	4	0,63	0,00	1,00	0,50	0,00
22	13	0,14	4,5	-76	-80,5	5,66	17,99	116,94	92,86	4	0,58	0,00	1,00	0,00	0,00
23	13	0,14	4,5	-80,5	-85	5,66	17,99	116,94	92,86	4	0,58	0,00	1,00	0,00	0,00
24	13	0,14	4,5	-85	-89,5	5,66	17,99	116,94	92,86	4	0,58	0,00	1,00	0,00	0,00
25	13	0,14	4,5	-89,5	-94	5,66	17,99	116,94	92,86	4	0,58	0,00	1,00	0,50	0,00
26	13	0,13	4,5	-94	-98,5	5,26	16,74	108,84	100,00	4	0,63	0,00	1,00	0,50	0,00
27	13	0,12	4,5	-98,5	-103	4,86	15,49	100,70	108,33	4	0,68	0,00	1,00	0,50	0,00
28	13	0,11	4,5	-103	-107,5	4,45	14,23	92,52	118,18	4	0,74	0,00	1,00	1,00	0,00
29	13	0,09	4,5	-107,5	-112	3,65	11,70	76,05	144,44	4	0,90	0,00	1,00	0,00	0,00
30	13	0,09	4,5	-112	-116,5	3,65	11,70	76,05	144,44	4	0,90	0,00	1,00	0,00	0,00
31	13	0,09	4,5	-116,5	-121	3,65	11,70	76,05	144,44	4	0,90	0,00	1,00	0,00	0,00
32	13	0,09	4,5	-121	-125,5	3,65	11,70	76,05	144,44	4	0,90	0,00	1,00	0,00	0,00
33	13	0,09	4,5	-125,5	-130	3,65	11,70	76,05	144,44	4	0,90	0,00	1,00	0,00	0,00

A.2. Ultimate Limit State

Ultimate Limit State										Yield check					Local Buckling, DNV				
Internal forces and stresses										Yield strength f _y [Mpa]	σ ₁ [Mpa]	ρ _a	ρ _b	Z ₁	f _{ei} [Mpa]	f _{es} [Mpa]	σ ₁ [Mpa]	ρ _a	ρ _b
Maximum force [N]	Maximum bending force [Nm]	Maximum shear force [N]	Maximum axial stress [Mpa]	Maximum bending stress [Mpa]	Maximum shear stress [Mpa]	Maximum axial stress [Mpa]	Maximum bending stress [Mpa]	Maximum shear stress [Mpa]	Maximum axial stress [Mpa]										
20562824	577934997	3645000	6,61	75,83	1,17				315	82,47	82,44	0,43	0,46	22667,50	0,16	1074,53	82,44	0,43	0,46
21576125	590692502	3645000	6,31	70,67	1,07				295	77,01	76,98	0,44	0,47	20606,82	0,19	1195,65	76,98	0,44	0,47
22878940	609034963	4913566	6,69	72,86	1,44				295	79,60	79,56	0,30	0,47	20606,82	0,19	1195,65	79,56	0,44	0,47
24214484	635996839	7053969	7,08	76,09	2,06				295	83,25	83,18	0,44	0,47	20606,82	0,19	1195,65	83,18	0,44	0,47
25698641	672813620	9668312	6,90	74,01	2,60				295	81,03	80,91	0,44	0,47	18889,59	0,22	1317,17	80,91	0,44	0,47
27182798	720923899	12069175	7,30	79,30	3,24				295	86,78	86,60	0,32	0,47	18889,59	0,22	1317,17	86,60	0,44	0,47
28679787	779111010	14189395	7,70	85,70	3,81				295	93,64	93,40	0,44	0,47	18889,59	0,22	1317,17	93,40	0,44	0,47
30280705	846085287	15967450	7,51	86,17	3,96				295	93,93	93,68	0,45	0,47	17436,54	0,26	1439,02	93,68	0,45	0,47
31894429	920704960	17464050	7,91	93,77	4,33				295	101,96	101,68	0,45	0,47	17436,54	0,26	1439,02	101,68	0,45	0,47
33611868	1002198878	18728631	7,75	95,06	4,32				295	103,09	102,81	0,45	0,47	16191,07	0,31	1561,13	102,81	0,45	0,47
35329308	1089224213	19801438	8,15	103,32	4,57				295	111,75	111,47	0,45	0,47	16191,07	0,31	1561,13	111,47	0,45	0,47
37046748	1180669120	20758939	8,54	111,99	4,79				295	120,82	120,54	0,45	0,47	16191,07	0,31	1561,13	120,54	0,45	0,47
38843005	1275995669	21720042	8,13	99,65	4,55				295	108,07	107,78	0,45	0,47	14719,16	0,31	1405,76	107,78	0,45	0,47
40670442	1375166820	22705707	8,39	96,63	4,68				295	105,33	105,02	0,44	0,47	14530,45	0,26	1175,43	105,02	0,44	0,47
42504867	1478232010	23707417	8,75	95,42	4,88				295	104,51	104,17	0,43	0,46	14530,45	0,22	981,70	104,17	0,43	0,46
44284021	1585130761	24658053	9,94	111,36	5,54				295	121,68	121,30	0,42	0,46	15851,40	0,19	889,23	121,30	0,42	0,46
46199296	1695468658	25494149	9,51	109,44	5,25				295	119,30	118,95	0,43	0,46	14530,45	0,22	981,70	118,95	0,43	0,46
48114571	1808844488	26237064	9,91	116,76	5,40				295	127,01	126,67	0,43	0,46	14530,45	0,22	981,70	126,67	0,43	0,46
50046627	1924934389	26905373	10,31	124,25	5,54				295	134,90	134,56	0,43	0,46	14530,45	0,22	981,70	134,56	0,43	0,46
52114589	2043481328	27515325	9,91	122,04	5,23				295	132,27	131,95	0,43	0,46	13412,72	0,26	1074,53	131,95	0,43	0,46
54199306	2164285847	28081067	10,31	129,25	5,34				295	139,87	139,57	0,43	0,46	13412,72	0,26	1074,53	139,57	0,43	0,46
56415177	2290517395	28614158	9,97	127,32	5,06				295	137,57	137,29	0,44	0,47	12454,67	0,31	1167,66	137,29	0,44	0,47
58571246	2395199558	28392752	10,36	133,14	5,02				295	143,75	143,49	0,44	0,47	12454,67	0,31	1167,66	143,49	0,44	0,47
60727316	2412671468	16029252	10,74	134,11	2,83				295	144,93	144,84	0,44	0,47	12454,67	0,31	1167,66	144,84	0,44	0,47
62866446	2387232711	50715858	11,11	132,69	8,97				295	144,64	143,81	0,44	0,47	12454,67	0,31	1167,66	144,64	0,44	0,47
64851102	2208246287	63816145	12,34	131,88	12,14				295	145,74	144,22	0,43	0,46	13412,72	0,26	1074,53	144,22	0,43	0,46
66687044	1940252271	74292256	13,73	125,24	15,30				295	141,48	138,97	0,43	0,46	14530,45	0,22	981,70	138,97	0,43	0,46
68350987	1620658774	78601707	15,34	113,86	17,65				295	132,77	129,20	0,42	0,46	15851,40	0,19	889,23	129,20	0,42	0,46
69742420	1272257625	79281414	19,11	108,74	21,72				315	133,27	127,85	0,41	0,45	19373,93	0,13	705,73	127,85	0,41	0,45
71133854	916434217	78595639	19,49	78,33	21,53				315	104,68	97,81	0,41	0,45	19373,93	0,13	705,73	97,81	0,41	0,45
72525288	573624106	73308553	19,87	49,03	20,08				315	77,18	68,90	0,41	0,45	19373,93	0,13	705,73	68,90	0,41	0,45
73916721	270798624	61531321	20,25	23,15	16,86				315	52,30	43,39	0,41	0,45	19373,93	0,13	705,73	43,39	0,41	0,45
75230853	60315138,9	33322419	20,61	5,16	9,13				315	30,23	25,77	0,41	0,45	19373,93	0,13	705,73	25,77	0,41	0,45

Local Buckling, Eurocode

$f_{b,0}$ [MPa]	$f_{t,c}$ [MPa]	λ	$f_{b,d}$ [MPa]	UC
1148,72	147,97	0,55	301,21	0,27
1271,88	166,69	0,51	285,67	0,27
1271,88	166,69	0,51	285,15	0,28
1271,88	166,69	0,53	284,29	0,29
1395,18	185,84	0,51	285,27	0,28
1395,18	185,84	0,52	284,67	0,30
1395,18	185,84	0,53	284,28	0,33
1518,58	205,40	0,51	285,79	0,33
1518,58	205,40	0,51	285,76	0,36
1642,07	225,33	0,49	287,15	0,36
1642,07	225,33	0,48	287,24	0,39
1642,07	225,33	0,48	287,35	0,42
1484,92	209,79	0,51	285,59	0,38
1251,34	179,15	0,56	281,74	0,37
1054,10	152,65	0,61	276,47	0,38
959,61	136,92	0,64	273,17	0,44
1054,10	152,65	0,61	276,96	0,43
1054,10	152,65	0,60	277,21	0,46
1054,10	152,65	0,60	277,47	0,48
1148,72	168,71	0,57	280,35	0,47
1148,72	168,71	0,57	280,55	0,50
1243,45	185,09	0,55	282,78	0,49
1243,45	185,09	0,54	283,01	0,51
1243,45	185,09	0,52	284,83	0,51
1243,45	185,09	0,58	279,48	0,51
1148,72	168,71	0,64	273,38	0,53
1054,10	152,65	0,70	264,42	0,53
959,61	136,92	0,78	252,45	0,51
771,17	106,54	0,96	232,23	0,55
771,17	106,54	1,03	215,42	0,45
771,17	106,54	1,13	193,81	0,36
771,17	106,54	1,25	168,87	0,26
771,17	106,54	1,22	175,84	0,15

α_x [MPa]	δ_{uk} [m]	α_x	λ_{yx}	u	$\sigma_{x,ker}$ [MPa]	λ_x	χ_x	τ_x	$\tau_{x,ker}$ [MPa]	λ_{pc}
82,44	0,03	0,47	1,09	154,15	2480,50	0,36	0,89	1,17	247,67	1,27
76,98	0,03	0,48	1,10	146,98	2728,55	0,33	0,91	1,07	279,01	1,27
79,56	0,03	0,48	1,10	146,98	2728,55	0,33	0,91	1,44	279,01	1,27
83,18	0,03	0,48	1,10	146,98	2728,55	0,33	0,91	2,06	279,01	1,27
80,91	0,03	0,49	1,10	140,72	2976,60	0,31	0,92	2,60	311,06	1,27
86,60	0,03	0,49	1,10	140,72	2976,60	0,31	0,92	3,24	311,06	1,27
93,40	0,03	0,49	1,10	140,72	2976,60	0,31	0,92	3,81	311,06	1,27
93,68	0,03	0,49	1,11	135,20	3224,65	0,30	0,93	3,96	343,80	1,27
101,68	0,03	0,49	1,11	135,20	3224,65	0,30	0,93	4,33	343,80	1,27
102,81	0,03	0,50	1,12	130,28	3472,70	0,29	0,94	4,32	377,17	1,27
111,47	0,03	0,50	1,12	130,28	3472,70	0,29	0,94	4,57	377,17	1,27
120,54	0,03	0,50	1,12	130,28	3472,70	0,29	0,94	4,79	377,17	1,27
107,78	0,04	0,49	1,11	124,22	3157,00	0,31	0,93	4,55	351,15	1,27
105,02	0,04	0,48	1,10	123,42	2687,21	0,33	0,91	4,68	299,86	1,27
104,17	0,04	0,47	1,08	123,42	2289,69	0,36	0,89	4,88	255,50	1,27
121,30	0,03	0,46	1,07	128,91	2098,88	0,37	0,88	5,54	229,17	1,27
118,95	0,04	0,47	1,08	123,42	2289,69	0,36	0,89	5,25	255,50	1,27
126,67	0,04	0,47	1,08	123,42	2289,69	0,36	0,89	5,40	255,50	1,27
134,56	0,04	0,47	1,08	123,42	2289,69	0,36	0,89	5,54	255,50	1,27
131,95	0,04	0,47	1,09	118,58	2480,50	0,34	0,90	5,23	282,39	1,27
139,57	0,04	0,47	1,09	118,58	2480,50	0,34	0,90	5,34	282,39	1,27
137,29	0,04	0,48	1,09	114,26	2671,31	0,33	0,91	5,06	309,80	1,27
143,49	0,04	0,48	1,09	114,26	2671,31	0,33	0,91	5,02	309,80	1,27
144,84	0,04	0,48	1,09	114,26	2671,31	0,33	0,91	2,83	309,80	1,27
143,81	0,04	0,48	1,09	114,26	2671,31	0,33	0,91	8,97	309,80	1,27
144,22	0,04	0,47	1,09	118,58	2480,50	0,34	0,90	12,14	282,39	1,27
139,97	0,04	0,47	1,08	123,42	2289,69	0,36	0,89	15,30	255,50	1,27
129,20	0,03	0,46	1,07	128,91	2098,88	0,37	0,88	17,65	229,17	1,27
127,85	0,03	0,44	1,05	142,51	1717,27	0,43	0,84	21,72	178,33	1,27
97,81	0,03	0,44	1,05	142,51	1717,27	0,43	0,84	21,53	178,33	1,27
68,90	0,03	0,44	1,05	142,51	1717,27	0,43	0,84	20,08	178,33	1,27
43,39	0,03	0,44	1,05	142,51	1717,27	0,43	0,84	16,86	178,33	1,27
25,77	0,03	0,44	1,05	142,51	1717,27	0,43	0,84	9,13	178,33	1,27

Column Buckling, DNV										Column Buckling, Eurocode				
λ_c	χ_c	k_c	$\sigma_{x,rd}$ [Mpa]	$\tau_{x,rd}$ [Mpa]	UC	i_c [m]	f_{sk} [Mpa]	λ_c	f_{kc} [Mpa]	f_E [Mpa]	UC	$A_{c,eff}$ [m²]	w_{eff} [m³]	
0,86	0,69	1,92	256,10	113,52	0,11	3,50	302,28	0,76	469,47	521,63	0,29	2,60	8,01	
0,78	0,74	1,94	245,06	114,34	0,11	3,50	286,41	0,74	468,53	520,59	0,29	3,10	9,15	
0,78	0,74	1,94	245,06	114,34	0,11	3,50	286,41	0,74	468,53	520,59	0,30	3,10	9,15	
0,78	0,74	1,94	245,06	114,34	0,12	3,50	286,41	0,74	468,53	520,59	0,31	3,10	9,15	
0,74	0,77	1,94	247,75	118,73	0,11	3,49	287,87	0,74	467,60	519,55	0,30	3,52	10,17	
0,74	0,77	1,94	247,75	118,73	0,13	3,49	287,87	0,74	467,60	519,55	0,32	3,52	10,17	
0,74	0,77	1,94	247,75	118,73	0,15	3,49	287,87	0,74	467,60	519,55	0,35	3,52	10,17	
0,70	0,79	1,95	250,08	122,57	0,15	3,49	288,99	0,75	466,66	518,51	0,35	3,97	11,21	
0,70	0,79	1,95	250,08	122,57	0,17	3,49	288,99	0,75	466,66	518,51	0,38	3,97	11,21	
0,67	0,81	1,96	252,13	125,95	0,17	3,49	289,87	0,75	465,73	517,48	0,38	4,43	12,26	
0,67	0,81	1,96	252,13	125,95	0,20	3,49	289,87	0,75	465,73	517,48	0,42	4,43	12,26	
0,67	0,81	1,96	252,13	125,95	0,24	3,49	289,87	0,75	465,73	517,48	0,45	4,43	12,26	
0,70	0,80	1,95	249,47	123,35	0,20	3,84	288,71	0,68	564,97	627,74	0,40	4,65	14,54	
0,75	0,76	1,93	244,57	117,28	0,20	4,20	286,13	0,62	674,91	749,90	0,39	4,36	15,52	
0,82	0,71	1,93	239,13	110,61	0,21	4,55	282,52	0,57	794,63	882,92	0,39	4,03	16,23	
0,86	0,68	1,91	235,90	105,76	0,28	4,56	279,99	0,56	795,85	884,28	0,46	3,54	14,59	
0,82	0,71	1,92	239,13	110,61	0,26	4,55	282,52	0,57	794,63	882,92	0,44	4,03	16,23	
0,82	0,71	1,93	239,13	110,61	0,30	4,55	282,52	0,57	794,63	882,92	0,47	4,03	16,23	
0,82	0,71	1,93	239,13	110,61	0,33	4,55	282,52	0,57	794,63	882,92	0,50	4,03	16,23	
0,78	0,74	1,93	241,93	114,84	0,31	4,55	284,47	0,57	793,40	881,56	0,49	4,54	17,90	
0,74	0,77	1,93	244,38	118,57	0,33	4,55	286,01	0,57	792,18	880,21	0,51	5,07	19,59	
0,74	0,77	1,93	244,38	118,57	0,36	4,55	286,01	0,57	792,18	880,21	0,53	5,07	19,59	
0,74	0,77	1,93	244,38	118,57	0,36	4,55	286,01	0,57	792,18	880,21	0,54	5,07	19,59	
0,74	0,77	1,93	244,38	118,57	0,37	4,55	286,01	0,57	792,18	880,21	0,53	5,07	19,59	
0,78	0,74	1,93	241,93	114,84	0,38	4,55	284,47	0,57	793,40	881,56	0,53	4,54	17,90	
0,82	0,71	1,93	239,13	110,61	0,38	4,55	282,52	0,57	794,63	882,92	0,51	4,03	16,23	
0,86	0,68	1,91	235,90	105,76	0,35	4,56	279,99	0,56	795,85	884,28	0,48	3,54	14,59	
1,01	0,58	1,88	240,26	96,17	0,37	4,56	287,65	0,57	798,30	887,00	0,45	2,54	11,22	
1,01	0,58	1,88	240,26	96,17	0,24	4,56	287,65	0,57	798,30	887,00	0,33	2,54	11,22	
1,01	0,58	1,88	240,26	96,17	0,15	4,56	287,65	0,57	798,30	887,00	0,22	2,54	11,22	
1,01	0,58	1,88	240,26	96,17	0,08	4,56	287,65	0,57	798,30	887,00	0,12	2,54	11,22	
1,01	0,58	1,88	240,26	96,17	0,03	4,56	287,65	0,57	798,30	887,00	0,05	2,54	11,22	

Eurocode														UC _{max}
N _{Ed} [MN]	M _{Ed} [MNm]	λ ₁	λ _{c,eff} [m]	λ	φ	χ	N _{Rk} [MN]	M _{Rk} [MNm]	N _{cr} [MN]	ζ _{gy}	μ	k _{yy}	UC	
20,56	577,93	80,14	3,83	0,65	0,82	0,76	744,32	2294,80	1622,37	0,99	1,00	1,00	0,29	0,29
21,58	590,69	82,82	3,67	0,68	0,85	0,74	830,17	2453,65	1779,25	0,99	1,00	1,00	0,28	0,29
22,88	609,03	82,82	3,67	0,68	0,85	0,74	830,17	2453,65	1779,25	0,99	1,00	1,00	0,29	0,30
24,21	636,00	82,82	3,67	0,68	0,85	0,74	830,17	2453,65	1779,25	0,99	1,00	1,00	0,30	0,31
25,70	672,81	82,82	3,59	0,71	0,88	0,72	944,95	2727,35	1935,16	0,99	1,00	1,00	0,29	0,30
27,18	720,92	82,82	3,59	0,71	0,88	0,72	944,95	2727,35	1935,16	0,99	1,00	1,00	0,31	0,32
28,68	779,11	82,82	3,59	0,71	0,88	0,72	944,95	2727,35	1935,16	0,99	1,00	1,00	0,33	0,35
30,28	846,09	82,82	3,52	0,74	0,91	0,70	1064,42	3005,28	2090,12	0,99	1,00	1,00	0,33	0,35
31,89	920,70	82,82	3,52	0,74	0,91	0,70	1064,42	3005,28	2090,12	0,98	1,00	1,00	0,36	0,38
33,61	1002,20	82,82	3,45	0,77	0,94	0,68	1188,36	3287,06	2244,12	0,99	1,00	1,00	0,35	0,38
35,33	1089,22	82,82	3,45	0,77	0,94	0,68	1188,36	3287,06	2244,12	0,98	0,99	0,99	0,38	0,42
37,05	1180,67	82,82	3,45	0,77	0,94	0,68	1188,36	3287,06	2244,12	0,98	0,99	0,99	0,42	0,45
38,84	1276,00	82,82	3,89	0,67	0,84	0,74	1247,97	3898,61	2998,40	0,99	1,00	1,00	0,38	0,40
40,67	1375,17	82,82	4,43	0,56	0,75	0,81	1168,57	4161,84	3635,37	0,99	1,00	1,00	0,38	0,39
42,50	1478,23	82,82	5,00	0,48	0,68	0,85	1080,43	4352,73	4287,13	0,99	1,00	1,00	0,40	0,40
44,28	1585,13	82,82	5,11	0,46	0,67	0,87	948,96	3913,19	3938,98	0,99	1,00	1,00	0,47	0,47
46,20	1695,47	82,82	5,00	0,48	0,68	0,85	1080,43	4352,73	4287,13	0,99	1,00	1,00	0,45	0,45
48,11	1808,84	82,82	5,00	0,48	0,68	0,85	1080,43	4352,73	4287,13	0,99	1,00	1,00	0,48	0,48
50,05	1924,93	82,82	5,00	0,48	0,68	0,85	1080,43	4352,73	4287,13	0,99	1,00	1,00	0,51	0,51
52,11	2043,48	82,82	4,90	0,50	0,70	0,84	1217,31	4799,64	4633,66	0,99	1,00	1,00	0,49	0,49
54,20	2164,29	82,82	4,90	0,50	0,70	0,84	1217,31	4799,64	4633,66	0,99	1,00	1,00	0,52	0,52
56,42	2290,52	82,82	4,80	0,52	0,71	0,83	1359,38	5253,32	4978,55	0,99	1,00	1,00	0,50	0,51
58,57	2395,20	82,82	4,80	0,52	0,71	0,83	1359,38	5253,32	4978,55	0,99	1,00	1,00	0,54	0,54
60,73	2412,67	82,82	4,80	0,52	0,71	0,83	1359,38	5253,32	4978,55	0,99	1,00	1,00	0,53	0,54
62,87	2387,23	82,82	4,80	0,52	0,71	0,83	1359,38	5253,32	4978,55	0,99	1,00	1,00	0,53	0,54
64,85	2208,25	82,82	4,90	0,50	0,70	0,84	1217,31	4799,64	4633,66	0,99	1,00	1,00	0,54	0,54
66,69	1940,25	82,82	5,00	0,48	0,68	0,85	1080,43	4352,73	4287,13	0,98	1,00	1,00	0,52	0,53
68,35	1620,66	82,82	5,11	0,46	0,67	0,87	948,96	3913,19	3938,98	0,98	1,00	1,00	0,50	0,51
69,74	1272,26	80,14	5,47	0,41	0,64	0,89	726,85	3213,43	3237,75	0,98	1,00	1,00	0,49	0,55
71,13	916,43	80,14	5,47	0,41	0,64	0,89	726,85	3213,43	3237,75	0,98	1,00	1,00	0,37	0,45
72,53	573,62	80,14	5,47	0,41	0,64	0,89	726,85	3213,43	3237,75	0,98	1,00	1,00	0,25	0,36
73,92	270,80	80,14	5,47	0,41	0,64	0,89	726,85	3213,43	3237,75	0,98	1,00	1,00	0,15	0,26
75,23	60,32	80,14	5,47	0,41	0,64	0,89	726,85	3213,43	3237,75	0,98	1,00	1,00	0,08	0,15

A.3. Fatigue Limit State

Fatigue Limit State Geometry and DEM		Stress Concentration Factors												
		Weld Number		z [m]	D	[m]	t _z [m]	ΔM _{eq} [MNm]	L [mm]	α	β	δ _t [mm]	δ _m [mm]	δ _{0.1n} [mm]
	Circular weld at bottom of can 1	13,00	10,00	0,10	0,11	272,15	40,00	0,03	1,75	5,00	4,00	0,00		
	Circular weld at bottom of can 2	9,50	10,00	0,11	0,11	280,08	0,00	0,00	1,77	0,00	4,00	0,00		
	Circular weld at bottom of can 3	5,00	10,00	0,11	0,11	290,40	0,00	0,00	1,77	0,00	4,00	0,00		
	Circular weld at bottom of can 4	0,50	10,00	0,11	0,12	300,85	40,00	0,03	1,77	5,00	4,00	0,00		
	Circular weld at bottom of can 5	-4,00	10,00	0,12	0,12	311,71	0,00	0,00	1,79	0,00	4,00	0,00		
	Circular weld at bottom of can 6	-8,50	10,00	0,12	0,12	323,49	0,00	0,00	1,79	0,00	4,00	0,00		
	Circular weld at bottom of can 7	-13,00	10,00	0,12	0,13	336,31	40,00	0,03	1,79	5,00	4,00	0,00		
	Circular weld at bottom of can 8	-17,50	10,00	0,13	0,13	350,29	0,00	0,00	1,81	0,00	4,00	0,00		
	Circular weld at bottom of can 9	-22,00	10,00	0,13	0,14	365,51	40,00	0,03	1,81	5,00	4,00	0,00		
	Circular weld at bottom of can 10	-26,50	10,00	0,14	0,14	381,99	0,00	0,00	1,83	0,00	4,00	0,00		
	Circular weld at bottom of can 11	-31,00	10,00	0,14	0,14	399,68	0,00	0,00	1,83	0,00	4,00	0,00		
	Circular weld at bottom of can 12	-35,50	10,00	0,14	0,14	418,49	0,00	0,00	1,83	0,00	4,00	0,00		
	Circular weld at bottom of can 13	-40,00	11,00	0,14	0,13	438,28	40,00	0,03	1,79	5,00	4,00	0,00		
	Circular weld at bottom of can 14	-44,50	12,00	0,13	0,12	458,97	40,00	0,03	1,75	5,00	4,00	0,00		
	Circular weld at bottom of can 15	-49,00	13,00	0,12	0,11	480,50	40,00	0,03	1,72	5,00	4,00	0,00		
	Circular weld at bottom of can 16	-53,50	13,00	0,11	0,12	502,80	40,00	0,03	1,72	5,00	4,00	0,00		
	Circular weld at bottom of can 17	-58,00	13,00	0,12	0,12	525,82	0,00	0,00	1,73	0,00	4,00	0,00		
	Circular weld at bottom of can 18	-62,50	13,00	0,12	0,12	549,53	0,00	0,00	1,73	0,00	4,00	0,00		
	Circular weld at bottom of can 19	-67,00	13,00	0,12	0,13	573,92	40,00	0,03	1,73	5,00	4,00	0,00		
	Circular weld at bottom of can 20	-71,50	13,00	0,13	0,13	598,99	0,00	0,00	1,75	0,00	4,00	0,00		
	Circular weld at bottom of can 21	-76,00	13,00	0,13	0,14	624,70	40,00	0,03	1,75	5,00	4,00	0,00		
	Circular weld at bottom of can 22	-80,50	13,00	0,14	0,14	651,01	0,00	0,00	1,77	0,00	4,00	0,00		
	Circular weld at bottom of can 23	-85,00	13,00	0,14	0,14	671,21	0,00	0,00	1,77	0,00	4,00	0,00		
	Circular weld at bottom of can 24	-89,50	13,00	0,14	0,14	664,42	0,00	0,00	1,77	0,00	4,00	0,00		
	Circular weld at bottom of can 25	-94,00	13,00	0,14	0,13	615,82	40,00	0,03	1,75	5,00	4,00	0,00		
	Circular weld at bottom of can 26	-98,50	13,00	0,13	0,12	541,64	40,00	0,03	1,73	5,00	4,00	0,00		
	Circular weld at bottom of can 27	-103,00	13,00	0,12	0,11	453,93	40,00	0,03	1,72	5,00	4,00	0,00		
	Circular weld at bottom of can 28	-107,50	13,00	0,11	0,09	358,31	80,00	0,06	1,68	10,00	4,00	0,00		
	Circular weld at bottom of can 29	-112,00	13,00	0,09	0,09	260,56	0,00	0,00	1,68	0,00	4,00	0,00		
	Circular weld at bottom of can 30	-116,50	13,00	0,09	0,09	166,01	0,00	0,00	1,68	0,00	4,00	0,00		
	Circular weld at bottom of can 31	-121,00	13,00	0,09	0,09	81,75	0,00	0,00	1,68	0,00	4,00	0,00		
	Circular weld at bottom of can 32	-125,50	13,00	0,09	0,09	20,72	0,00	0,00	1,68	0,00	4,00	0,00		

Fatigue damage external weld					Fatigue damage internal weld									
$\delta_{\text{e,out}}$ [mm]	SCF inside	SCF inside	Thk. Factor	$\Delta\sigma_{\text{nom}}$ [MPa]	$\Delta\sigma_{\text{e}}$ [MPa]	Fatigue damage	D_{ext} [m]	$\Delta\sigma_{\text{nom}}$ [MPa]	Thk. Factor	$\Delta\sigma_{\text{e}}$ [MPa]	Fatigue damage			
0,00	1,24	0,97		10,00	34,99	1,15	49,82	0,25		9,80	35,71	1,15	39,93	0,08
0,00	1,11	1,11		10,00	32,77	1,16	42,15	0,11		9,78	33,51	1,16	43,10	0,12
0,00	1,11	1,11		10,00	33,98	1,16	43,70	0,13		9,78	34,74	1,16	44,69	0,15
0,00	1,22	0,98		10,00	35,20	1,16	49,78	0,25		9,78	35,99	1,16	40,72	0,09
0,00	1,10	1,10		10,00	33,46	1,17	43,06	0,12		9,76	34,29	1,17	44,12	0,14
0,00	1,10	1,10		10,00	34,73	1,17	44,69	0,15		9,76	35,58	1,17	45,79	0,17
0,00	1,20	0,98		10,00	36,11	1,17	50,79	0,28		9,76	36,99	1,17	42,30	0,11
0,00	1,09	1,09		10,00	34,75	1,18	44,76	0,15		9,74	35,68	1,18	45,95	0,17
0,00	1,19	0,98		10,00	36,26	1,18	50,80	0,28		9,74	37,23	1,18	42,98	0,12
0,00	1,09	1,09		10,00	35,22	1,19	45,43	0,16		9,72	36,23	1,19	46,74	0,19
0,00	1,09	1,09		10,00	36,85	1,19	47,53	0,20		9,72	37,91	1,19	48,90	0,23
0,00	1,09	1,09		10,00	38,58	1,19	49,77	0,25		9,72	39,70	1,19	51,20	0,29
0,00	1,19	0,98		11,00	35,89	1,18	50,30	0,27		10,74	36,76	1,18	42,44	0,11
0,00	1,20	0,98		12,00	34,15	1,17	48,08	0,21		11,76	34,85	1,17	39,85	0,08
0,00	1,22	0,98		13,00	33,19	1,16	46,99	0,19		12,78	33,76	1,16	38,19	0,07
0,00	1,22	0,98		13,00	34,73	1,16	49,17	0,24		12,78	35,32	1,16	39,96	0,08
0,00	1,10	1,10		13,00	33,31	1,17	42,87	0,12		12,76	33,94	1,17	43,68	0,13
0,00	1,10	1,10		13,00	34,82	1,17	44,80	0,15		12,76	35,47	1,17	45,65	0,16
0,00	1,20	0,98		13,00	36,36	1,17	51,21	0,29		12,76	37,05	1,17	42,36	0,11
0,00	1,09	1,09		13,00	35,06	1,18	45,16	0,16		12,74	35,77	1,18	46,08	0,17
0,00	1,19	0,98		13,00	36,56	1,18	51,27	0,29		12,74	37,31	1,18	43,07	0,12
0,00	1,09	1,09		13,00	35,41	1,19	45,67	0,16		12,72	36,19	1,19	46,67	0,18
0,00	1,09	1,09		13,00	36,50	1,19	47,09	0,19		12,72	37,31	1,19	48,12	0,21
0,00	1,09	1,09		13,00	36,14	1,19	46,61	0,18		12,72	36,93	1,19	47,64	0,20
0,00	1,19	0,98		13,00	36,04	1,18	50,54	0,27		12,74	36,78	1,18	42,46	0,11
0,00	1,20	0,98		13,00	34,32	1,17	48,33	0,22		12,76	34,96	1,17	39,97	0,08
0,00	1,22	0,98		13,00	31,35	1,16	44,39	0,14		12,78	31,89	1,16	36,08	0,05
0,00	1,37	0,84		13,00	30,20	1,14	46,94	0,19		12,82	30,62	1,14	29,33	0,02
0,00	1,13	1,13		13,00	21,96	1,14	28,29	0,02		12,82	22,27	1,14	28,69	0,02
0,00	1,13	1,13		13,00	13,99	1,14	18,03	0,00		12,82	14,19	1,14	18,28	0,00
0,00	1,13	1,13		13,00	6,89	1,14	8,88	0,00		12,82	6,99	1,14	9,00	0,00
0,00	1,13	1,13		13,00	1,75	1,14	2,75	0,00		12,82	1,77	1,14	2,22	0,00

B

Results Guyed Monopile

B.1. Geometry

Geometry										Geometric design criteria				
Cans	Diameter [m]	thickness [m]	Length [m]	Top elev.[m]	Bottom elev.[m]	Area [m²]	Section Modulus [m³]	Moment of inertia [m⁴]	Slenderness [-]	Cross section class[-]	D/t ratio [-]	thickness s [-]	length [-]	Thickness slope [-]
1	10	0,11	4	16	12	3,417739	8,3584387	41,792194	90,90909	4	0,57	0,00	0,89	0,00
2	10	0,11	4,5	12	7,5	3,417739	8,3584387	41,792194	90,90909	4	0,57	0,00	1,00	0,00
3	10	0,11	4,5	7,5	3	3,417739	8,3584387	41,792194	90,90909	4	0,57	0,00	1,00	0,00
4	10	0,11	4,5	3	-1,5	3,417739	8,3584387	41,792194	90,90909	4	0,57	0,00	1,00	0,50
5	10	0,1	4,5	-1,5	-6	3,110177	7,6214881	38,10744	100	4	0,63	0,00	1,00	0,00
6	10	0,1	4,5	-6	-10,5	3,110177	7,6214881	38,10744	100	4	0,63	0,00	1,00	0,00
7	10	0,1	4,5	-10,5	-15	3,110177	7,6214881	38,10744	100	4	0,63	0,00	1,00	0,50
8	10	0,09	4,5	-15	-19,5	2,801986	6,8800116	34,400058	111,1111	4	0,69	0,00	1,00	0,00
9	10	0,09	4,5	-19,5	-24	2,801986	6,8800116	34,400058	111,1111	4	0,69	0,00	1,00	0,00
10	10	0,09	4,5	-24	-28,5	2,801986	6,8800116	34,400058	111,1111	4	0,69	0,00	1,00	0,00
11	10	0,09	4,5	-28,5	-33	2,801986	6,8800116	34,400058	111,1111	4	0,69	0,00	1,00	0,50
12	10	0,08	4,5	-33	-37,5	2,493168	6,1339909	30,669955	125	4	0,78	0,00	1,00	0,00
13	10	0,08	4,5	-37,5	-42	2,493168	6,1339909	30,669955	125	4	0,78	0,00	1,00	0,00
14	10	0,08	4,5	-42	-46,5	2,493168	6,1339909	30,669955	125	4	0,78	0,00	1,00	0,00
15	10	0,08	4,5	-46,5	-51	2,493168	6,1339909	30,669955	125	4	0,78	0,00	1,00	0,00
16	10	0,08	4,5	-51	-55,5	2,493168	6,1339909	30,669955	125	4	0,78	0,00	1,00	0,00
17	10	0,08	4,5	-55,5	-60	2,493168	6,1339909	30,669955	125	4	0,78	0,00	1,00	0,00
18	10	0,08	4,5	-60	-64,5	2,493168	6,1339909	30,669955	125	4	0,78	0,00	1,00	0,00
19	10	0,08	4,5	-64,5	-69	2,493168	6,1339909	30,669955	125	4	0,78	0,00	1,00	0,00
20	10	0,08	4,5	-69	-73,5	2,493168	6,1339909	30,669955	125	4	0,78	0,00	1,00	0,00
21	10	0,08	4,5	-73,5	-78	2,493168	6,1339909	30,669955	125	4	0,78	0,00	1,00	0,00
22	10	0,08	4,5	-78	-82,5	2,493168	6,1339909	30,669955	125	4	0,78	0,00	1,00	0,50
23	10	0,07	4,5	-82,5	-87	2,183721	5,3834074	26,917037	142,8571	4	0,89	0,00	1,00	0,00
24	10	0,07	4,5	-87	-91,5	2,183721	5,3834074	26,917037	142,8571	4	0,89	0,00	1,00	0,00
25	10	0,07	4,5	-91,5	-96	2,183721	5,3834074	26,917037	142,8571	4	0,89	0,00	1,00	0,00
26	10	0,07	4,5	-96	-100,5	2,183721	5,3834074	26,917037	142,8571	4	0,89	0,00	1,00	0,00
27	10	0,07	4,5	-100,5	-105	2,183721	5,3834074	26,917037	142,8571	4	0,89	0,00	1,00	0,00

B.2. Ultimate Limit State

Ultimate Limit State										Yield check				Local Buckling, DNV						
Internal forces and stresses										Yield check				Local Buckling, DNV						
Maximum axial force [N]	Maximum bending force [Nm]	Maximum shear force [N]	Maximum axial stress [Mpa]	Maximum bending stress [Mpa]	Maximum shear stress [Mpa]					Yield strength f_y [Mpa]	σ_1 [Mpa]	σ_2 [Mpa]	UC	σ_1 [Mpa]	ρ_a	ρ_b	Z_1	f_{t1} [Mpa]	f_{t3} [Mpa]	
20930499	593516233	13771507	6,12	71,01	4,03					295,00	77,45	77,13	0,29	77,13	0,44	0,47	19488,11	0,20	1195,65	
22233314	623346997	13771507	6,51	74,58	4,03					295,00	81,38	81,08	0,30	81,08	0,44	0,47	19488,11	0,20	1195,65	
23534552	652891715	13771507	6,89	78,11	4,03					295,00	85,28	85,00	0,32	85,00	0,44	0,47	19488,11	0,20	1195,65	
24874526	675647378	13739893	7,28	80,83	4,02					295,00	88,39	88,11	0,33	88,11	0,44	0,47	19488,11	0,20	1195,65	
26124442	684035246	11534053	8,40	89,75	3,71					315,00	98,36	98,15	0,34	98,15	0,43	0,46	21436,92	0,16	1074,53	
27374358	684163209	8667697	8,80	89,77	2,79					315,00	98,69	98,57	0,34	98,57	0,43	0,46	21436,92	0,16	1074,53	
28611363	680073806	6336176	9,20	89,23	2,04					315,00	98,49	98,43	0,34	98,43	0,43	0,46	21436,92	0,16	1074,53	
29743799	666827970	6420515	10,62	96,92	2,29					315,00	107,61	107,54	0,38	107,54	0,43	0,46	23818,80	0,13	953,92	
30876235	645181941	7778090	11,02	93,78	2,78					315,00	104,91	104,80	0,37	104,80	0,43	0,46	23818,80	0,13	953,92	
32008672	616125972	8952941	11,42	89,55	3,20					315,00	101,13	100,98	0,35	100,98	0,43	0,46	23818,80	0,13	953,92	
33128171	581613870	9968405	11,82	84,54	3,56					315,00	96,56	96,36	0,34	96,36	0,43	0,46	23818,80	0,13	953,92	
34142888	541958115	10927073	13,69	88,35	4,38					325,00	102,33	102,05	0,35	102,05	0,42	0,45	26796,15	0,11	833,96	
35157605	498351458	11756973	14,10	81,24	4,72					325,00	95,70	95,35	0,32	95,35	0,42	0,45	26796,15	0,11	833,96	
36172322	451886387	12474643	14,51	73,67	5,00					325,00	88,60	88,18	0,30	88,18	0,42	0,45	26796,15	0,11	833,96	
37187040	403885571	13099041	14,92	65,84	5,25					325,00	81,27	80,76	0,28	80,76	0,42	0,45	26796,15	0,11	833,96	
38201757	385610410	13646323	15,32	62,86	5,47					325,00	78,76	78,19	0,27	78,19	0,42	0,45	26796,15	0,11	833,96	
39216474	410099704	14130344	15,73	66,86	5,67					325,00	83,17	82,59	0,28	82,59	0,42	0,45	26796,15	0,11	833,96	
40231191	439201803	14563061	16,14	71,60	5,84					325,00	88,32	87,74	0,30	87,74	0,42	0,45	26796,15	0,11	833,96	
41245908	470906593	14954852	16,54	76,77	6,00					325,00	93,89	93,31	0,32	93,31	0,42	0,45	26796,15	0,11	833,96	
42260625	504075620	15314715	16,95	82,18	6,14					325,00	99,70	99,13	0,34	99,13	0,42	0,45	26796,15	0,11	833,96	
43275343	538596659	15650210	17,36	87,81	6,28					325,00	105,72	105,16	0,36	105,16	0,42	0,45	26796,15	0,11	833,96	
44242358	570962349	15828105	17,75	93,08	6,35					325,00	111,37	110,83	0,38	110,83	0,42	0,45	26796,15	0,11	833,96	
45074775	573155562	15393473	20,64	106,47	7,05					325,00	127,69	127,11	0,43	127,11	0,41	0,45	30624,17	0,08	714,85	
45907192	538422656	38548020	21,02	100,02	17,65					325,00	124,84	121,04	0,42	121,04	0,41	0,45	30624,17	0,08	714,85	
46739610	401042255	42803128	21,40	74,50	19,64					325,00	101,75	95,90	0,34	95,90	0,41	0,45	30624,17	0,08	714,85	
47572027	211092438	41522801	21,78	39,21	19,01					325,00	69,32	61,00	0,23	61,00	0,41	0,45	30624,17	0,08	714,85	
48358199	53334027	27279517	22,14	9,91	12,49					325,00	38,67	32,05	0,13	32,05	0,41	0,45	30624,17	0,08	714,85	

Local Buckling, Eurocode

f_{tb} [Mpa]	f_{ec} [Mpa]	λ	$f_{t,b,d}$ [Mpa]	UC	α_x [Mpa]	$\delta_{a,k}$ [m]	α_x	λ_{px}	w	$\sigma_{x,RCF}$ [Mpa]	λ_x	χ_x	τ_x	$\tau_{x0,RCF}$ [Mpa]	λ_{pt}
1271,88	169,03	0,57	280,61	0,27	77,13	0,03	0,48	1,10	142,93	2728,55	0,33	0,91	4,03	282,93	1,27
1271,88	169,03	0,57	280,98	0,29	81,08	0,03	0,48	1,10	142,93	2728,55	0,33	0,91	4,03	282,93	1,27
1271,88	169,03	0,56	281,30	0,30	85,00	0,03	0,48	1,10	142,93	2728,55	0,33	0,91	4,03	282,93	1,27
1271,88	169,03	0,56	281,55	0,31	88,11	0,03	0,48	1,10	142,93	2728,55	0,33	0,91	4,02	282,93	1,27
1148,72	150,05	0,60	296,83	0,33	98,15	0,03	0,47	1,09	149,91	2480,50	0,36	0,89	3,71	251,15	1,27
1148,72	150,05	0,58	298,66	0,33	98,57	0,03	0,47	1,09	149,91	2480,50	0,36	0,89	2,79	251,15	1,27
1148,72	150,05	0,57	300,06	0,33	98,43	0,03	0,47	1,09	149,91	2480,50	0,36	0,89	2,04	251,15	1,27
1025,74	131,53	0,60	296,34	0,36	107,54	0,03	0,46	1,08	158,02	2232,45	0,38	0,88	2,29	220,16	1,27
1025,74	131,53	0,61	295,14	0,36	104,80	0,03	0,46	1,08	158,02	2232,45	0,38	0,88	2,78	220,16	1,27
1025,74	131,53	0,62	293,92	0,34	100,98	0,03	0,46	1,08	158,02	2232,45	0,38	0,88	3,20	220,16	1,27
1025,74	131,53	0,63	292,64	0,33	96,36	0,03	0,46	1,08	158,02	2232,45	0,38	0,88	3,56	220,16	1,27
903,00	113,52	0,70	292,21	0,35	102,05	0,03	0,45	1,07	167,60	1984,40	0,40	0,86	4,38	190,02	1,27
903,00	113,52	0,71	290,00	0,33	95,35	0,03	0,45	1,07	167,60	1984,40	0,40	0,86	4,72	190,02	1,27
903,00	113,52	0,73	287,49	0,31	88,18	0,03	0,45	1,07	167,60	1984,40	0,40	0,86	5,00	190,02	1,27
903,00	113,52	0,74	284,57	0,28	80,76	0,03	0,45	1,07	167,60	1984,40	0,40	0,86	5,25	190,02	1,27
903,00	113,52	0,75	282,82	0,28	78,19	0,03	0,45	1,07	167,60	1984,40	0,40	0,86	5,47	190,02	1,27
903,00	113,52	0,75	283,32	0,29	82,59	0,03	0,45	1,07	167,60	1984,40	0,40	0,86	5,67	190,02	1,27
903,00	113,52	0,75	284,05	0,31	87,74	0,03	0,45	1,07	167,60	1984,40	0,40	0,86	5,84	190,02	1,27
903,00	113,52	0,74	284,86	0,33	93,31	0,03	0,45	1,07	167,60	1984,40	0,40	0,86	6,00	190,02	1,27
903,00	113,52	0,74	285,68	0,35	99,13	0,03	0,45	1,07	167,60	1984,40	0,40	0,86	6,14	190,02	1,27
903,00	113,52	0,73	286,48	0,37	105,16	0,03	0,45	1,07	167,60	1984,40	0,40	0,86	6,28	190,02	1,27
903,00	113,52	0,73	287,32	0,39	110,83	0,03	0,45	1,07	167,60	1984,40	0,40	0,86	6,35	190,02	1,27
780,57	96,07	0,78	277,43	0,46	127,11	0,02	0,44	1,05	179,17	1736,35	0,43	0,84	7,05	160,81	1,27
780,57	96,07	0,96	239,61	0,51	121,04	0,02	0,44	1,05	179,17	1736,35	0,43	0,84	17,65	160,81	1,27
780,57	96,07	1,06	216,71	0,44	95,90	0,02	0,44	1,05	179,17	1736,35	0,43	0,84	19,64	160,81	1,27
780,57	96,07	1,22	181,57	0,34	61,00	0,02	0,44	1,05	179,17	1736,35	0,43	0,84	19,01	160,81	1,27
780,57	96,07	1,33	160,46	0,20	32,05	0,02	0,44	1,05	179,17	1736,35	0,43	0,84	12,49	160,81	1,27

Column Buckling, DNV										Column Buckling,		
λ_c	χ_c	k_χ	k_c	$\sigma_{x,rd}$ [MPa]	$\tau_{x,rd}$ [MPa]	UC	i_c [m]	f_{ak} [Mpa]	λ_c	f_{kc} [Mpa]	f_E [Mpa]	UC
0,78	0,74	1,94	1,94	245,06	114,92	0,11	3,50	286,41	0,72	495,43	550,48	0,29
0,78	0,74	1,94	1,94	245,06	114,92	0,12	3,50	286,41	0,72	495,43	550,48	0,30
0,78	0,74	1,94	1,94	245,06	114,92	0,13	3,50	286,41	0,72	495,43	550,48	0,32
0,78	0,74	1,94	1,94	245,06	114,92	0,14	3,50	286,41	0,72	495,43	550,48	0,33
0,85	0,69	1,92	1,92	256,10	114,19	0,16	3,50	302,28	0,74	496,42	551,58	0,35
0,85	0,69	1,92	1,92	256,10	114,19	0,16	3,50	302,28	0,74	496,42	551,58	0,35
0,85	0,69	1,92	1,92	256,10	114,19	0,16	3,50	302,28	0,74	496,42	551,58	0,35
0,91	0,65	1,91	1,91	251,98	107,62	0,20	3,50	299,11	0,74	497,41	552,68	0,39
0,91	0,65	1,91	1,91	251,98	107,62	0,19	3,50	299,11	0,74	497,41	552,68	0,38
0,91	0,65	1,91	1,91	251,98	107,62	0,18	3,50	299,11	0,74	497,41	552,68	0,36
0,91	0,65	1,91	1,91	251,98	107,62	0,16	3,50	299,11	0,74	497,41	552,68	0,34
0,99	0,59	1,89	1,90	253,55	101,11	0,18	3,51	302,82	0,74	498,41	553,79	0,36
0,99	0,59	1,89	1,90	253,55	101,11	0,16	3,51	302,82	0,74	498,41	553,79	0,33
0,99	0,59	1,89	1,90	253,55	101,11	0,14	3,51	302,82	0,74	498,41	553,79	0,31
0,99	0,59	1,89	1,90	253,55	101,11	0,12	3,51	302,82	0,74	498,41	553,79	0,28
0,99	0,59	1,89	1,90	253,55	101,11	0,11	3,51	302,82	0,74	498,41	553,79	0,27
0,99	0,59	1,89	1,90	253,55	101,11	0,12	3,51	302,82	0,74	498,41	553,79	0,28
0,99	0,59	1,89	1,90	253,55	101,11	0,14	3,51	302,82	0,74	498,41	553,79	0,30
0,99	0,59	1,89	1,90	253,55	101,11	0,16	3,51	302,82	0,74	498,41	553,79	0,32
0,99	0,59	1,89	1,90	253,55	101,11	0,17	3,51	302,82	0,74	498,41	553,79	0,35
0,99	0,59	1,89	1,90	253,55	101,11	0,19	3,51	302,82	0,74	498,41	553,79	0,37
0,99	0,59	1,89	1,90	253,55	101,11	0,21	3,51	302,82	0,74	498,41	553,79	0,39
1,08	0,53	1,88	1,88	247,05	90,99	0,30	3,51	295,86	0,73	499,41	554,90	0,46
1,08	0,53	1,88	1,88	247,05	90,99	0,31	3,51	295,86	0,73	499,41	554,90	0,43
1,08	0,53	1,88	1,88	247,05	90,99	0,22	3,51	295,86	0,73	499,41	554,90	0,34
1,08	0,53	1,88	1,88	247,05	90,99	0,12	3,51	295,86	0,73	499,41	554,90	0,20
1,08	0,53	1,88	1,88	247,05	90,99	0,05	3,51	295,86	0,73	499,41	554,90	0,09

Column Buckling,

 $A_{c,eff}$
[m²] W_{eff} [m³]

, Eurocode

N_{Ed} [MN]	M_{Ed} [MNm]	λ_1	$i_{c,eff}$ [m]	λ	ϕ	χ	N_{Rk} [MN]	M_{Rk} [MNm]	N_{cr} [MN]	c_{my}	μ	k_{yy}	UC	UC _{max}
20,93	593,52	82,82	3,67	0,66	0,83	0,75	830,17	2453,65	1881,38	0,99	1,00	1,00	0,28	0,29
22,23	623,35	82,82	3,67	0,66	0,83	0,75	830,17	2453,65	1881,38	0,99	1,00	1,00	0,30	0,30
23,53	652,89	82,82	3,67	0,66	0,83	0,75	830,17	2453,65	1881,38	0,99	1,00	1,00	0,31	0,32
24,87	675,65	82,82	3,67	0,66	0,83	0,75	830,17	2453,65	1881,38	0,99	1,00	1,00	0,32	0,33
26,12	684,04	80,14	3,83	0,63	0,81	0,77	744,32	2294,80	1715,50	0,98	1,00	1,00	0,35	0,35
27,37	684,16	80,14	3,83	0,63	0,81	0,77	744,32	2294,80	1715,50	0,98	1,00	1,00	0,35	0,35
28,61	680,07	80,14	3,83	0,63	0,81	0,77	744,32	2294,80	1715,50	0,98	1,00	1,00	0,35	0,35
29,74	666,83	80,14	3,94	0,60	0,78	0,79	636,15	2017,69	1548,61	0,98	1,00	1,00	0,39	0,39
30,88	645,18	80,14	3,94	0,60	0,78	0,79	636,15	2017,69	1548,61	0,98	1,00	1,00	0,38	0,38
32,01	616,13	80,14	3,94	0,60	0,78	0,79	636,15	2017,69	1548,61	0,98	1,00	1,00	0,37	0,37
33,13	581,61	80,14	3,94	0,60	0,78	0,79	636,15	2017,69	1548,61	0,98	1,00	1,00	0,35	0,35
34,14	541,96	78,90	4,09	0,56	0,75	0,81	542,07	1788,14	1380,69	0,98	1,00	1,00	0,37	0,37
35,16	498,35	78,90	4,09	0,56	0,75	0,81	542,07	1788,14	1380,69	0,97	0,99	0,99	0,34	0,34
36,17	451,89	78,90	4,09	0,56	0,75	0,81	542,07	1788,14	1380,69	0,97	0,99	0,99	0,32	0,32
37,19	403,89	78,90	4,09	0,56	0,75	0,81	542,07	1788,14	1380,69	0,97	0,99	0,99	0,29	0,29
38,20	385,61	78,90	4,09	0,56	0,75	0,81	542,07	1788,14	1380,69	0,97	0,99	0,99	0,28	0,28
39,22	410,10	78,90	4,09	0,56	0,75	0,81	542,07	1788,14	1380,69	0,97	0,99	0,99	0,29	0,29
40,23	439,20	78,90	4,09	0,56	0,75	0,81	542,07	1788,14	1380,69	0,97	0,99	0,99	0,31	0,31
41,25	470,91	78,90	4,09	0,56	0,75	0,81	542,07	1788,14	1380,69	0,97	0,99	0,99	0,33	0,33
42,26	504,08	78,90	4,09	0,56	0,75	0,81	542,07	1788,14	1380,69	0,97	0,99	0,99	0,36	0,36
43,28	538,60	78,90	4,09	0,56	0,75	0,81	542,07	1788,14	1380,69	0,97	0,99	0,99	0,38	0,38
44,24	570,96	78,90	4,09	0,56	0,75	0,81	542,07	1788,14	1380,69	0,97	0,99	0,99	0,40	0,40
45,07	573,16	78,90	4,23	0,53	0,72	0,83	444,13	1517,81	1211,74	0,96	0,99	0,99	0,47	0,47
45,91	538,42	78,90	4,23	0,53	0,72	0,83	444,13	1517,81	1211,74	0,96	0,99	0,99	0,45	0,51
46,74	401,04	78,90	4,23	0,53	0,72	0,83	444,13	1517,81	1211,74	0,96	0,99	0,99	0,35	0,44
47,57	211,09	78,90	4,23	0,53	0,72	0,83	444,13	1517,81	1211,74	0,96	0,99	0,99	0,22	0,34
48,36	53,33	78,90	4,23	0,53	0,72	0,83	444,13	1517,81	1211,74	0,96	0,99	0,99	0,10	0,20

B.3. Fatigue Limit State

Fatigue Limit State Geometry and DEM			Stress Concentration Factors										
			Weld Number	z [m]	D	[m]	t _s [m]	ΔM _{eq} [MNm]	L [mm]	α	β	δ _t [mm]	δ _e [mm]
		Circular weld at bottom of can 1	12,00	10,00	0,11	0,11	315,73	0,00	0,00	1,77	0,00	4,00	0,00
		Circular weld at bottom of can 2	7,50	10,00	0,11	0,11	303,53	0,00	0,00	1,77	0,00	4,00	0,00
		Circular weld at bottom of can 3	3,00	10,00	0,11	0,11	291,73	0,00	0,00	1,77	0,00	4,00	0,00
		Circular weld at bottom of can 4	-1,50	10,00	0,11	0,10	280,34	40,00	0,03	1,75	5,00	4,00	0,00
		Circular weld at bottom of can 5	-6,00	10,00	0,10	0,10	269,62	0,00	0,00	1,75	0,00	4,00	0,00
		Circular weld at bottom of can 6	-10,50	10,00	0,10	0,10	259,47	0,00	0,00	1,75	0,00	4,00	0,00
		Circular weld at bottom of can 7	-15,00	10,00	0,10	0,09	249,81	40,00	0,03	1,73	5,00	4,00	0,00
		Circular weld at bottom of can 8	-19,50	10,00	0,09	0,09	240,67	0,00	0,00	1,73	0,00	4,00	0,00
		Circular weld at bottom of can 9	-24,00	10,00	0,09	0,09	232,15	0,00	0,00	1,73	0,00	4,00	0,00
		Circular weld at bottom of can 10	-28,50	10,00	0,09	0,09	224,37	0,00	0,00	1,73	0,00	4,00	0,00
		Circular weld at bottom of can 11	-33,00	10,00	0,09	0,08	217,42	40,00	0,04	1,71	5,00	4,00	0,00
		Circular weld at bottom of can 12	-37,50	10,00	0,08	0,08	211,29	0,00	0,00	1,71	0,00	4,00	0,00
		Circular weld at bottom of can 13	-42,00	10,00	0,08	0,08	205,95	0,00	0,00	1,71	0,00	4,00	0,00
		Circular weld at bottom of can 14	-46,50	10,00	0,08	0,08	201,37	0,00	0,00	1,71	0,00	4,00	0,00
		Circular weld at bottom of can 15	-51,00	10,00	0,08	0,08	197,49	0,00	0,00	1,71	0,00	4,00	0,00
		Circular weld at bottom of can 16	-55,50	10,00	0,08	0,08	194,31	0,00	0,00	1,71	0,00	4,00	0,00
		Circular weld at bottom of can 17	-60,00	10,00	0,08	0,08	191,87	0,00	0,00	1,71	0,00	4,00	0,00
		Circular weld at bottom of can 18	-64,50	10,00	0,08	0,08	190,20	0,00	0,00	1,71	0,00	4,00	0,00
		Circular weld at bottom of can 19	-69,00	10,00	0,08	0,08	189,38	0,00	0,00	1,71	0,00	4,00	0,00
		Circular weld at bottom of can 20	-73,50	10,00	0,08	0,08	189,46	0,00	0,00	1,71	0,00	4,00	0,00
		Circular weld at bottom of can 21	-78,00	10,00	0,08	0,08	190,45	0,00	0,00	1,71	0,00	4,00	0,00
		Circular weld at bottom of can 22	-82,50	10,00	0,08	0,07	191,34	40,00	0,04	1,68	5,00	4,00	0,00
		Circular weld at bottom of can 23	-87,00	10,00	0,07	0,07	176,06	0,00	0,00	1,68	0,00	4,00	0,00
		Circular weld at bottom of can 24	-91,50	10,00	0,07	0,07	132,08	0,00	0,00	1,68	0,00	4,00	0,00
		Circular weld at bottom of can 25	-96,00	10,00	0,07	0,07	72,03	0,00	0,00	1,68	0,00	4,00	0,00
		Circular weld at bottom of can 26	-100,50	10,00	0,07	0,07	20,65	0,00	0,00	1,68	0,00	4,00	0,00

$\delta_{\theta, out}$ [mm]	SCF inside	SCF inside	Fatigue damage external weld					Fatigue damage internal weld					Fatigue Damage UC
			D_{ext} [m]	$\Delta\sigma_{nom}$ [MPa]	Thk. Factor	$\Delta\sigma_a$ [MPa]	Fatigue damage	D_{int} [m]	$\Delta\sigma_{nom}$ [MPa]	Thk. Factor	$\Delta\sigma_a$ [MPa]	Fatigue damage	
0,00	1,11	1,11	10,00	36,94	1,16	47,52	0,20	9,78	37,77	1,16	48,58	0,22	0,67
0,00	1,11	1,11	10,00	35,52	1,16	45,68	0,17	9,78	36,31	1,16	46,71	0,18	0,55
0,00	1,11	1,11	10,00	34,13	1,16	43,90	0,14	9,78	34,90	1,16	44,89	0,15	0,45
0,00	1,24	0,97	10,00	36,05	1,15	51,32	0,30	9,80	36,78	1,15	41,13	0,10	0,89
0,00	1,12	1,12	10,00	34,67	1,15	44,60	0,15	9,80	35,38	1,15	45,51	0,16	0,49
0,00	1,12	1,12	10,00	33,36	1,15	42,92	0,12	9,80	34,04	1,15	43,80	0,13	0,40
0,00	1,26	0,97	10,00	35,66	1,14	51,20	0,29	9,82	36,31	1,14	40,06	0,09	0,88
0,00	1,13	1,13	10,00	34,35	1,14	44,25	0,14	9,82	34,98	1,14	45,06	0,15	0,46
0,00	1,13	1,13	10,00	33,14	1,14	42,69	0,12	9,82	33,74	1,14	43,47	0,13	0,39
0,00	1,13	1,13	10,00	32,03	1,14	41,26	0,10	9,82	32,61	1,14	42,01	0,11	0,33
0,00	1,29	0,97	10,00	34,88	1,12	50,65	0,28	9,84	35,44	1,12	38,52	0,07	0,83
0,00	1,15	1,15	10,00	33,89	1,12	43,79	0,13	9,84	34,45	1,12	44,50	0,14	0,43
0,00	1,15	1,15	10,00	33,04	1,12	42,68	0,12	9,84	33,58	1,12	43,38	0,13	0,38
0,00	1,15	1,15	10,00	32,30	1,12	41,73	0,11	9,84	32,83	1,12	42,41	0,11	0,34
0,00	1,15	1,15	10,00	31,68	1,12	40,93	0,10	9,84	32,20	1,12	41,59	0,10	0,31
0,00	1,15	1,15	10,00	31,17	1,12	40,27	0,09	9,84	31,68	1,12	40,92	0,10	0,29
0,00	1,15	1,15	10,00	30,78	1,12	39,76	0,08	9,84	31,28	1,12	40,41	0,09	0,27
0,00	1,15	1,15	10,00	30,51	1,12	39,42	0,08	9,84	31,01	1,12	40,06	0,09	0,26
0,00	1,15	1,15	10,00	30,38	1,12	39,25	0,08	9,84	30,87	1,12	39,88	0,08	0,25
0,00	1,15	1,15	10,00	30,39	1,12	39,26	0,08	9,84	30,89	1,12	39,90	0,08	0,25
0,00	1,15	1,15	10,00	30,55	1,12	39,47	0,08	9,84	31,05	1,12	40,11	0,09	0,26
0,00	1,33	0,96	10,00	35,05	1,11	51,65	0,31	9,86	35,54	1,11	37,95	0,07	0,92
0,00	1,17	1,17	10,00	32,25	1,11	41,87	0,11	9,86	32,70	1,11	42,46	0,11	0,34
0,00	1,17	1,17	10,00	24,19	1,11	31,41	0,03	9,86	24,53	1,11	31,86	0,03	0,08
0,00	1,17	1,17	10,00	13,19	1,11	17,13	0,00	9,86	13,38	1,11	17,37	0,00	0,00
0,00	1,17	1,17	10,00	3,78	1,11	4,91	0,00	9,86	3,84	1,11	4,98	0,00	0,00

C

Geometries parametric study

C.1. 60-meter water depth

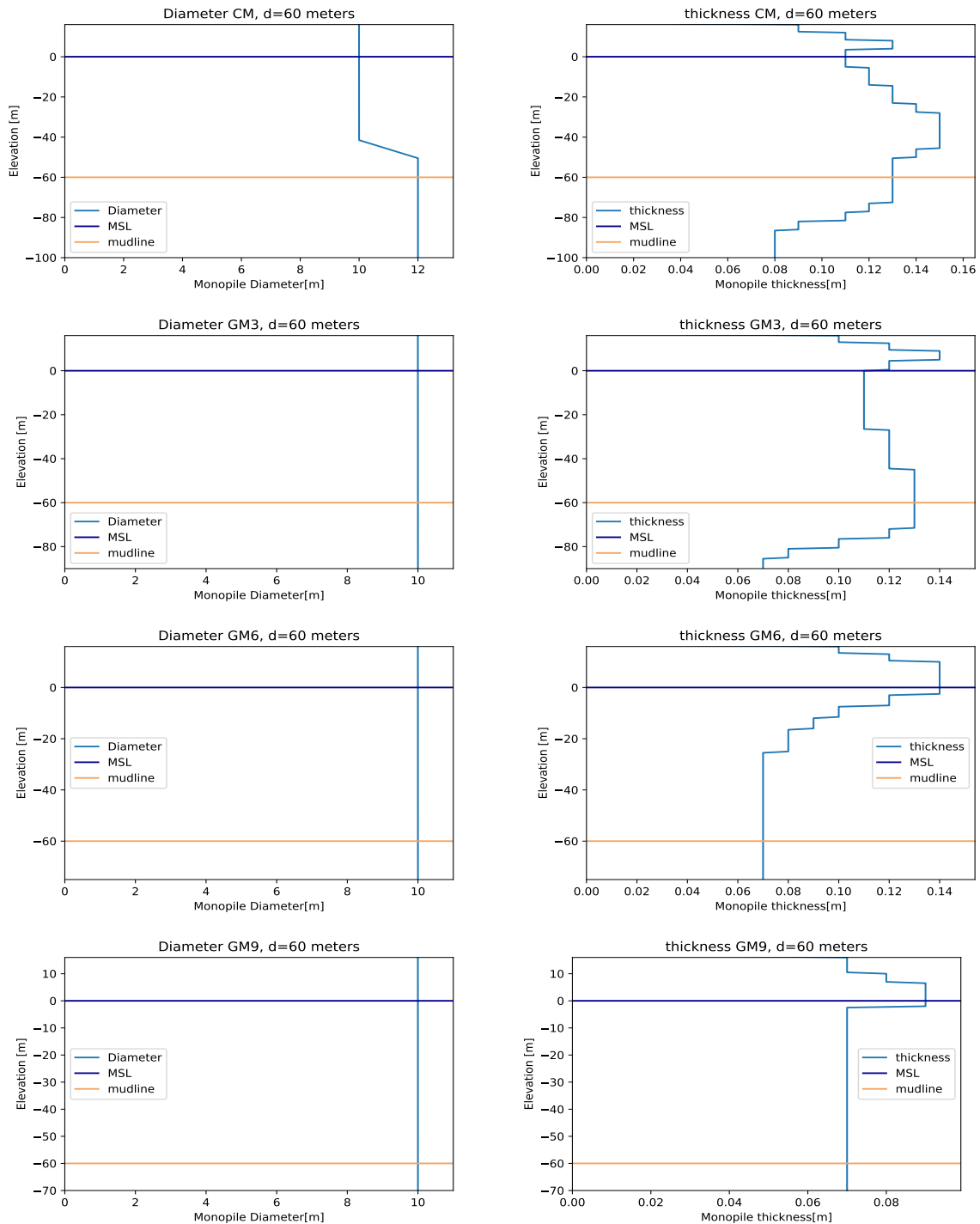


Figure C.1: All geometries for 60-meter water depth

C.2. 80-meter water depth

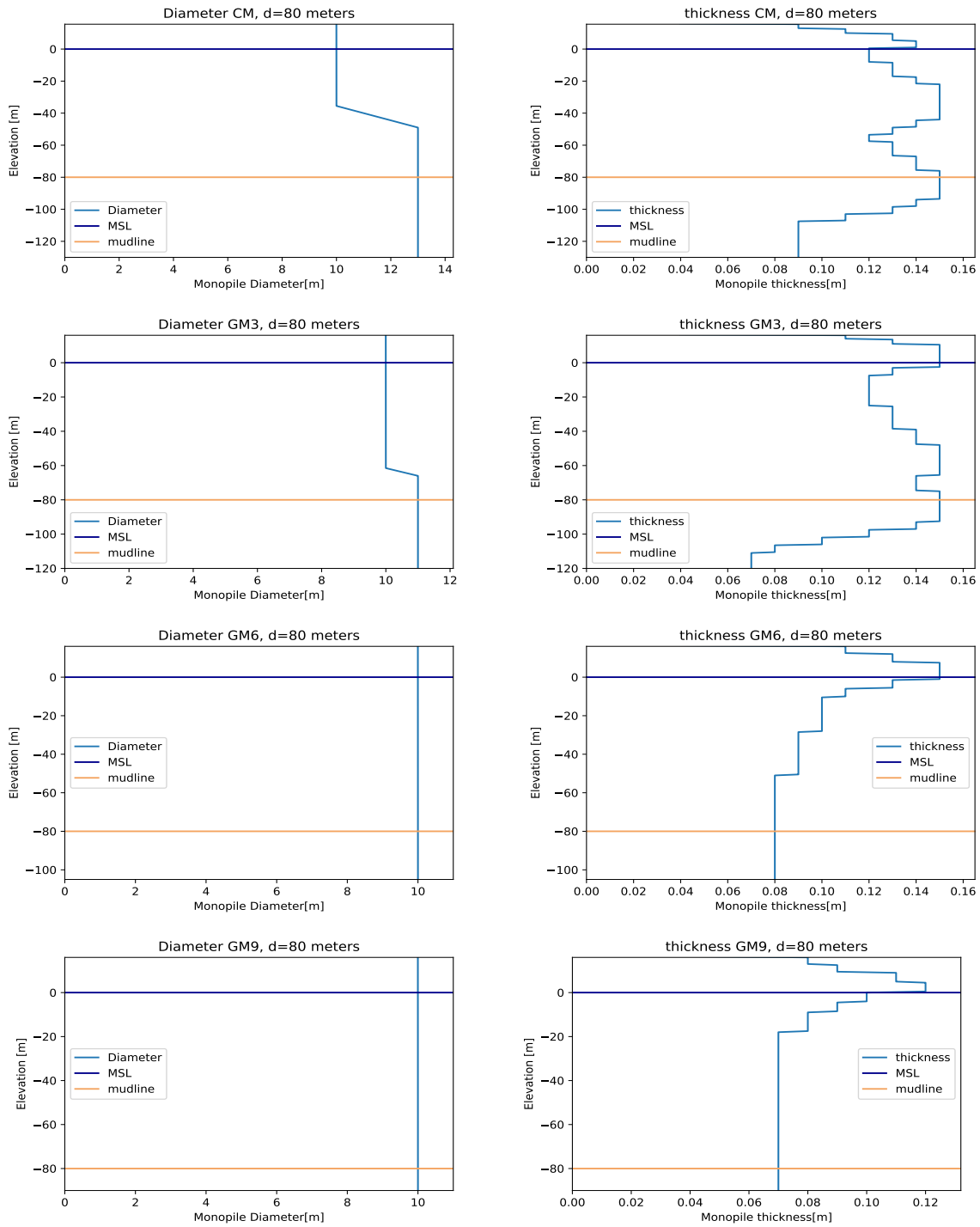


Figure C.2: All geometries for 80-meter water depth

C.3. 100-meter water depth

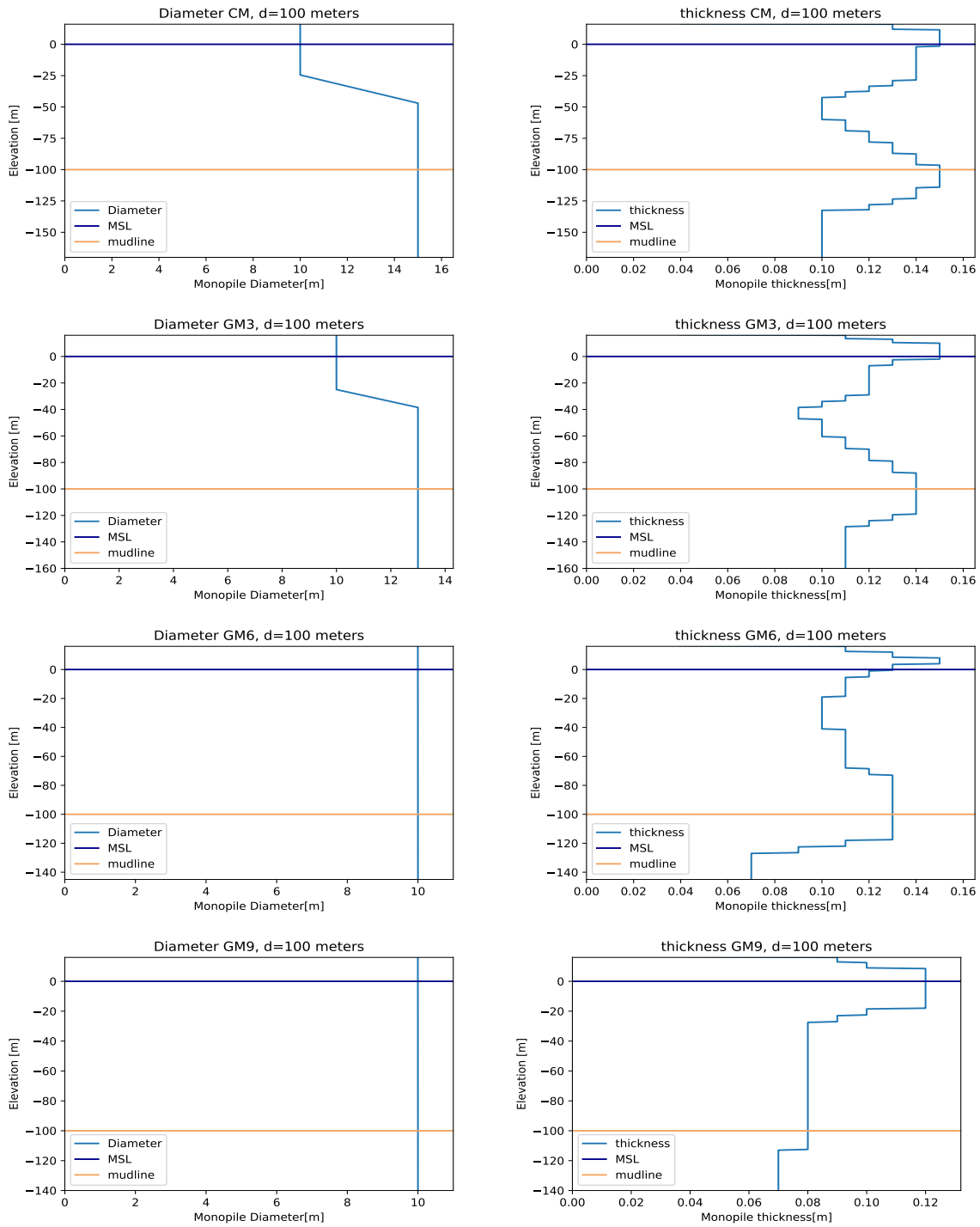


Figure C.3: All geometries for 100-meter water depth

C.4. 120-meter water depth

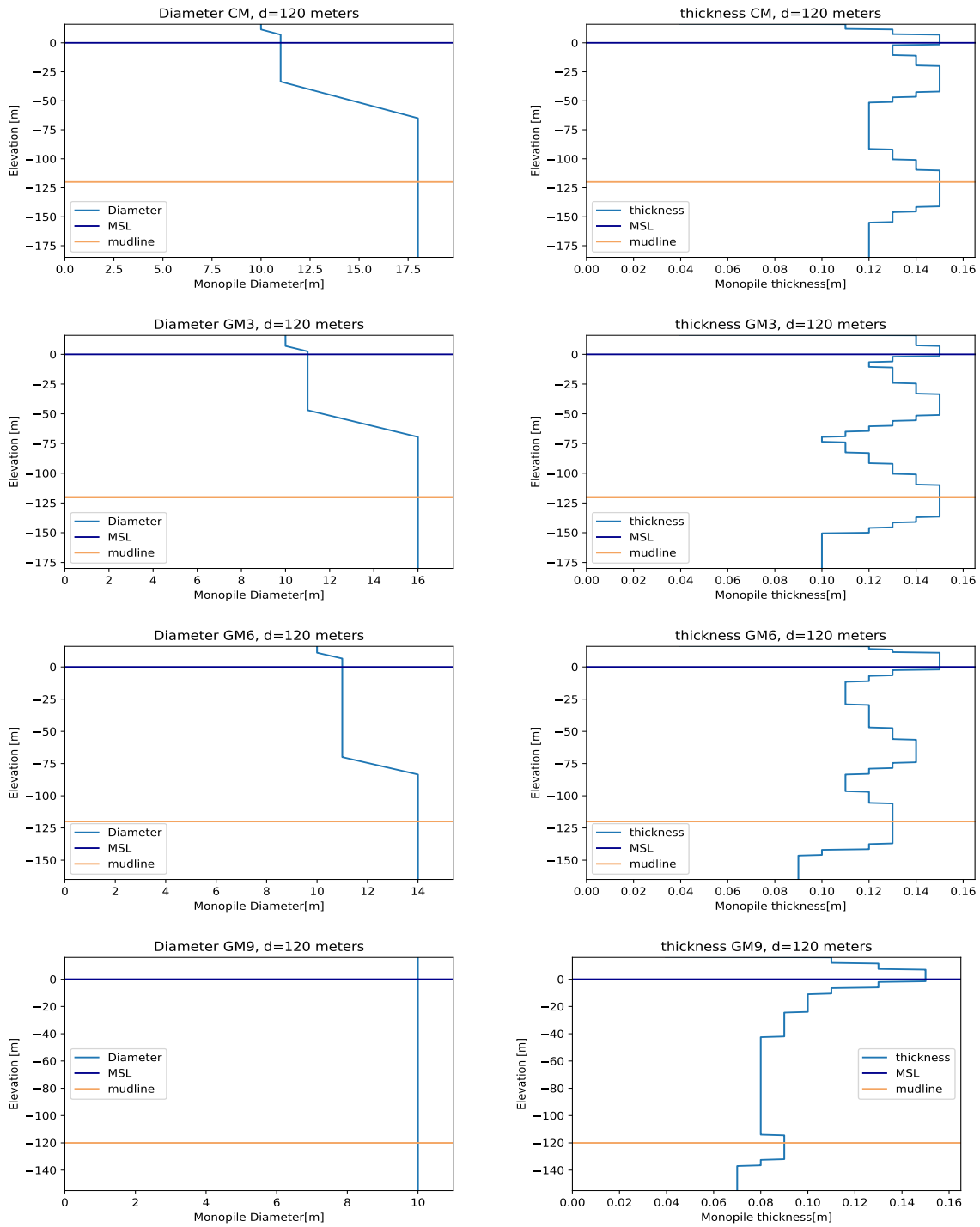


Figure C.4: All geometries for 120-meter water depth

D

Modal results parametric study

D.1. 60-meter water depth

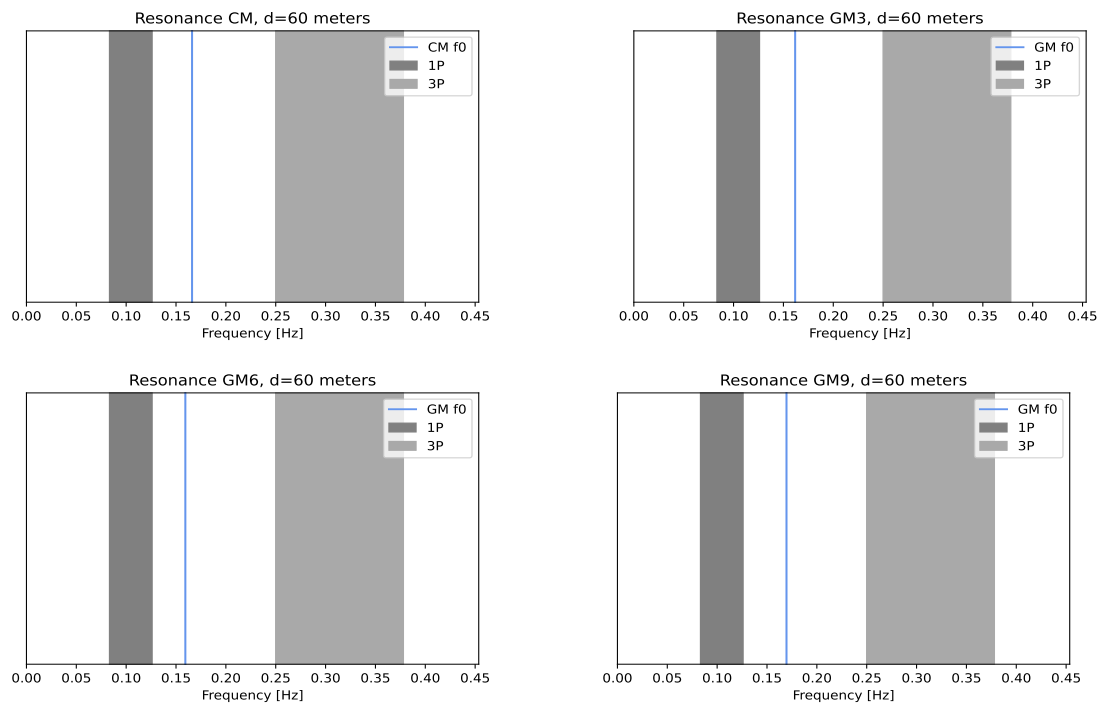


Figure D.1: All resonance checks for 60-meter water depth

D.2. 80-meter water depth

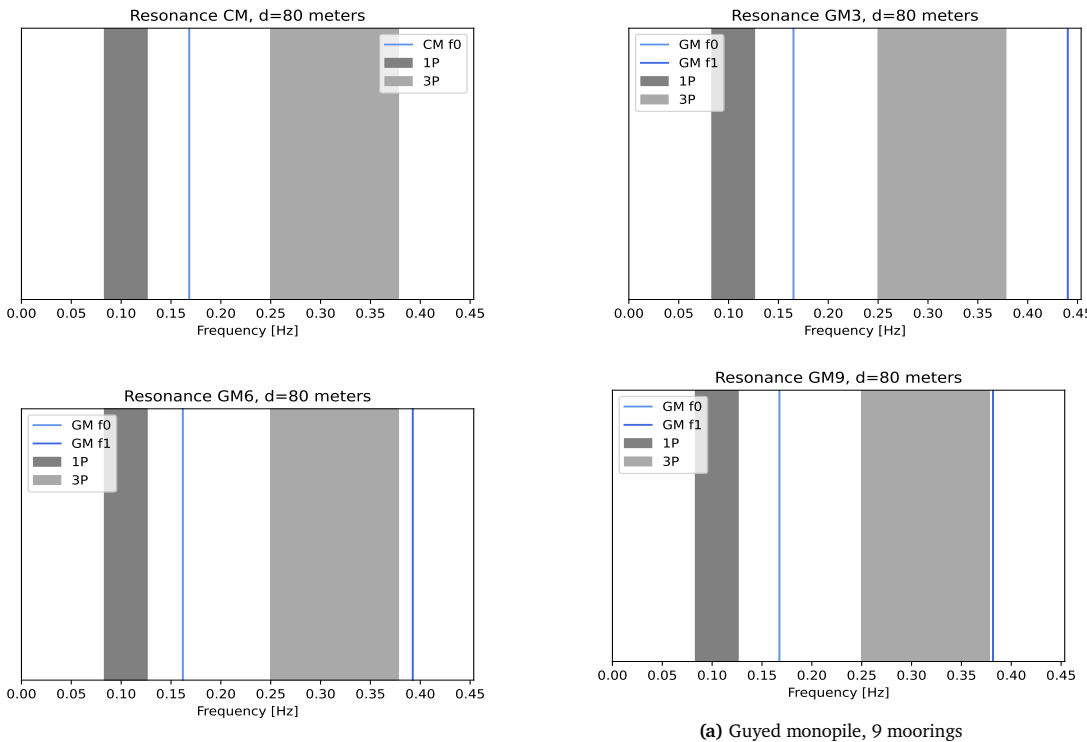


Figure D.2: All resonance checks for 80-meter water depth

D.3. 100-meter water depth

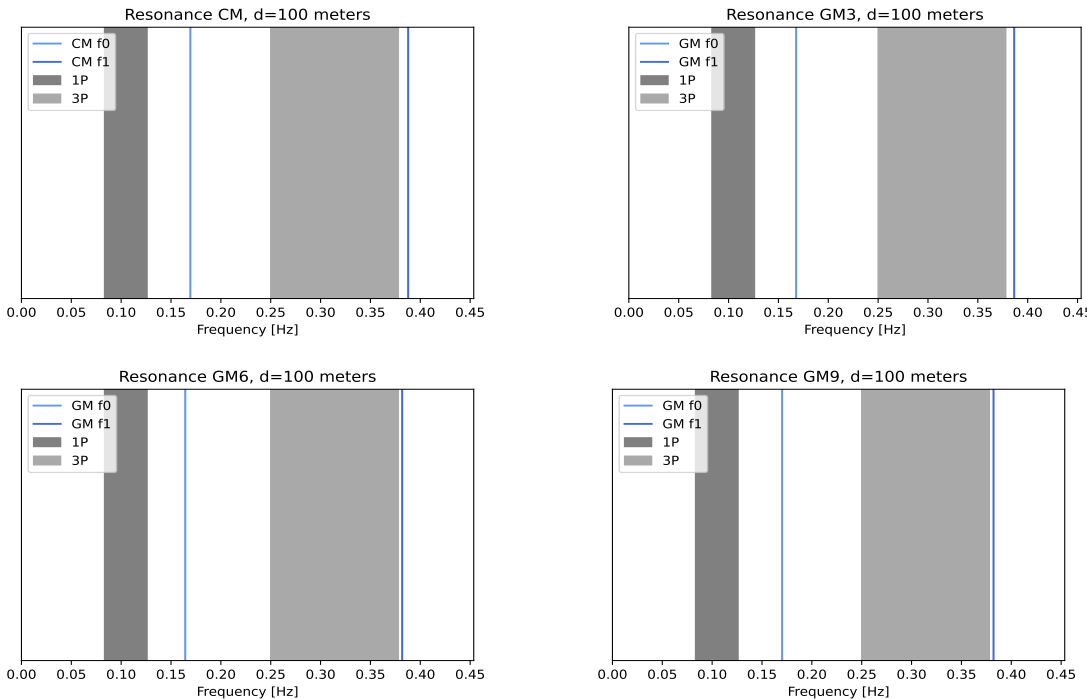


Figure D.3: All resonance checks for 100-meter water depth

D.4. 120-meter water depth

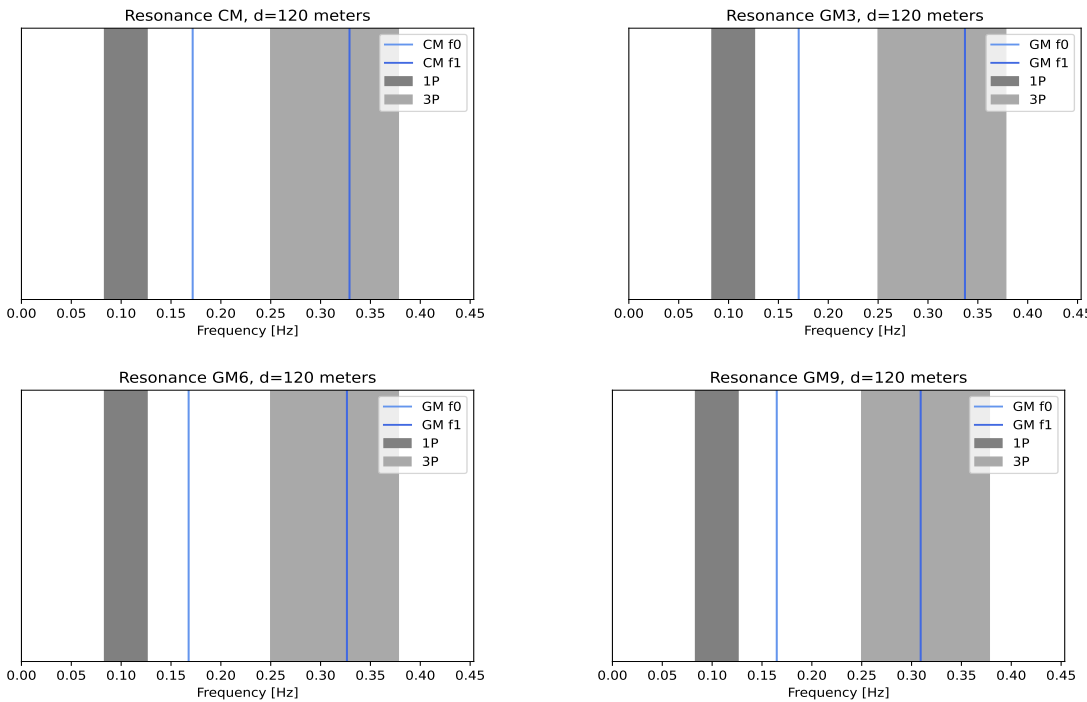


Figure D.4: All resonance checks for 120-meter water depth

E

ULS and FLS results parametric study

E.1. 60-meter water depth

GM			
Can no.	ULS	FLS	
0	0,31	0,55	
1	0,31	0,28	
2	0,31	0,76	
3	0,31	0,67	
4	0,32	0,93	
5	0,32	0,65	
6	0,34	0,89	
7	0,34	0,66	
8	0,37	0,90	
9	0,37	0,81	
10	0,38	0,66	
11	0,41	0,75	
12	0,44	0,87	
13	0,44	0,79	
14	0,44	0,68	
15	0,44	0,65	
16	0,47	0,73	
17	0,49	0,82	
18	0,50	0,78	
19	0,53	0,88	
20	0,53	0,63	
21	0,61	0,63	
22	0,62	0,35	
23	0,62	0,30	
24	0,62	0,30	
25	0,62		

GM3			
Can no.	ULS	FLS	
0	0,28	0,61	
1	0,28	0,29	
2	0,28	0,77	
3	0,29	0,90	
4	0,29	0,71	
5	0,29	0,71	
6	0,29	0,71	
7	0,29	0,72	
8	0,29	0,74	
9	0,30	0,97	
10	0,30	0,63	
11	0,31	0,66	
12	0,33	0,70	
13	0,35	0,92	
14	0,35	0,65	
15	0,38	0,70	
16	0,40	0,76	
17	0,42	0,81	
18	0,43	0,70	
19	0,43	0,60	
20	0,43	0,46	
21	0,47	0,32	
22	0,47	0,30	
23	0,47		

GM6			
Can no.	ULS	FLS	
0	0,29	0,81	
1	0,29	0,31	
2	0,29	0,95	
3	0,29	0,78	
4	0,29	0,56	
5	0,32	0,80	
6	0,35	0,73	
7	0,39	0,87	
8	0,39	0,53	
9	0,42	0,84	
10	0,42	0,50	
11	0,42	0,43	
12	0,42	0,38	
13	0,42	0,35	
14	0,42	0,33	
15	0,42	0,32	
16	0,42	0,31	
17	0,42	0,31	
18	0,42	0,30	
19	0,42	0,30	
20	0,42		

GM9			
Can no.	ULS	FLS	
0	0,47	0,36	
1	0,47	0,47	
2	0,47	0,80	
3	0,47	0,79	
4	0,50	0,96	
5	0,50	0,48	
6	0,50	0,42	
7	0,50	0,38	
8	0,50	0,35	
9	0,50	0,33	
10	0,50	0,32	
11	0,50	0,31	
12	0,50	0,30	
13	0,50	0,30	
14	0,50	0,30	
15	0,50	0,30	
16	0,50	0,30	
17	0,50	0,30	
18	0,50	0,30	
19	0,50		

E.2. 80-meter water depth

CM	GM9		
	Can no.	ULS	FLS
	0	0,31	0,64
	1	0,31	0,30
	2	0,31	0,79
	3	0,31	0,85
	4	0,31	0,64
	5	0,31	0,87
	6	0,31	0,64
	7	0,33	0,86
	8	0,33	0,77
	9	0,34	0,63
	10	0,36	0,72
	11	0,39	0,83
	12	0,39	0,56
	13	0,39	0,54
	14	0,39	0,50
	15	0,41	0,69
	16	0,43	0,79
	17	0,43	0,59
	18	0,45	0,81
	19	0,45	0,62
	20	0,46	0,84
	21	0,46	0,66
	22	0,47	0,72
	23	0,47	0,70
	24	0,50	0,81
	25	0,50	0,70
	26	0,57	0,86
	27	0,67	0,83
	28	0,67	0,34
	29	0,67	0,30
	30	0,67	0,30
	31	0,67	0,30
	32	0,67	

GM6	GM3		
	Can no.	ULS	FLS
	0	0,26	0,41
	1	0,26	0,23
	2	0,26	0,88
	3	0,26	0,90
	4	0,26	0,71
	5	0,27	0,77
	6	0,27	0,66
	7	0,27	0,69
	8	0,28	0,72
	9	0,29	0,95
	10	0,29	0,66
	11	0,31	0,71
	12	0,33	0,94
	13	0,33	0,69
	14	0,35	0,90
	15	0,35	0,70
	16	0,38	0,77
	17	0,40	0,86
	18	0,40	0,75
	19	0,40	0,71
	20	0,42	0,94
	21	0,42	0,72
	22	0,44	0,79
	23	0,44	0,73
	24	0,44	0,75
	25	0,47	0,79
	26	0,50	0,60
	27	0,59	0,42
	28	0,59	0,31
	29	0,59	0,30
	30	0,59	

GM9	GM6		
	Can no.	ULS	FLS
	0	0,28	0,61
	1	0,28	0,27
	2	0,28	0,93
	3	0,28	0,64
	4	0,32	0,99
	5	0,33	0,97
	6	0,33	0,67
	7	0,33	0,61
	8	0,33	0,56
	9	0,33	0,89
	10	0,33	0,62
	11	0,33	0,58
	12	0,33	0,55
	13	0,33	0,53
	14	0,33	0,92
	15	0,33	0,65
	16	0,33	0,64
	17	0,33	0,63
	18	0,34	0,62
	19	0,36	0,63
	20	0,38	0,64
	21	0,39	0,65
	22	0,39	0,53
	23	0,43	0,36
	24	0,43	0,30
	25	0,43	0,30
	26	0,43	

E.3. 100-meter water depth

GM9	Can no. ULS			FLS		
	Can no.	ULS	FLS	Can no.	ULS	FLS
	0	0,33	0,40			
	1	0,33	0,30			
	2	0,33	0,80			
	3	0,33	0,38			
	4	0,33	0,37			
	5	0,33	0,36			
	6	0,33	0,35			
	7	0,33	0,51			
	8	0,35	0,51			
	9	0,39	0,63			
	10	0,39	0,47			
	11	0,39	0,45			
	12	0,39	0,43			
	13	0,39	0,41			
	14	0,39	0,40			
	15	0,39	0,39			
	16	0,39	0,39			
	17	0,39	0,38			
	18	0,39	0,38			
	19	0,39	0,38			
	20	0,39	0,39			
	21	0,39	0,40			
	22	0,39	0,41			
	23	0,41	0,43			
	24	0,44	0,46			
	25	0,46	0,49			
	26	0,47	0,53			
	27	0,47	0,50			
	28	0,56	0,68			
	29	0,56	0,37			
	30	0,56	0,32			
	31	0,56	0,30			
	32	0,56	0,30			
	33	0,56	0,30			
	34	0,56				

GM6	Can no. ULS			FLS		
	Can no.	ULS	FLS	Can no.	ULS	FLS
	0	0,27	0,49			
	1	0,27	0,24			
	2	0,27	0,69			
	3	0,28	0,69			
	4	0,31	0,85			
	5	0,31	0,65			
	6	0,31	0,63			
	7	0,31	1,00			
	8	0,31	0,77			
	9	0,31	0,75			
	10	0,31	0,74			
	11	0,31	0,75			
	12	0,31	0,99			
	13	0,31	0,60			
	14	0,31	0,62			
	15	0,32	0,64			
	16	0,34	0,67			
	17	0,36	0,71			
	18	0,38	0,95			
	19	0,38	0,76			
	20	0,38	0,56			
	21	0,38	0,60			
	22	0,39	0,64			
	23	0,42	0,69			
	24	0,44	0,76			
	25	0,46	0,84			
	26	0,47	0,90			
	27	0,47	0,83			
	28	0,47	0,61			
	29	0,48	0,89			
	30	0,52	0,84			
	31	0,65	0,75			
	32	0,65	0,32			
	33	0,65	0,30			
	34	0,65	0,30			
	35	0,65				

GM3	Can no. ULS			FLS		
	Can no.	ULS	FLS	Can no.	ULS	FLS
	0	0,26	0,39			
	1	0,26	0,22			
	2	0,26	0,86			
	3	0,26	0,90			
	4	0,26	0,72			
	5	0,28	0,80			
	6	0,28	0,70			
	7	0,28	0,74			
	8	0,29	0,79			
	9	0,31	0,86			
	10	0,31	0,84			
	11	0,31	0,74			
	12	0,33	0,72			
	13	0,35	0,61			
	14	0,38	0,91			
	15	0,38	0,58			
	16	0,38	0,64			
	17	0,40	0,95			
	18	0,40	0,63			
	19	0,43	0,90			
	20	0,43	0,62			
	21	0,43	0,87			
	22	0,43	0,63			
	23	0,44	0,87			
	24	0,44	0,65			
	25	0,45	0,73			
	26	0,48	0,82			
	27	0,49	0,89			
	28	0,49	0,84			
	29	0,49	0,68			
	30	0,49	0,73			
	31	0,49	0,62			
	32	0,49	0,50			
	33	0,49	0,34			
	34	0,49	0,31			
	35	0,49	0,30			
	36	0,49	0,30			
	37	0,49	0,30			
	38	0,49	0,30			
	39	0,49				

CM	Can no. ULS			FLS		
	Can no.	ULS	FLS	Can no.	ULS	FLS
	0	0,22	0,21			
	1	0,22	0,14			
	2	0,22	1,00			
	3	0,24	0,58			
	4	0,25	0,56			
	5	0,27	0,62			
	6	0,30	0,69			
	7	0,32	0,78			
	8	0,35	0,90			
	9	0,35	0,85			
	10	0,35	0,74			
	11	0,36	0,70			
	12	0,37	0,70			
	13	0,37	0,47			
	14	0,38	0,51			
	15	0,41	0,57			
	16	0,43	0,85			
	17	0,43	0,58			
	18	0,45	0,84			
	19	0,45	0,60			
	20	0,46	0,84			
	21	0,46	0,62			
	22	0,46	0,85			
	23	0,46	0,64			
	24	0,47	0,87			
	25	0,47	0,67			
	26	0,47	0,73			
	27	0,47	0,73			
	28	0,51	0,95			
	29	0,51	0,62			
	30	0,51	0,68			
	31	0,52	0,60			
	32	0,61	0,80			
	33	0,61	0,38			
	34	0,61	0,32			
	35	0,61	0,30			
	36	0,61	0,30			
	37	0,61	0,30			
	38	0,61	0,30			
	39	0,61	0,30			
	40	0,61	0,30			
	41	0,61				

E.4. 120-meter water depth

CM	GM3			GM6			GM9		
	Can no.	ULS	FLS	Can no.	ULS	FLS	Can no.	ULS	FLS
	0	0,26	0,73		0	0,21	0	0,29	0,59
	1	0,26	0,58		1	0,22	1	0,29	0,26
	2	0,26	0,92		2	0,22	2	0,29	0,89
	3	0,26	0,81		3	0,22	3	0,29	0,62
	4	0,26	0,63		4	0,24	4	0,34	0,95
	5	0,26	0,84		5	0,24	5	0,36	0,93
	6	0,26	0,65		6	0,24	6	0,36	0,65
	7	0,28	0,87		7	0,24	7	0,36	0,59
	8	0,29	0,70		8	0,26	8	0,38	0,93
	9	0,31	0,81		9	0,26	9	0,38	0,63
	10	0,34	0,96		10	0,28	10	0,38	0,58
	11	0,34	0,65		11	0,29	11	0,38	0,53
	12	0,34	0,67		12	0,31	12	0,38	0,89
	13	0,34	0,64		13	0,33	13	0,38	0,60
	14	0,35	0,63		14	0,33	14	0,38	0,56
	15	0,35	0,79		15	0,33	15	0,38	0,53
	16	0,35	0,64		16	0,34	16	0,38	0,51
	17	0,35	0,55		17	0,36	17	0,38	0,49
	18	0,35	0,62		18	0,37	18	0,38	0,47
	19	0,35	0,72		19	0,39	19	0,38	0,46
	20	0,37	0,83		20	0,39	20	0,38	0,45
	21	0,39	0,52		21	0,40	21	0,38	0,45
	22	0,41	0,58		22	0,40	22	0,38	0,46
	23	0,43	0,82		23	0,40	23	0,38	0,46
	24	0,43	0,60		24	0,40	24	0,38	0,48
	25	0,43	0,83		25	0,40	25	0,38	0,50
	26	0,43	0,63		26	0,40	26	0,39	0,54
	27	0,43	0,86		27	0,40	27	0,41	0,58
	28	0,43	0,66		28	0,40	28	0,43	0,86
	29	0,43	0,73		29	0,41	29	0,43	0,53
	30	0,44	0,82		30	0,42	30	0,43	0,57
	31	0,44	0,87		31	0,42	31	0,43	0,54
	32	0,45	0,81		32	0,43	32	0,47	0,64
	33	0,45	0,68		33	0,45	33	0,55	0,47
	34	0,48	0,77		34	0,47	34	0,55	0,31
	35	0,51	0,80		35	0,50	35	0,55	0,30
	36	0,51	0,73		36	0,61	36	0,55	0,30
	37	0,51	0,70		37	0,61	37	0,55	0,30
	38	0,51	0,37		38	0,61	38	0,59	0,30
	39	0,51	0,37		39	0,61	39	0,59	0,30
	40	0,51	0,37		40	0,61	40	0,59	0,30
	41	0,51	0,37		41	0,61	41	0,59	0,30
	42	0,51	0,37		42	0,61	42	0,59	0,30
	43	0,51	0,37		43	0,61	43	0,59	0,30
	44	0,51			44	0,61	44	0,59	

F

Stream function wave

